University of South-Eastern Norway
Faculty of Health and Social Sciences

Doctoral dissertation no. 67
2020

Hilde Røgeberg Pedersen

The Retina in Congenital Aniridia - Structural, Functional and Genetic Variability

Hilde Røgeberg Pedersen

The Retina in Congenital Aniridia - Structural, Functional and Genetic Variability

A PhD dissertation in
Person-Centred Healthcare

Faculty of Health and Social Sciences
University of South-Eastern Norway
Kongsberg, 2020

Doctoral dissertations at the University of South-Eastern Norway no.67

ISSN: 2535-5244 (print)
ISSN: 2535-5252 (online)

ISBN: 978-82-7206-552-1 (print)
ISBN: 978-82-7206-553-8 (online)

Print: University of South-Eastern Norway

To Kent, Ellen, Kåre & Stine

Acknowledgements

The work presented in this thesis has been carried out at the National Centre for Optics, Vision and Eye Care, Faculty of Health and Social Sciences at the University of South-Eastern Norway and was funded by the Norwegian Ministry of Education and Research. The genetic analysis was conducted at the Neitz Lab at the University of Washington and was supported by National Eye Institute grants P30EY001730 and R01EY028118, and by unrestricted funds from Research to Prevent Blindness.

First, I want to thank my supervisors, Rigmor C. Baraas and Stuart J. Gilson. A special thanks to Rigmor, who has been my main supervisor and a great inspiration along the way. Thank you for sharing your immense knowledge, for always believing in me and for challenging me a little bit extra when needed. I learn from you every day and am forever grateful! I am deeply thankful to Stuart for proof-reading and for his invaluable support and feedback. This work would not have been possible without his remarkable programming skills. I am very grateful to Maureen Neitz for her work with the genetic analysis and for sharing her great expertise. I want to thank Erlend S. Landsend, Tor P. Utheim and Øygunn Aas Utheim for the great collaboration we have had during this project. Tor enthusiastically introduced me to aniridia research in 2015 and played an important role in the initiation of this project. A great thanks to my colleges and my fellow PhD-candidates, Lene A. Hagen and Nickolai G. Nilsen, for all support, valuable discussions and friendship. I also want to thank Lene, Ragnhild Bjørgum and Jon Gjelle for contributing in this project, and to Kenneth Knoblauch for patiently teaching me R.

I would like to express my gratitude to Aniridi Norge for their continuous support. I am appreciative of and thank the participants and their families. Their interest, contributions and patience are fundamental and have been a great inspiration.

And last, but not least, I am deeply thankful to my family and friends for always being supportive. A special thanks to my dear Kent for always being there for me.

Kongsberg, February 2020

Hilde Røgeberg Pedersen

Abstract

Aniridia is a rare, congenital eye disorder most commonly caused by a mutation in the *PAX6* gene, which affects eye development and leads to a range of ocular anomalies, including iris- and foveal hypoplasia and vision impairment. However, the phenotypes vary considerably between individuals. Research investigating the retina in aniridia remains limited. The main purpose of this thesis is therefore to gain more in-depth knowledge about variation in genotype and retinal phenotype in persons with aniridia.

The thesis includes three cross-sectional studies that characterize macular structure and foveal development, their importance to visual performance, and genotype-phenotype correlations. Data from genetic analysis and retinal imaging were combined with clinical and psychophysical measures of high-contrast visual acuity and colour vision.

High-resolution retinal imaging shows that persons with aniridia have varying foveal hypoplasia grades (paper I), reduced cone photoreceptor density and mosaic regularity (paper II) and decreased thicknesses and morphology of the retinal layers (paper III), relative to normal healthy controls. High-contrast visual acuity and colour discrimination thresholds not only varied greatly between individuals, but also within families carrying the same genetic mutation, and were associated with grade of foveal hypoplasia and thickness of the outer retinal layers. Despite the large variation in phenotype, analysis of genotype-phenotype correlations indicate that the retinal phenotype is associated with the position and extent of the mutation, within non-coding, coding or flanking regulatory regions of the *PAX6* gene.

This knowledge is of great significance in the clinical management of persons with congenital aniridia to understand limits and potential related to visual function, to determine when an intervention is advisable, and for presenting well-founded individual alternatives of facilitation, rehabilitation or treatment options.

Keywords: Aniridia, *PAX6*, foveal hypoplasia, retinal development, photoreceptors, colour vision, visual acuity, optical coherence tomography, adaptive optics, person-centred eye care.

List of papers

Paper I

Pedersen, H. R., Hagen, L. A., Landsend, E. C. S., Gilson, S. J., Utheim, Ø. A., Utheim, T. P., Neitz M., & Baraas, R. C. (2018). Color Vision in Aniridia. *Investigative Ophthalmology & Visual Science, 59*(5), 2142-2152. doi:10.1167/iovs.17-23047

Paper II

Pedersen, H. R., Neitz M., Gilson, S. J., Landsend, E. C. S., Utheim, Ø. A., Utheim, T. P., & Baraas, R. C. (2019). The cone photoreceptor mosaic in aniridia: within-family phenotype-genotype discordance. *Ophthalmology Retina*, 3:523-534. https://doi.org/10.1016/j.oret.2019.01.020

Paper III

Pedersen, H. R., Baraas, R. C., Landsend, E. C. S., Utheim, Ø. A., Utheim, T. P., Gilson, S. J., Neitz, M. (Accepted). *PAX6* Genotypic and Retinal Phenotypic Characterization in Congenital Aniridia. *Investigative Ophthalmology & Visual Science.*

Research presentations

Work presented in this thesis has been presented at several international conferences.

Conference abstracts

Pedersen H.R., Neitz M., Gilson S. J, Landsend E. S., Utheim Ø. A., Utheim T. P., Baraas R.C. (2019) PAX6 genotype and thickness of retinal layers in aniridia. ARVO meeting abstracts, Investigative Ophthalmology and Visual Science 60(9):1896

Pedersen H. R., Landsend E. S., Neitz M., Gilson S. J, Hagen L. A., Utheim Ø. A., Utheim T. P., Baraas R.C. (2018) Vision in congenital aniridia. Scandinavian Journal of Optometry and Visual Science; Volume 11(2) s. 1-2

Pedersen H.R., Neitz M., Gilson S. J, Landsend E. S., Utheim Ø. A., Utheim T. P., Baraas R.C (2018) Within-family phenotype-genotype discordance in congenital aniridia. 4th European Conference on Aniridia, Paris, France; 2018-08-25 – 2018-08-26

Pedersen H.R., Neitz M., Gilson S. J, Landsend E. S., Utheim Ø. A., Utheim T. P., Baraas R.C (2018) Retinal structure variation in congenital aniridia: within family phenotype-genotype discordance. ARVO meeting abstracts, Investigative Ophthalmology and Visual Science, 59(9): 667

Pedersen H. R, Gjelle J. V., Hagen L. A., Landsend E.S., Gilson S. J., Utheim Ø. A., Utheim T. P., Baraas R. C. (2017) Investigation of ocular biometry in persons with congenital aniridia. Scandinavian Journal of Optometry and Visual Science, Volume 10(2) s. 8-9

Pedersen H. R, Gjelle J. V., Hagen L. A., Landsend E. S., Gilson S. J., Utheim Ø. A., Utheim T. P., Baraas R. C. (2017) Refractive errors and ocular biometry in congenital aniridia. The 16th International Myopia Conference; Ophthalmic and Physiological Optics 2018 May;38(3): S3

Pedersen H. R., Hagen L. A., Landsend E. S., Gilson S. J., Gjelle J. V., Utheim Ø. A., Utheim T. P., Neitz M., Baraas R. C. (2017) Chromatic Sensitivity in Aniridia. The 24th symposium of the international colour vision society; 2017-08-17 – 2017-08-22

Pedersen H. R., Hagen L. A., Landsend E. S., Gjelle J. V., Utheim Ø. A., Gilson S. J., Utheim T. P., Baraas R. C. (2016) Color vision, dark adaptation and retinal structure in Aniridia. ARVO meeting abstracts, Investigative Ophthalmology and Visual Science 57(12):623

List of tables

List of figures

Abbreviations

AAK – Aniridia-associated keratopathy

AOSLO – Adaptive optics scanning light ophthalmoscope

bHLH – basic-Helix-Loop-Helix

BM – Bruch's membrane

CTE – C-terminal extension

DCDC1 – Doublecortin domain-containing 1 gene

ELM – External limiting membrane

*ELP*4 – Elongator acetyltransferase complex subunit 4

EZ – Ellipsoid zone

FAZ – Foveal avascular zone

FOXC1 – Forkhead box C1 gene

Fwk – Fetal week

FH – Foveal hypoplasia

GCL – Ganglion cell layer

HFL – Henle's fiber layer

HD – Homeo domain

ILM – Inner limiting membrane

IPL – Inner plexiform layer

INL – Inner nuclear layer

IS – Inner segment

IZ – Interdigitation zone

MPLA – multiplex ligation-dependent probe amplification

NMD – Nonsense mediated decay

ONL – Outer nuclear layer

OPL – Outer plexiform layer

OS – Outer segment

PAX6 – Human paired box 6 gene

PAX6 – Paired box 6 protein

Pax6 – Mouse paired box 6 gene

PD – Paired domain

PITX2 – Pituitary homeobox 2 gene

PCR – Polymerase chain reaction

PST – Proline serine–threonine domain

PTC – Premature termination codon

RNFL – Retinal nerve fiber layer

RPC – Retinal progenitor cell

RPE – Retinal pigment epithelium

SD-OCT – Spectral domain optical coherence tomography

Sey – Small eye

UTR – Untranslated region

WT1 – Wilms' tumor 1 gene

Table of contents

1 Introduction

1.1 Background

The physical parameters of the eye are unique to each person, giving each their very own subjective visual experience. Sight has long been considered the most highly valued of our senses, which was recently supported in a cross-sectional study in UK [1]. Hence, to have a visual impairment may have a large impact on people's lives and identities and creates major challenges in many areas of life such as learning, communication, work and spare time, social relations and independence in daily life [2].

Rare eye disorders affect a limited number of individuals and is often overshadowed by conditions affecting larger patient populations. In most of Europe including Norway, a disease is defined as rare if the population prevalence is less than 1:2000 [3]. With a reported prevalence of 1:72 000 (95% CI: 1:63 000–1:84 000) in Norway and Sweden [4], congenital aniridia is classified as a rare genetic eye disorder. There is no official register for aniridia in Norway but the Norwegian Association of Aniridia (Aniridi Norge) had registered about 70 known cases in 2017. Rare diseases such as aniridia are a challenge, both for the persons who are affected and their families, but also for health care professionals because reliable and scientifically grounded information often is insufficient. Individuals with aniridia commonly experience that healthcare providers and society lack knowledge about the disorder. This may have negative consequences, such as inappropriate treatment or advice, treatment delay, and reduced options for vision rehabilitation and facilitation [5].

Although the name aniridia means without iris, the diagnosis aniridia includes a spectrum of disorders in addition to varying degree of iris hypoplasia. Congenital aniridia is often called a "pan-ocular" disorder of abnormal eye development [6-8]. This reflects that the whole eye is affected by misdirected ocular development, causing vision impairment from early childhood ranging from mild vision impairment to blindness. The

majority of persons with aniridia have foveal hypoplasia [9] which may be one of the main limiting factors in the visual function achieved.

Congenital aniridia can result from more than 450 different *PAX6* mutations [8] and is associated with large variability in phenotype and severity, even among family members who have an identical genetic mutation [9]. Consequently, despite having the same diagnosis the impact of the disease can vary a lot between persons with aniridia. This person-to-person variability can be a challenge in the clinical management of aniridia. Thus, genotypic and phenotypic variation and complexity in aniridia requires more detailed attention.

There is a particular lack of knowledge related to variation in retinal structure and how it correlates with visual function in persons with aniridia. Only a few studies have investigated the retinal layers in aniridia before the present study was initiated. Those described the presence of foveal hypoplasia and/or different grades of foveal hypoplasia [10-13]. None had reported analysis of the photoreceptor mosaic. Functional consequences and retinal phenotype in relation to genotype remains largely unexplored and can make it difficult to provide evidence based and person-centred rehabilitation and treatment options. This indicates the need to increase the understanding of morphological abnormalities and variation in retinal development, both between and within individuals and families with aniridia.

The work presented in this thesis focuses on characterizing retinal structure and foveal development, its importance to visual performance, and genotype-phenotype correlations in aniridia. The use of high-resolution retinal imaging techniques allows thickness measurements of the retinal layers and imaging of the retina in living humans at a cellular resolution. Data from genetic analysis and retinal imaging combined with visual functional measurements such as colour vision and visual acuity will contribute to increased knowledge about the large spectrum of between-individual variations, limitations and possibilities related to visual function. Such knowledge is crucial if we are to understand each individual's needs for facilitation and visual rehabilitation and

how their vision can be utilized in the best possible way, which is essential for learning, communication, work and each person's independence in daily life.

1.2 The retina

The initial step in seeing begins in the retina, which is considered a part of the central nervous system [14]. The retina comprises highly organized layers of neurons including the light-sensitive cells which detect and process visual information [15]. Retinal function requires photoreceptors. Light stimulates the photopigment in the cone and rod outer segments and is converted into electrical signals by phototransduction. That is, activation of the visual pigment results in a cascade of several biochemical reactions and hyperpolarisation of the cell. This generates a response to light in the form of an electrical signal [15]. Rods are very light-sensitive and operate at low light levels as they are able to respond to a single photon of light, whereas cones require higher light levels to generate signals. All rods contain the same photopigment, rhodopsin [15].

Normal trichromatic colour vision is initiated by differential activation of the three cone types which have their peak sensitivity at different wavelengths depending on the type of photopigment their respective outer segments contain. The long (L), medium (M) and short (S) wavelength cones have peak sensitivities at ~560 nm, ~530 nm and ~420 nm, respectively [16, 17], but with considerable overlap in absorption spectra [18, 19]. The L and M cone opsin genes (OPN1LW and OPN1MW) are localized on the X-chromosome at Xq28 whereas the genes for the S cone opsin (OPN1SW) is localized to an autosome on chromosome 7 at 7q32. Mutations in one of these genes cause inherited colour vision deficiencies [20].

A network of different cell types forms neural circuits and carry signals from the photoreceptors via ganglion cells and the lateral geniculate nucleus (LGN) to the brain in at least three major pathways: parvo-, magno- and koniocellular pathways. In short, the parvocellular pathway carries information about red-green colour opponency and fine spatial details, the magnocellular pathway conveys luminance and motion signals and the koniocellular pathway signals blue-yellow opponency, amongst others [21-23].

1.2.1 The retinal layers

The human retina has a layered structure. The outermost layer, the retinal pigment epithelium (RPE), is formed by a single layer of pigmented epithelial cells that closely interacts with the photoreceptors in the maintenance of visual function [24]. The RPE is also critical for normal retinal development [24]. The photoreceptor layer is located adjacent to the RPE and consists of the outer segments (OS) and inner segments (IS) of the rods and cones. Their cell bodies comprise the outer nuclear layer (ONL) and form synapses with horizontal and bipolar cells in the outer plexiform layer (OPL). Bipolar, horizontal, amacrine and Müller glia cell bodies are located in the inner nuclear layer (INL). Bipolar cells connect directly to the photoreceptors, whereas horizontal and amacrine cells laterally inhibit bipolar cells. The inner layer of synapses is the inner plexiform layer (IPL) where bipolar cell dendrites connect to the ganglion cells, either directly or indirectly via amacrine cells. The retinal ganglion cell layer (GCL) consist mainly of ganglion cell nuclei, but also displaced amacrine cells [25]. The retinal ganglion cells transmit signals via their axons in the retinal nerve fiber layer (RNFL) through the optic nerve to the LGN and visual cortex where the sensory information is interpreted as vision. Most of the retinal cell types have multiple subtypes that perform different functions (reviewed in [26]).

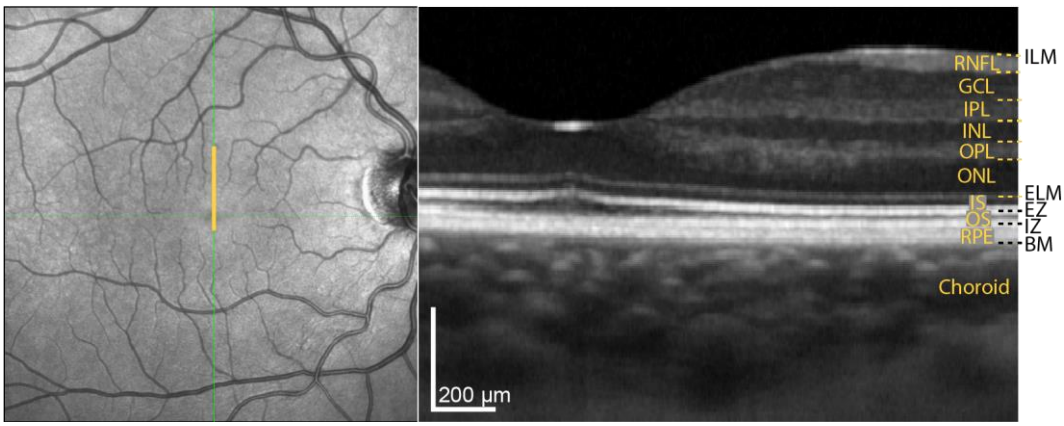

Figure 1. SD-OCT image (right) that shows the different retinal layers. The scan is taken along the yellow line shown in the infra-red fundus image (left). Müller cell end feet and astrocytes form the inner limiting membrane (ILM), while Junctions between photoreceptors and Müller cells form the external limiting membrane (ELM). EZ, ellipsoid zone (also termed IS/OS); IZ, interdigitation zone; BM, Bruch's membrane.

1.2.2 Normal distribution of photoreceptors

Retinal thickness and cellular organization differ based on location in the retina. The retinal photoreceptor arrangement is well described *ex-vivo* by histology [27-29] and *in-vivo* by high-resolution imaging [30-35]. The photoreceptor mosaic is organised in a regular triangular pattern with nearly hexagonal packing, although some cones have fewer or more than six neighbour cones. In reality, on average 50–60% of the cones have six neighbours [36]. There are considerably more rods than cones across the retina with a total ratio of rods to cones of approximately 20:1, but this ratio varies substantially with retinal eccentricity [29]. In a normal retina, the foveal center, out to a region approximately 200–400 µm in diameter, is rod-free [29, 37]. The fovea contains the highest density of cone photoreceptors with thick outer retinal layers. However, the density decreases quickly as a function of distance from the foveal center. In the foveal center, cone inner segment diameters are 1-3 µm but increase in diameter towards the more peripheral regions [29, 38]. The gaps between the cones are filled with an increasing number of rods which dominates the more peripheral regions and peaks at around 15–20 degrees from the center of the fovea [29, 35].

In addition to different rod and cone distributions, the number and distribution of the three cone subtypes varies. S cones are absent from the foveal center and are randomly but more sparsely distributed than the L and M cones [27, 39, 40]. The L and M cones are found to be randomly arranged, but the same classes of cones occasionally tend to clump together [39-41]. There is a large variation in relative densities of L and M cones, with L:M cone ratios being recorded as high as 16.5:1 and as low as 1.1:1 in males with normal colour vision [40-42].

The cone density varies substantially between normal individuals, particularly in the foveal center where peak cone density has a wide normal range of less than 100 000 up to about 250 000 cones/mm^2 (imaged *in-vivo*) [43-45]. The inner retinal layers are thickest in a concentric zone around the foveal center. This zone contains the cells that receive input from the foveal cones and has the highest density of ganglion cells. Ganglion cell density decreases rapidly with eccentricity [25].

Variation and changes in the composition of nerve cells in the retina such as cone density, mosaic regularity, L:M cone ratio, or how the cells connect to each other can alter the visual information that travels to the brain. All these factors can influence detail and colour perception [e.g. 46, 47].

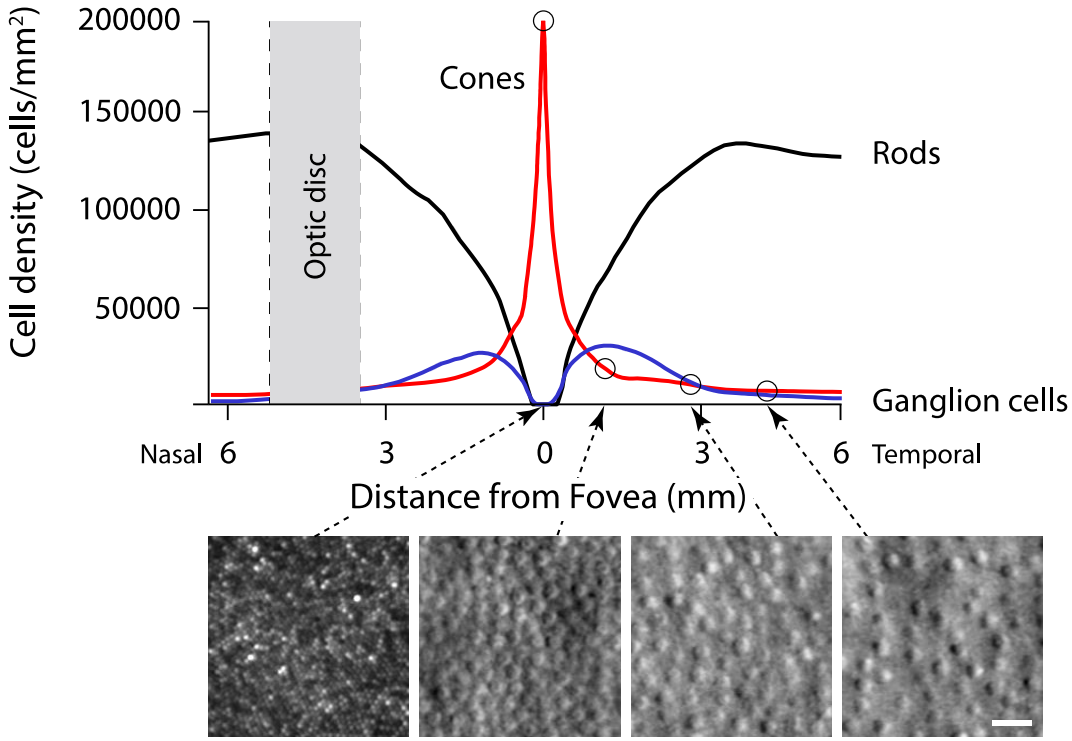

Figure 2. Normal distribution of photoreceptors and retinal ganglion cells. Density of cones, rods and ganglion cells as a function of distance from the foveal center in a normal retina. The plot is based on data from Curcio et al. [29] and Curio & Allen [25]. Images of the cone photoreceptors are taken with the Kongsberg adaptive optics scanning light ophthalmoscope and shows cones from the foveal center in confocal mode and images from approximately 1.4, 2.9 and 4.4 mm retinal eccentricity in split-detector mode. Scale bar = 20 µm.

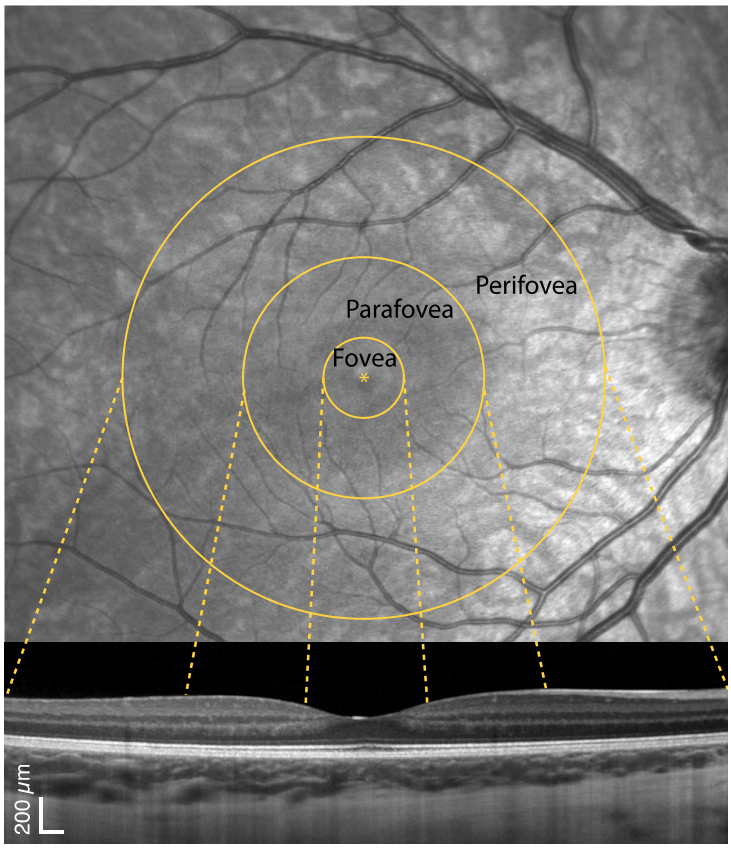

Figure 3. Definition of the macula. The central 6 mm (corresponds to ~ 20 degrees of visual field) of the retina is called the macula and can be divided into three concentric zones: Fovea (central 1 mm), parafovea (0.5–1.5 mm from the foveal center) and perifovea (1.5–3.0 mm from the foveal center). The foveal center is marked with an asterisk.

1.2.3 Retinal development

The retina originates from the neural ectoderm and develops over several years, both before and after birth. Retinal development starts within the eye field of the anterior neural plate forming the optic vesicles. The optic cup is formed from invaginations of each optical vesicle by embryonic day 32. The retinal pigment epithelium (RPE) develops from the outer posterior layer of the optic cup, and the neural retina from the inner posterior layer (reviewed in [48]). Proliferation and differentiation of the inner layer of the optic cup begins around fetal week 7–8 developing into the different neural retinal layers. All the retinal cells, including Müller glial cells, are generated at different times from multipotent retinal progenitor cells (RPCs). That is, RPCs have the ability to give

rise to more than one type of cell and become any of the seven major cell types of the retina. The ganglion cells, cones, horizontal cells and amacrine cells are born in an early phase and overlaps with a late phase with birth of the rods followed by Müller glial cells and bipolar cells [49-51]. Expression of cone opsins takes place in S cones before M and L cones [52].

Development of the retina follows a central-to-peripheral gradient where the retinal cells are generated in the incipient fovea first and continues sequentially more peripherally [53]. Although cone migration mechanisms are not very well-known, it is shown that the cells migrate in all three planes during retinal development and maturation. In early development post mitotic cells migrate from the scleral surface towards the surface of the vitreous (z-axis) to their respective cellular locations [54]. This results in the characteristic laminar structure formed by the different retinal layers [14]. Later, the cells migrate (x and y-axis) to form the fovea [55].

The inner and outer retina develop differently. The inner plexiform layer and ganglion cell layer form first and reaches the peripheral areas around mid-gestation, while the outer plexiform layer develops slower and is not complete before 30 fetal weeks [53]. All retinal layers are present from the central to peripheral retina before birth but are immature. Particularly, foveal photoreceptors are far from mature, continues to develop after birth and are the last to complete development (reviewed in [56]). This development process is regulated by a network of genetic factors, including *PAX6* (described in section 1.4.4), that is important to produce each class of cell in the right order and number, place them correctly through migration and for formation of neural circuits [57]. Abnormal regulation or mutations in one or several of the early retinal developmental genes can lead to inherited retinal diseases (reviewed in [58]).

1.2.4 Foveal development

The fovea is a specialized region of the retina that dominates the visual perception including colour vision and high spatial acuity. The fovea is characterized by a pit where the inner retinal layers are translocated outwards. Blood vessels are absent from the

foveal center, forming an avascular zone. The high visual resolution is enabled by the high cone photoreceptor density, elongated waveguides and that the foveal cones sends information through a non-convergent pathway, where at least two midget ganglion cells receives input from only one cone via one cone bipolar cell. In contrast, in the periphery many cones are connected to each ganglion cell [59]. Information from the fovea and its retinal circuitry employs a large part of the visual cortex and plays a crucial role in normal cortical development, regulating calcarine fissure volume and symmetry [60]. Hence, adequate stimulation of the visual system is important for normal development.

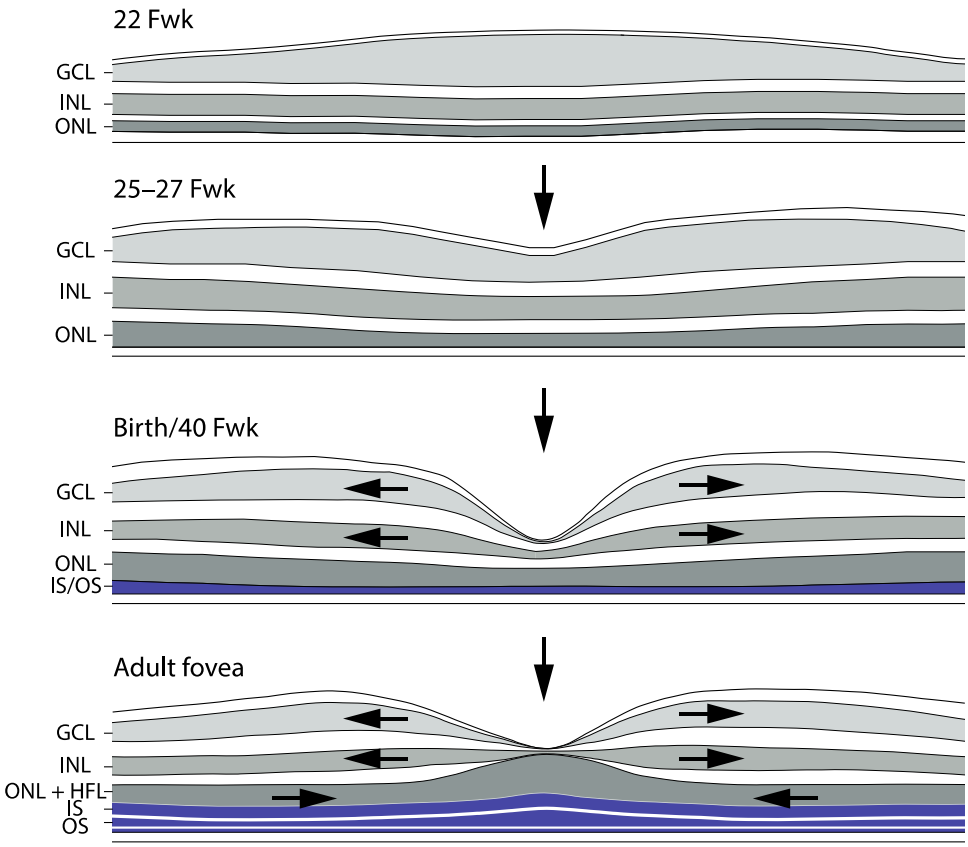

Figure 4. Schematic illustration of foveal development. There is an initial thickening of the ganglion cell layer (GCL) before the foveal pit gradually forms after formation of a foveal avascular zone. Cells from the GCL and inner nuclear layer (INL) migrate away from the foveal center, and cone photoreceptors migrate towards the foveal center. At birth, the foveal cone inner and outer segments are short and immature (coloured blue) and cone packing and elongation continues through adolescence [55].

Foveal development is a complex process with a combination of biochemical and mechanical factors involved [56]. Photoreceptor differentiation begins very early in the fovea and is complete earlier than in other regions for all the retinal cell types [61]. The fovea can be identified morphologically as early as around fetal week (Fwk) 11-12 by the presence of cones and initial thickening of the central retina. The pit, however, does not begin to form until the foveal avascular zone (FAZ) is defined after mid-gestation and gradually forms with migration of inner retinal layers away from the center (reviewed in [56]). The pit shape changes from narrow and deep to wide and shallow after birth, presumably as a consequence of stretching of the retina as the eye grows [62].

At birth, foveal outer segments are extremely short and cone density is only around 25,000 cones/mm^2 [63, 64]. Cone packing to raise foveal cone density mainly occur after birth [65]. During childhood, the cones migrate towards the foveal pit, individual cones become thinner and the outer segments elongates, referred to as cone specialization. The cone axons elongate as a result of displacement of the inner retinal neurons and centripetal cone migration, forming the Henle's fiber layer together with Müller cell processes. This indicates that the foveal outer retina forms synapses with the inner retinal neurons before the onset of pit formation and cone packing, as also found by histology [66]. An exact timeframe for final maturation is not clearly defined. Recently, studies of postnatal development using OCT indicates that foveal maturation continues until at least 12–16 years of age [67, 68]. It is, however, a significant amount of variation between individuals [67]. In the developing retina, there is a correlation between thickness of the outer retinal layers and visual acuity [67]. Also, normal colour vision develops over several years after birth. The best chromatic detection sensitivity is reached at around 20 years of age [69].

1.2.5 Foveal hypoplasia

Disruption of the foveal development process leads to foveal hypoplasia, characterized by lack of a foveal avascular zone and incursion of inner retinal layers. Clinically, foveal hypoplasia can be graded based on whether a foveal pit, outer nuclear layer widening, and outer segment lengthening are present or not. This is thought to reflect the major

development steps in foveal formation: centrifugal displacement of inner retinal layers, centripetal migration of cones, and cone specialization [70]. This grading system is applied and described in more detail in paper I.

Foveal hypoplasia can have large functional consequences since the normal human fovea underlies a large part of our visual function, including the ability to distinguish details and colours [71]. Increasing grades of foveal hypoplasia have been linked to increasingly poor visual acuity [70]. To the best of the authors knowledge, no previous studies have investigated the association between degree of foveal hypoplasia and colour sensitivity.

Many inherited retinal diseases, e.g. albinism and achromatopsia, are associated with foveal hypoplasia, decreased cone density and mosaic regularity and/or disruption of the photoreceptor structure and function [e.g. 46, 72]. Studies of albinism have shown that cone specialization can occur in the absence of a foveal pit [73, 74] and that the reduced foveal cone density is correlated with outer segment length [75].

1.3 Aniridia phenotype

Aniridia was first described in the early 1800s [76]. The name aniridia describe the most noticeable characteristic feature, that is complete or partial absence of the iris. Consequently, the eye is not able to adjust to differing levels of light. The classical ocular phenotype in congenital aniridia is, however, a combination of congenital under- or abnormal development of several eye structures including the iris, cornea, anterior chamber angle, lens and retina. Clinically, the most common findings in childhood, besides varying degrees of iris hypoplasia, are thickened corneas, foveal hypoplasia, nystagmus, significant visual impairment and photophobia [7, 9, 77]. A smaller proportion of cases also have optic nerve hypoplasia [78]. Ocular complications, like early onset cataract, glaucoma, aniridia-associated keratopathy (AAK, progressive opacification of the cornea) and dry eye disease [79-82], often develop progressively during lifetime [83] and may cause increasing visual impairment.

Foveal hypoplasia is one of the most common features associated with congenital aniridia [9] and may be one of the crucial limitations for visual outcome. Foveal hypoplasia in congenital aniridia was confirmed by histology in the early 1900s [84]. More than a century later, OCT was shown to be a useful tool in confirming foveal hypoplasia and quantify macular thickness in persons with aniridia [10, 11]. The central macula in children with aniridia was reported to be significantly thicker compared with that in healthy children and described as a flattened retinal profile [11] or a dome-shaped macular profile [12]. Thickening of the outer nuclear layer normally seen at the fovea could not be identified [12]. Clinically, foveal hypoplasia is most often described as present or not based on absence or presence of the macula reflex evaluated using ophthalmoscopy. Recently, qualitative OCT-based grading [70] have demonstrated variable degrees of foveal hypoplasia across persons who have aniridia [85, 86], implying that visual potential differs markedly between individuals. Detailed descriptive quantitative data on foveal, parafoveal and perifoveal architecture in aniridia is, however, limited.

Abnormal development of the foveal region has been associated with reduced length of the calcarine fissure, where the primary visual cortex is located, assessed with MRI in aniridia [60]. Both cone and rod function has been reported to be affected in congenital aniridia as measured with electroretinogram (ERG), but with dysfunction ranging from nearly normal to severely abnormal [87-89]. There are a limited number of previous studies of colour vision in aniridia, however, in a report from 1981, Weber and Petersen described reduced colour vision in a family with congenital aniridia [90].

A wide variety of phenotypes and severity have been described in aniridia [e.g. 9, 91]. This large between-individual variation in phenotypes also occurs within families [85]. The reason for variable expressivity among persons with the same or different genetic mutations is unclear.

1.4 Genetics of congenital aniridia

In approximately one-third of persons who have aniridia the condition has occurred sporadically, whereas two-thirds have a family history of aniridia [9]. The majority of genetic mutations leading to aniridia are inherited dominantly and often results in multiple persons with aniridia across familial generations. These mutations occur within the *paired box gene 6* (*PAX6;* OMIM 607108) and result in loss of function of one copy (haploinsufficiency) of the gene (recently reviewed in [8, 92]). Disease-causing mutations can also occur in neighbouring regions of DNA that normally regulate the expression of the *PAX6* gene [93-95]. In a few cases, other genes such as *FOXC1* and *PITX2* have been implicated in aniridia-like phenotypes [96].

Aniridia can also occur as part of a syndrome, such as WAGR syndrome where the adjacent *WT1* locus is involved in addition to *PAX6,* and may cause Wilms' tumour, aniridia, genitourinary abnormalities and mental retardation [97]. Another rare form of aniridia is observed in Gillespie's syndrome which is characterized by iris hypoplasia along with cerebellar ataxia and intellectual disability [96, 98]. Only non-syndromic aniridia is discussed further in this thesis.

1.4.1 The *PAX6* gene

The *Pax6* gene is highly conserved in a variety of species. Based on the genotypic and phenotypic similarities, the Small eye (*Sey*) mouse [99] and Drosophila eyeless (*ey*) [100] have served as major model systems for human aniridia. In humans, *PAX6* was identified as the gene causing aniridia by positional cloning [101] and the genomic exon/intron structure was mapped by isolating cDNA clones [102].

PAX6 is a transcription factor and plays important roles in development of the central nervous system, olfactory system, spinal cord and pancreas, in addition to its essential role in normal eye development. It is considered the master regulator or selector gene of eye development [103], which means that it acts as a "molecular switch" by interacting with other transcription factors in the gene regulatory network to direct cell type specification, differentiation, proliferation and migration [104]. In other words, the

PAX6 gene provides instructions for making PAX6 protein that regulate activity and controls the expression of other genes that are involved in normal ocular and neural development (reviewed in [105]). However, *PAX6* is also regulated through interactions with other transcription factors and multiple enhancers to carry out and fulfil its role [103].

Correct PAX6 dosage is of importance for normal eye development [106]. A single functional copy of the *PAX6* gene does not produce a sufficient level of the PAX6 protein to activate its target genes. Hence, normal eye development requires two functional copies of *PAX6.* The amount of protein within a cell may also alter which target genes would be expressed, which in turn influences development. Too high levels of PAX6 are also known to lead to congenital eye anomalies [106].

The human *PAX6* gene is mapped to the short arm of chromosome 11 (11p13) and is 22 kilobase pairs (kb) long. It contains 14 exons (the first 3 being non-coding), including an alternatively spliced exon 5a, encoding two different major isoforms: a 422 amino acid PAX6 protein (canonical PAX6) and an 436 amino acid PAX6 (5a) protein, that exhibits different DNA-binding properties [101, 102]. The canonical PAX6 contains two DNA-binding domains, the paired domain (PD) and the homeodomain (HD), separated by a linker region (LNK), as well as a proline serine–threonine-rich C-terminal transactivation domain (PST) which regulates the transcription of target genes. The PD comprises an N-terminal sub-domain (NTS or PAI domain) and a C-terminal sub-domain (CTS or RED domain) [102].

A third isoform, in which the PD is lost (Pax6ΔPD), has been described [107] and shown to have a distinct function in mammalian ocular development [108, 109]. Another alternative PAX6 transcript initiation site has been identified in intron 7 [110]. In humans, *PAX6* uses at least three promoters (P0, P1 and Pα) for production of the different PAX6 isoforms, though the regulation and different downstream target genes of each isoform in the eye are not fully understood.

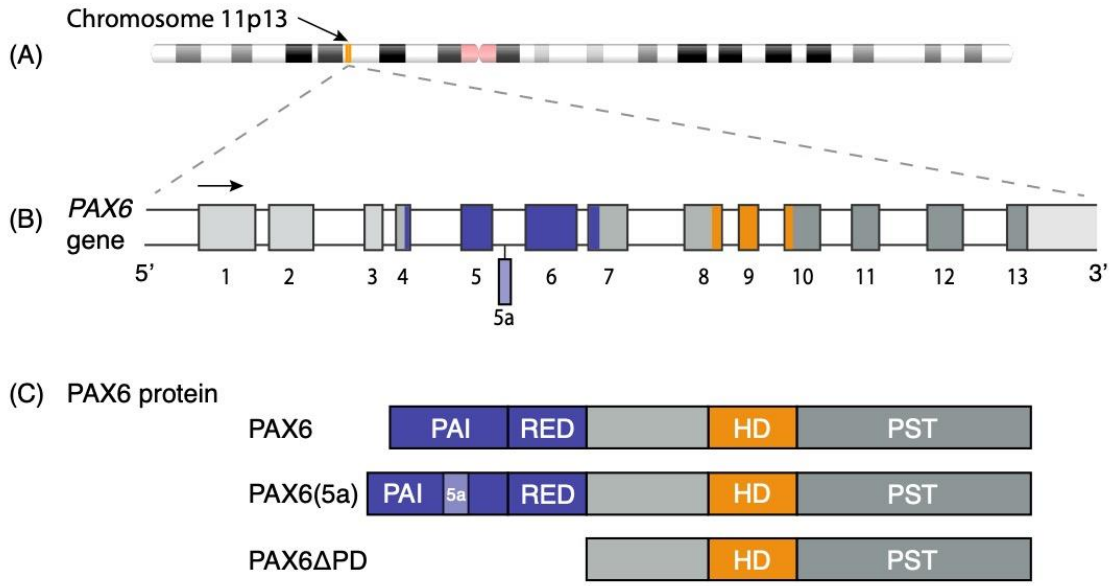

Figure 5. Schematic presentation of chromosome 11p13 (A), the PAX6 gene (B) and the PAX6, PAX6(5a*), and* PAX6ΔPD *proteins (C). PAX6 is one of several genes located at chromosome 11p13 (marked in orange in A). The PAX6 exons are represented by coloured boxes indicating the different protein domains (light grey: 5'UTR, blue: PD, grey: linker region, orange: HD and dark grey: PST domain). PAI and RED are sub-domains of the paired domain. PD: paired domain, HD: homeodomain, PST: proline-serine-threonine rich domain.*

Cis-regulatory elements have been identified both within introns of the gene, upstream and downstream of *PAX6* [93, 94, 109, 111, 112]. An important downstream regulatory region is located within introns of the *ELP4* gene adjacent of *PAX6*. This region contains a number of regulatory elements including the so-called SIMO enhancer, involved in the self-amplifying loop of *PAX6* [93], and a retina-specific enhancer [111], among others. Deletions in this region were described previously in persons with aniridia who have no intragenic mutations in the *PAX6* coding region [93-95], suggesting that these 3' regulatory elements are required for *PAX6* transcription. Although the role of all elements is not known, important tissue-specific regulators are located in this region [109].

1.4.2 The spectrum of *PAX6* mutations

More than 490 unique *PAX6* mutation variants were reported in the "*PAX6* Mutation Database" (http://lsdb.hgu.mrc.ac.uk/home.php?select_db=PAX6) until its last update in 2018. The most common mutations found in *PAX6* includes nonsense, frameshift and splice-site variants that introduce premature termination codons (PTCs), which results in the loss of one functional copy of *PAX6* (haploinsufficiency). These account for approximately 70 % of all reported *PAX6* mutations [8, 92, 113]. It is hypothesized that the mRNAs containing PTCs located before 50 base pairs upstream of the last exon-exon junction are detected and degraded by the nonsense-mediated decay (NMD) pathway to prevent the accumulation of truncated proteins in the cell [113, 114]. Most mutations in the PST region result from frameshift or point mutations that change the stop codon to cause run-on translation [113]. These are predicted to create a longer transcript, C-terminal extensions (CTE), which escape the NMD and may result in dominant negative effects. However, the underlying mechanisms of how CTE mutations cause loss of function remains to be investigated [92].

Mutations in non-coding regions of *PAX6,* have also been reported in aniridia. Deletions or point mutations in 5' untranslated region (UTR) are likely to affect normal splicing resulting in skipping of one or several exons and presumably formation of PTCs [95, 115]. Although, the exact effect on the mRNA are not known. An increasing number of reports have demonstrated that changes in *PAX6* regulatory regions at the 3' end of the transcribed gene, leaving the *PAX6* exons intact, can cause aniridia [93-96, 116-118]. Large deletions involving the whole or a part of the *PAX6* gene, including or not including regulatory regions, also account for a considerable proportion of aniridia cases [119, 120].

1.4.3 Genotype-phenotype correlations

Genotype-phenotype correlations refer to the relationship between specific gene mutations (genotype) and the resulting expression of the disease (phenotype). To date, no accurate genotype-phenotype correlations in aniridia have been established. PTC

mutations generally present a classical aniridia phenotype, including foveal hypoplasia [9], but the type or location of the different mutations does not seem to influence the expressed phenotype. It is assumed that this is because the truncated proteins are subject to NMD [113], resulting in *PAX6* haploinsufficiency. CTE variants have been associated with moderate and severe aniridic phenotypes, similar to PTC-causing mutations [9, 121, 122]. Missense mutations, which cause one amino acid to be replaced by another during translation, have been reported in milder phenotypes, atypical and non-aniridia phenotypes, but with quite variable severity [9, 113, 123]. Classical aniridia has been reported as a consequence of changes in 3' regulatory *PAX6* regions [96, 116]. More recently, deletions in this region have also been associated with milder anterior segment phenotypes such as mild, non-progressive keratopathy [83] and varying foveal hypoplasia grades [85]. Phenotypes associated with *FOXC1* and *PITX2* genes are most commonly described as anterior segment dysgenesis rather than classical aniridia [96, 124, 125].

1.4.4 The role of *PAX6* in retinal development

Spatially, temporally and quantitatively correct expression of *PAX6* is important for normal development of the eye [126, 127]. This expression pattern is complex and not well understood. During early human eye development, *PAX6* is expressed on the surface and neural ectoderm. PAX6 is required for the optic vesicle to invaginate to form the optic cup, giving rise to the neural retina and the retinal pigment epithelium [128, 129].

PAX6 is involved in RPE specification and pigmentation through a regulatory interaction with the transcription factor *MITF* [130]. In the neural retina, the *Pax6* gene has at least three, overlapping functions: promote proliferation of retinal progenitor cells, maintain potential of progenitors to generate all retinal cell types (RPC multipotency) [131], and regulate cellular differentiation timing [126, 132].

Pax6 is widely expressed in retinal progenitor cells and is required for activating and regulating the expression of several different transcription factors, including basic-Helix-

Loop-Helix (bHLH) transcription factors, to control the development of individual retinal cell types [105, 131, 133]. *Pax6* is involved in regulation of *Crx* and *Otx*, through a transcriptional network that regulates specification and differentiation of both rod and cone photoreceptors [127]. In addition to its role as an activator, Pax6 has been shown to inhibit the transcription of several genes. For example, inhibition of Crx in the peripheral optic cup prevents premature activation of photoreceptor differentiation which is essential for determination and survival of the photoreceptors [127]. In the differentiated human retina, *PAX6* is expressed in retinal ganglion, amacrine and horizontal cells [128]. Variable continuous expression of *PAX6* is also seen in the inner layers of the adult human retina [134], suggesting a possible role in maintenance of the aging retina.

Multiple downstream target genes are most likely affected by PAX6 during foveal formation. These need to be determined to understand the mechanism of how *PAX6* haploinsufficiency leads to arrested foveal development. As mentioned in the aniridia phenotype section, foveal hypoplasia is the most common retinal deficit associated with aniridia [135]. This suggests that PAX6 plays a critical role in foveal formation. Quantitative measurements of intra-retinal layer thicknesses across a spectrum of *PAX6* mutations have not been reported before in aniridia.

2 Motivation and aim of research

2.1 Motivation

To provide the best possible care for persons with congenital aniridia, clinical management and healthcare should be guided according to experience and evidence that exists from best available research information. As mentioned in the introduction, foveal hypoplasia is a very common finding and is the main cause of congenital vision loss in aniridia. Despite this, scientific research investigating variation in retinal structure and visual function in aniridia remains limited, and little is known about the underlying mechanisms of foveal hypoplasia. This entails difficulties in providing accurate and early diagnosis, prognosis and subsequent provision of personalized early intervention, facilitation and treatment. Hence, the main motivation behind this research project is to gain new and better knowledge about the retina in aniridia, including associations between structure and function, retinal phenotype and genotype, which can contribute to better future eye health care for persons with aniridia.

2.2 Aims and objectives

The aim of this thesis is to increase knowledge about the complexity and variation in retinal structure and development, its association with genotype and how it affects visual function in persons who have congenital aniridia.

The primary objectives for each of the papers were:

I. To quantify the association between the degree of arrested foveal formation and impairment of colour vision in congenital aniridia.
II. To investigate the variation in retinal phenotype in family members possessing the same aniridia genotype.
III. To investigate *PAX6* genotype and phenotype correlations in congenital aniridia, specifically with regards to thickness of the retinal layers within the macula and its association with visual function.

3 Materials and Methods

3.1 Research design, recruitment and study sample

This thesis is a self-contained part of a larger project entitled “Aniridia and vision” that was initiated and planned in close collaboration with Aniridi Norge and Oslo University Hospital. The study had a cross-sectional, observational and comparative design. High-resolution imaging of the retina and quantitative methods were employed to provide a detailed evaluation of retinal phenotypic variability in aniridia. Clinical and psychophysical measures of visual function (visual acuity, colour vision) were considered to be important to increase knowledge about the retinal function and understand the consequences of changes in retinal- and optical structures in aniridia. These methods are non-invasive and have been applied successfully for retinal and functional characterization in other inherited retinal diseases [e.g. 46, 72, 136].

The participants were recruited through Aniridi Norge. Anyone in Norway, aged 10 years or older during the year of data collection, and diagnosed with congenital aniridia, was invited to participate in the study. In addition, one participant from another Nordic country who heard about the study and volunteered to participate, was included. This gave a total study sample of 37. The diagnosis of aniridia was confirmed clinically by the presence of iris hypoplasia or/and foveal hypoplasia at the initial visit. Age-matched healthy controls were recruited through the National Centre for Optics, Vision and Eye Care, University of South-Eastern Norway. Inclusion criteria were no history of systemic or ocular diseases. Refractive errors that could be corrected with glasses or contact lenses were permitted. Additionally, all participants (both participants with aniridia and controls) who were included in paper I had to have normal trichromatic colour vision, confirmed by analysis of the cone opsin genes as a part of the initial data collection. Unaffected family members in one family with aniridia were included as normal controls in paper II. These were recruited through the family members who were already included in the study. A total of 68 normal controls were included in the three studies combined.

Table 1. Overview of the overall study sample and data that were collected in all the participants, and the number of participants and additional data included in paper I-III.

CROSS-SECTIONAL STUDY		
ANIRIDIA GROUP Total sample 37 participants Age: 9 – 72 years	NORMAL CONTROL GROUP Total sample 68 participants Age: 10 – 74 years	DATA: • Genetic analysis • Extensive eye examination • Ocular biometry • Colour fundus photo • Anterior and posterior segment OCT

Paper I	Paper II	Paper III
31 participants with aniridia Age: 9–67 years 52 normal controls Age: 10–74 years Additional data: • Cone opsin genetics • Colour vision tests • Grading of foveal hypoplasia	8 participants with aniridia Age: 24–66 years 33 normal controls Age: 14–69 years Additional data: • High-resolution retinal imaging - OCT - AOSLO • Ocular biometry	37 participants with aniridia Age: 9–72 years 55 normal controls Age: 10–74 years Additional data: • Detailed *PAX6* genotyping • Quantitative analysis of retinal layers

3.1.1 Data collection

The initial data collection for this project was carried out at the National Centre for Optics, Vision and Eye Care, Kongsberg between October 2015 and February 2016 with follow-up measures in June 2016, October 2016, May 2017 and January-February 2018. For most of the participants with aniridia, a large part of the data included in paper I and III was collected as a part of the initial data collection. All the participants underwent an extensive eye examination conducted over 2–3 days. In addition to giving a saliva sample for genetic analysis, clinical and psychophysical testing of visual function, posterior segment imaging, refraction and ocular biometry, the examination included a

comprehensive assessment of the anterior segment [79, 137], among others. Follow-up measures of colour vision, a part of paper I, were collected at Hurdal syn- og mestringssenter, Hurdal in June 2016, 3–6 months after the initial visit. The data included in the second study (paper II), was collected on a separate day, between October 2016 and February 2018. Collection of data from normal healthy controls was carried out at the National Centre for Optics, Vision and Eye Care between March 2016 and February 2019.

3.2 Principles guiding the study process

An essential part of development of this study has been through dialogue with members of Aniridi Norge, and their wish to gain more knowledge about their eyes and vision. Two persons who have aniridia, representing different age groups (young adult and middle-aged) and representatives from the board of Aniridi Norge took part in the planning, discussions and reflections during the project. This gave us an opportunity to seek advice before and during the project on how the data collection could be performed in the best possible way for the participants.

The intended outcome of this thesis is geared towards increasing knowledge to be able to help individuals. Thus, it was essential to involve persons with aniridia and parents of children with aniridia to ensure that the research carried out will culminate into knowledge that is relevant for the person with aniridia. Each person's history was essential to further identify what is important for each of them in their daily life, to build understanding about symptoms and needs. In this way, the studies were conducted with and on behalf of the persons who have aniridia to fill knowledge gaps that may contribute to a more personalized eye healthcare for this patient group.

Person-centred research principles like respecting each person and their individual experiences needs and preferences, guided the research process [138]. These principles were, for example, important when participants were recruited, in communication and collaboration with the participants before, during and after the data collection.

3.3 Ethical considerations

Rare disorders do present particular research challenges. Because of the small population, it may be difficult to recruit participants. On the other hand, individuals who have a rare disease are often highly motivated and willing to participate in research to help science and for the community [139]. It is especially important to be careful when researching small groups with rare diseases, even if common ethical guidelines for confidentiality and de-identifying data are followed [140]. Because they represent a small group, it may be more challenging to preserve their anonymity. In small countries like Norway, many individuals who have aniridia know or know of each other. Hence, it is possible that one can be identified by other persons, at least by other participants or members the patient organization. Specific information about this was therefore given to all the participants.

Each participant, and/or their guardians, were given detailed information about the project and provided his or her informed consent to participate voluntarily in the different parts of the project. Specific consent was obtained from all family members included in paper II, which includes a family pedigree as a supplementary figure. All participants, also the unaffected family members were given the opportunity to look through the pedigree and ask questions prior to giving consent.

It is of importance to be aware of ethical issues related to the inclusion of children in the research project. Children and young people are persons with their own rights and need to be given recognition, respect and a voice in the research. We strived to communicate in a way that they understood, ensuring that the child got appropriate information and a choice about participation, including the right not to participate. None of the examinations were considered harmful to the participants but some could be perceived as unpleasant due to increased light sensitivity in the participant with aniridia. The participants were actively given the opportunity to withdraw from an examination at any time without explanation. This underlined the importance of good dialogue and explanation also during the investigations.

An ethical dilemma in DNA analysis is that it may generate intentional or unintentional predictive gene information of potentially medical significance. However, this study only includes analyses of exons from a connected region, candidate genes, or a subset of candidate genes. Therefore, the gene analyses were not likely to reveal random findings of potential medical significance unrelated to the patient's eye condition. The vast majority of the research participants were already diagnosed with aniridia and were familiar with its heredity before enrolled in the study. One participant whose diagnosis was not previously discovered, was referred to the specialist health services to ensure appropriate follow-up.

The project was approved by the Regional Committee for Medical and Health Research Ethics (Southern Norway Regional Health Authority), 2010/449 REC South-East B, and the research was conducted in compliance with the ethical principles for medical research involving human subjects, embodied in the Declaration of Helsinki [140].

3.4 Genetic analysis

A mutation is defined as a permanent alteration in the sequence of nucleotides [141], however it does not say anything about the functional effect of the variant. In this thesis, the term “mutation” refers to a pathogenic genetic variant, unless otherwise specified. The genetics part of these studies was conducted in the Neitz Lab at University of Washington, Seattle. The participants gave saliva samples (Oragene-DNA, OG-500, DNA Self-Collection Kit, DNA Genotek Inc., Ottawa, ON, Canada) for genetic analysis of both cone opsin genes and for analysis of the aniridia genotype.

To classify colour-normal from colour-deficient observers, the cone opsin genes were analysed for all the participants in paper I. For details, please refer to paper I. To identify the genetic cause of aniridia, DNA was first extracted and amplified by polymerase chain reaction (PCR) using the primers showed in table 2. Direct fluorescent sequencing of the 13 exons of the *PAX6* gene was performed on both DNA strands using the BigDye Terminator v3.1 (Applied BioSystems). Reactions were analysed on an ABI 3500 Genetic

Analyzer. Two other target genes, *FOXC1* and *PITX2,* were amplified and sequenced if no *PAX6* mutations were detected.

In paper III, further analyses of the *PAX6* genomic region were performed to determine copy number variation of *PAX6* and known regulatory regions with the use of multiplex ligation-dependent probe amplification (MPLA). For details, please refer to paper III. The inclusion of MLPA has previously shown to substantially increase the mutation detection rate in aniridia [142].

Table 2. List of PCR primer sequences used to perform amplification and sequencing of PAX6. The sequences are listed 5' to 3'. These primers are described previously by Yokoi et al. [120].

***PAX6* Exon**	**Forward primer**	**Reverse primer**
1	CTCATTTCCCGCTCTGGTTC	AAGAGTGTGGGTGAGGAAGT
2	TTATCTCTCACTCTCCAGCC	AAGCGAGAAGAAAGAAGCGG
3	TCAGAGAGCCCATCGACGTAT	CTGTTTGTGGGTTTTGAGCC
4	TTGGGAGTTCAGGCCTACCT	GAAGTCCCAGAAAGACCAGA
5	CCTCTTCACTCTGCTCTCTT	ATGAAGAGAGGGCGTTGAGA
5a	TGAAAGTATCATCATATTTGTAG	GGGAAGTGGACAGAAAACCA
6	GTGGTTTTCTGTCCACTTCC	AGGAGAGAGCATTGGGCTTA
7	CAGGAGACACTACCATTTGG	ATGCACATATGGAGAGCTGC
8	GGGAATGTTTTGGTGAGGCT	CAAAGGGCCCTGGCTAAATT
9	GTAGTTCTGGCACAATATGG	GTACTCTGTACAAGCACCTC
10	GTAGACACAGTGCTAACCTG	CCCGGAGCAAACAGGTTTAA
11	TTAAACCTGTTTGCTCCGGG	TTATGCAGGCCACCACCAGC
12	GCTGTGTGATGTGTTCCTCA	TGCAGCCTGCAGAAACAGTG
13	CATGTCTGTTTCTCAAAGGGA	GAACAATTAACTTTTGCTGGCC

The SALSA probemix P219-B3 (MRC-Holland, Amsterdam, The Netherlands) contains probes for all the *PAX6* exons (except exon 11), including the sequence upstream of the main *PAX6* transcript. Moreover, it contains probes for genes downstream of *PAX6*, including *ELP4*, as well as probes for genes upstream of *PAX6*, among them *WT1*. MLPA was performed according to the manufacturer's recommendations (MRC-Holland). In short, MLPA is based on PCR amplification of probes that each detect a specific DNA

sequence. The MLPA reactions result in a set of unique PCR amplicons [143]. These were separated based on their length by capillary electrophoresis using the ABI 3500 Genetic Analyzer. The relative peak heights of each individual probe compared with those obtained from the reference samples, reflect the relative copy number of each target sequence. This enables detection of deletions or duplications in the genomic region (Figure 6). Data analysis and normalization were performed using the Coffalyser.Net software (MRC-Holland). Copy number changes detected with MLPA were confirmed by quantitative real-time PCR as described in paper III.

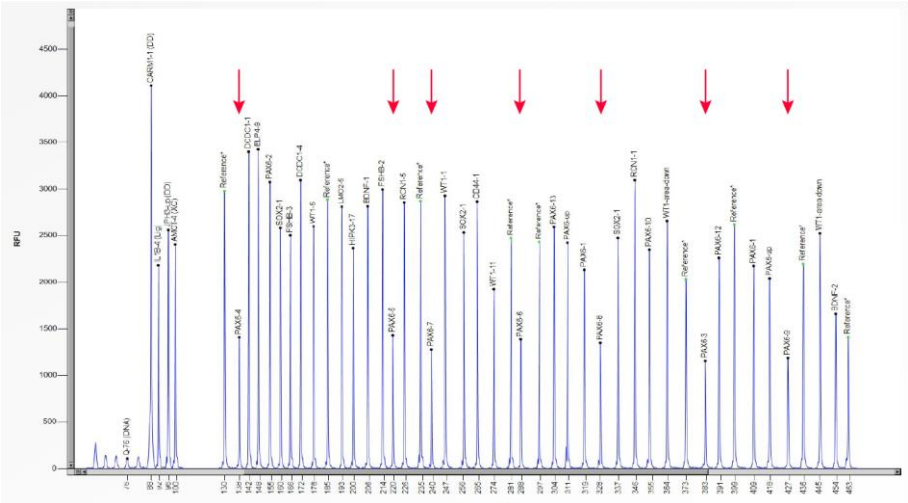

Figure 6. Example of a graph of the capillary electrophoresis of the amplified DNA. Electropherograms are from a participant with deletion of exon 3-9 of the PAX6 gene. The deletion is apparent by a ~50% reduction in RFU (relative fluorescence units) of the PAX6 exon 3-9 probes (red arrows).

3.5 Visual function

3.5.1 High-contrast visual acuity

High-contrast visual acuity was measured with a logMAR chart on an electronic display-screen and scored letter-by-letter, which provides a precise measure of visual acuity [144, 145]. The measurements were basically measured under standard lighting conditions, an even lit room with a general luminance of 130–160 cd/m^2, with no direct glare sources. However, these lighting conditions were not experienced as comfortable

or optimal for all participants with aniridia, due to the large individual differences in iris and ocular media abnormalities. Individual adjustments of the room illumination were therefore allowed to minimize the experience of discomfort and glare, and the impact that may have on visual function. The logMAR chart was displayed with 5 letters per row. This limits the range that can be measured at the standard testing distance at 6 m to maximum 1.0 logMAR. To overcome this, viewing distance was shortened to first 3 m and then 1 m for those with more severe visual impairments, which extended the range to 1.80 logMAR. Very severe impairment beyond this upper limit, was registered as counting fingers (CF), hand movements (HM) or light perception (LP).

3.5.2 Colour vision

Colour vision was assessed with two different pseudoisochromatic plate tests, two computerized colour vision tests and an anomaloscope. The two plate tests were carried out under controlled illumination (True Daylight Illuminator with Easel, colour temperature 6200 K, model number 1339R, Richmond Products, Albuquerque, NM) measured at the surface of the test plates with a digital lux meter (Hagner Model EC1, Hagner AB, Solna, Sweden), and averaged about 800 lux. The Colour Assessment and Diagnosis Test (CAD) test was modified to compensate for low vision, while the Cambridge Colour Test (CCT) and the anomaloscope were tested following standard conditions and procedures. For a detailed description of the specific colour vision tests, please refer to paper I.

3.6 Retinal imaging and analysis

3.6.1 Colour fundus photography

A 45-degrees colour fundus photography (Topcon TRC-NW6S nonmydriatic fundus camera; Topcon Corp., Tokyo, Japan) were taken of all the participants at the initial examination. Additionally, the same camera was used to image the red reflex, lens and iris, by adjusting the camera focus. These images were useful as a supplement to the

slit-lamp examination and anterior segment OCT when evaluating the degree of iris hypoplasia and ocular media opacities (See e.g. Figure 2 in paper II).

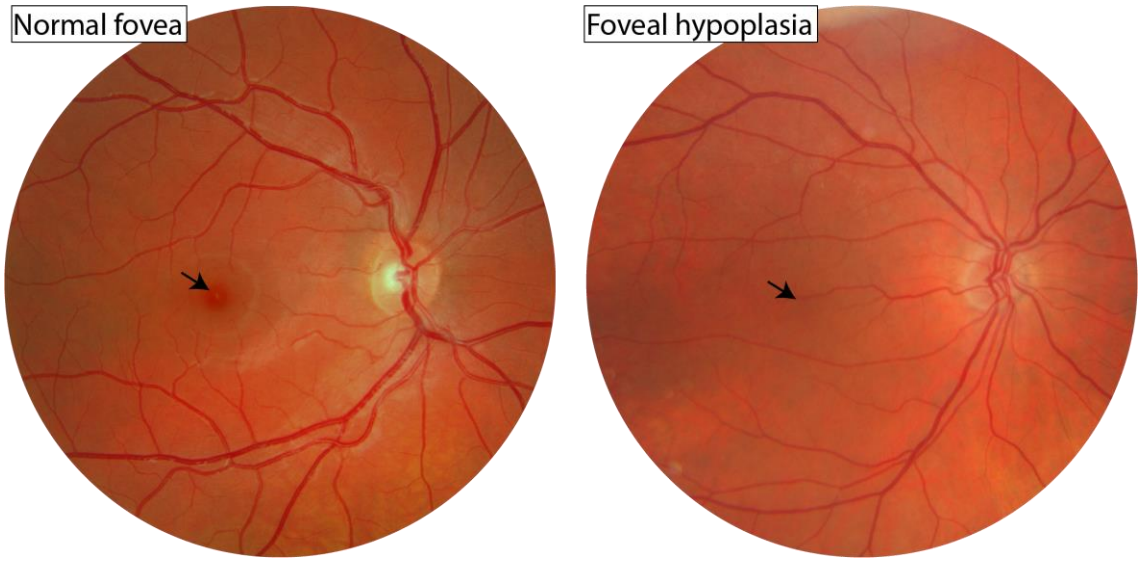

Figure 7. Colour fundus photographs (45-degree field of view) showing a retina with a normal fovea (left) and a retina with foveal hypoplasia (right). The retinal vessels transverse the expected foveal area (arrows) in the retina with foveal hypoplasia.

3.6.2 Optical coherence tomography

Optical coherence tomography (OCT) enables *in vivo* examination of retinal layers. Different retinal layers have different reflectivity profiles and depth which makes them possible to detect and differentiate by measuring the back-reflected light. The reflected light from various depths in the retina is referred to as an A-scan. Multiple adjacent A-scans build cross-sectional images, or B-scans of the retina.

The Heidelberg Spectralis SD-OCT2 Module (Heidelberg Engineering GmbH, Heidelberg, Germany) was used to obtain images of the retinal layers for the papers included in this thesis. The scan protocol is described in more detail in the respective papers. Two different methods were used for segmentation of the retinal layers. Longitudinal reflectivity profiles (LRP; plots of OCT reflectivity), averaged over 5 adjacent pixels (~28.3 µm), were generated to delineate the outer retinal layers and assist in defining the

expected foveal center as described in paper I. The subsequent qualitative grading of foveal hypoplasia is based on the unique developmental steps that occurs during foveal formation [65, 146]. In short, the fovea is graded from 1–4 based on the presence or absence of three structural landmarks [70]. This grading scheme is described in more detail in paper I.

To segment the intra-retinal layers across the macula, an active contour-based method [147, 148], implemented in custom software, was applied for analysing the OCT images in paper II and III. The active contour was first used to segment the inner limiting membrane. Successive layers were then segmented using the contour of the previous layer as a seed. Definitions of the segmented layers are described in the respective papers. To obtain precise segmentations, manual adjustment of the relative weightings of the contour's internal and external forces and/or the position of contour nodes was possible, if needed. The internal forces specify the tension or smoothness of the contour while external forces push the contour towards image features such as peaks or edges (Figure 8).

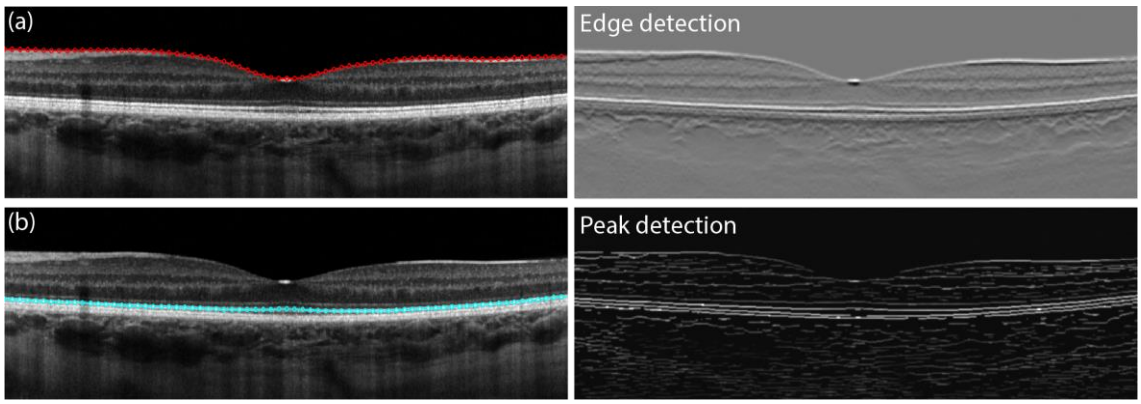

Figure 8. Segmentation of retinal layers using active contours. The retinal layer boundaries are defined by transition from light-to-dark or dark-to-light or as peaks in brightness for the different layers. The segmentation line nodes are attracted towards edges (a) or peaks (b), according to the brightness characteristics of the to-be-extracted layer.

3.6.3 Adaptive optics scanning light ophthalmoscopy (AOSLO)

Single-cell imaging of the living human retina is made possible through adaptive optics (AO) ophthalmoscopy, which is designed to measure and correct for optical imperfections in the eye. Light from the retina is detected by a wavefront sensor to measure the ocular monochromatic aberrations and a deformable mirror to correct for the aberrations [149, 150]. This allows numerous structural features down to ~2 µm in size to be resolved, such as individual foveal photoreceptor cells and the organization of the photoreceptor mosaic.

In paper II, Kongsberg AOSLO was used to obtain high-resolution images of the photoreceptor mosaic. The Kongsberg AOSLO was constructed in collaboration with Boston Micromachines Corporation (Cambridge, MA), and has the same design as that described by Dubra and Sulai [151] and Scoles, Sulai et al. [38]. The instrument uses an 850 nm light source for wavefront sensing and a broadband 790 nm light source for imaging (SLD; Superlum, Carrigtwohill, Co., Cork, Ireland), that is scanned across the retina as a single-point beam. Incident powers for these light sources were measured at the cornea prior to each imaging session, and all exposures were kept more than 6 times below the maximum permissible exposure [152, 153].

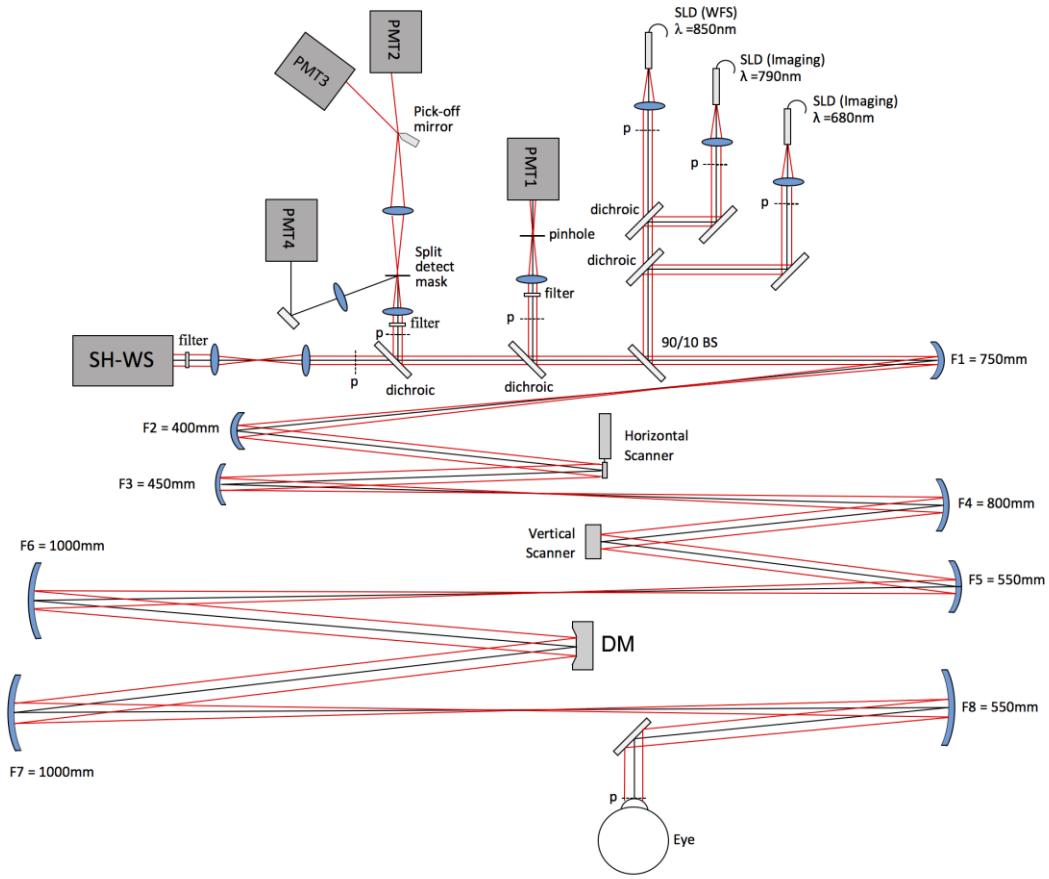

Figure 9. Schematic diagram of the Kongsberg AOSLO. The beam from the SLD's are coaxially aligned and are projected into the eye via horizontal and vertical scanning mirrors and spherical mirrors (F1-8). Infrared light is reflected back through the optical system and a Shack-Hartmann wavefront sensor (SH-WS) sample the light and measures the wavefront aberrations which is then compensated for by the deformable mirror (DM). The wavefront is continuously corrected in a closed loop. The light scattered from the retina is captured by photomultiplier modules (PMTs).

The instrument is a split detection system that allows simultaneously imaging of both photoreceptor outer and inner segments, as well as RPE cells (Figure 10). The reflectance confocal AOSLO modality relies on waveguided light that has passed through both the outer and inner segment of the photoreceptor, while the split-detector modality allows visualization of the photoreceptor inner segment and is independent of the waveguiding properties of the cell [38].

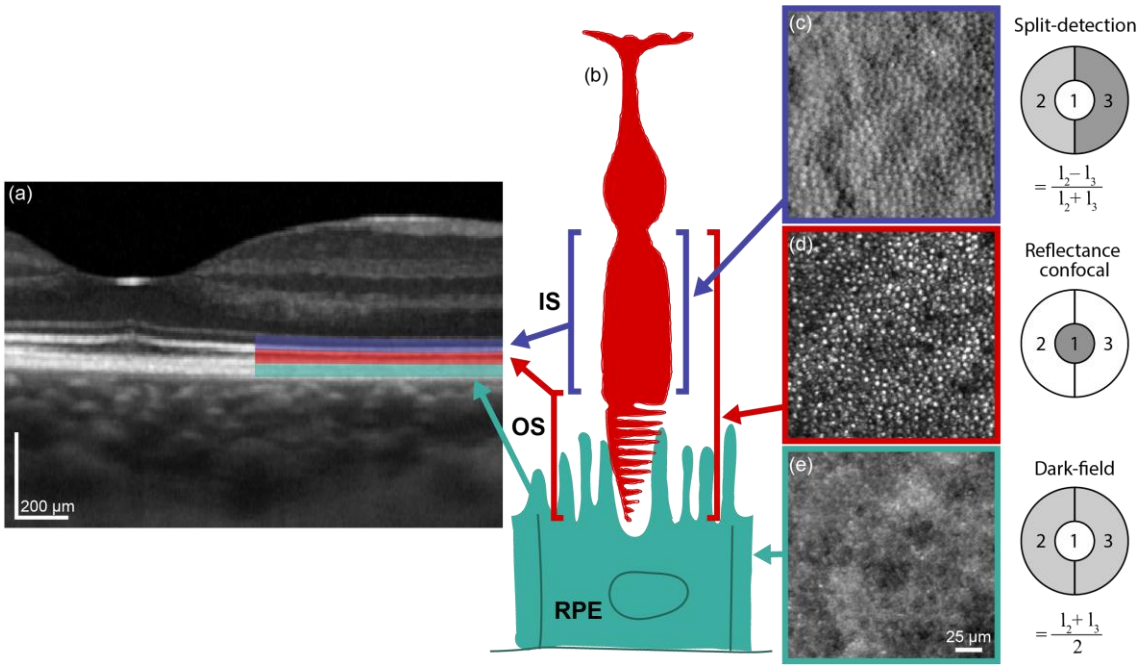

Figure 10. Illustration of the AOSLO image modalities. (a) OCT image showing the photoreceptor inner (blue) and outer segment (red) layers and the retinal pigment epithelium (turquoise) in a healthy retina. (b) A drawing of a cone photoreceptor with its inner and outer segment which is the origin of the light. The right columns show AOSLO images of cone inner segments (c), reflective cones (d) and RPE cells (e) and the detector views showing the annular reflective mirror that reflects the confocal light to a light detector while the multiple scattered light is transmitted and then split between two different detectors [38, 154]. This figure is a modified version of figure 1 in [47].

The imaging protocol is described in detail in paper II. In short, confocal and non-confocal image sequences were acquired across the macula in the participants with aniridia and the normal controls. At the end of each imaging session we imaged a Ronchi ruling with known spacing, positioned at the focal plane of a lens with a 19-mm focal length. This calibration step was necessary for converting field of view in degrees to image pixels, and to estimate how the image warping, resulting from the sinusoidal motion of the horizontal scanner, affected the spacing of the grid. To correct for these distortions, a desinusoiding algorithm was applied to each image sequence [151, 155]. Then, a reference frame from each image sequence was selected manually before the image frames were divided into strips and registered to the reference frame using image

registration software [156]. The 20–50 frames with the highest normalized cross correlation were registered and averaged to improve signal-to-noise ratio [156].

We used ocular biometry measurements (IOL Master 700) and the Liou and Brennan eye model [157] to approximate individual retinal magnification factors (in µm/degree), calculated with optical design software (Zemax EE, Radiant Zemax, Redmond, WA), and the registered AOSLO images were scaled accordingly. To estimate cone photoreceptor density and mosaic organization, individual cones were identified in the confocal AOSLO images via a semi-automatic algorithm, which located cone centers based on identification of local intensity maxima, implemented in custom software. This algorithm is previously described by Li and Roorda [158] and validated by Garrioch et al. [159]. Figure 11 shows an illustration of the metrics used for analysis of the photoreceptor mosaic.

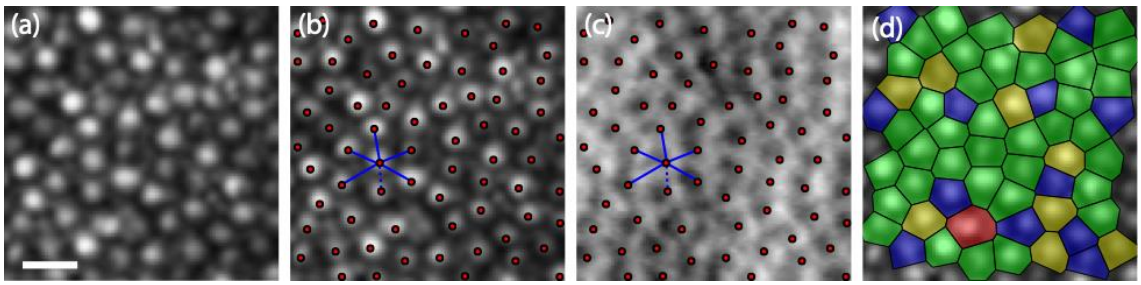

Figure 11. Analysis of the cone photoreceptors mosaic. Cones were identified in the confocal (a and b) and non-confocal (c) images (red dots). Voronoi analysis was applied to measure nearest neighbour distance (dashed line) and the mean inter-cell distance (average of all lines). The Voronoi diagrams (d) give an estimate of the packing regularity, the colours illustrate how many neighbours each cell has. Blue = 5; Green = 6; Yellow = 7; Red = 8. Scale bar = 10 µm.

4 Results

4.1 Main results Paper I

Paper I combined measurements from computerized colour vision tests and retinal imaging (OCT and colour fundus photo) to examine colour vision and the degree of arrested foveal formation in congenital aniridia compared with normal controls. The paper shows that there is no association between age and colour discrimination threshold in children, adolescences and adults with congenital aniridia. Individuals with aniridia have a quantifiable loss of red-green colour discrimination which correlates with their degree of foveal hypoplasia, based on grading of OCT images. This suggests that arrested retinal development and maturation is likely to be the primary reason for decreased red-green colour vision in aniridia. Some have, in addition, a quantifiable loss of blue-yellow colour discrimination, but this was typically associated with secondary pathology, such as glaucoma.

4.2 Main results Paper II

The paper describes for the first time, with the use of adaptive optics *in-vivo* cell-resolved retinal imaging, that individuals with congenital aniridia have significantly lower than normal cone density and mosaic regularity within the macular area (within the central 20 degrees). The foveal cone density varied between 19 899 and 55 128 cones/mm^2, which is more than three standard deviations below the foveal cone density measured in the normal controls. Varying relationships between foveal cone density and visual acuity suggests that visual function in aniridia also may be affected by other factors such as altered development and maturation of post-receptoral neurons and associated pathways.

Furthermore, the results show a large between-individual variation in how the fovea has developed in family members with aniridia caused by the same *PAX6* gene mutation. DNA sequencing revealed a splice site mutation in the 5'UTR of the *PAX6* gene, IV2-2delA (c.-128-2delA), in all the affected family members. The mutation was not found in

unaffected family members, confirming that this variant is likely to be the disease-causing mutation.

There was also a great interfamilial variation in iris hypoplasia which had a poor association, if any, with foveal hypoplasia. This underscores the importance of a thorough iris and retinal examination, even in apparently unaffected members of families with aniridia.

4.3 Main results Paper III

Paper III quantified the structural variability and thickness of the retinal layers in congenital aniridia and explored the relationship between genotype and retinal phenotype. The paper describes in detail how different *PAX6* related mutations are associated with varying degrees of arrested foveal development and significant alterations of retinal cell layer morphology, not only in the foveal center, but the whole macula.

Abnormal foveal architecture was observed in all participants, from whom it was possible to acquire SD-OCT images of, who had a mutation within the *PAX6* gene. The participants with aniridia had greater central retinal thickness and significantly thinner outer retinal layers than unaffected individuals, although with large variability between individuals. The outer retinal layers were thicker in the foveal center relative to the perifovea in a subset of those with aniridia, indicating that postnatal foveal maturation takes place in some of the *PAX6* mutations. The parafoveal and perifoveal retinal thickness was significantly decreased in aniridia from a reduction of both inner and outer retinal layer thicknesses. Together, these findings confirm abnormal foveal formation. Furthermore, it reflects that other aspects of retinal development also are affected, including the generation of the individual cell types within the retina resulting in thinning of the retinal layers also outside the foveal center.

The paper also shows that location of the mutation may influence retinal phenotype. Mutations outside the *PAX6* gene (3’ regulatory regions *ELP4-DCDC1*) were associated with the mildest retinal phenotypes. Further, participants with mutations before the

translational start codon (*PAX6* 5'UTR, non-coding regions) had better developed retinas than those with mutations within coding regions of the *PAX6* gene. The phenotype of those with large *PAX6* deletions was dependent on if the retina enhancer in the downstream regulatory region was intact or not, with milder phenotypes observed when the retina enhancer was deleted.

5 Discussion

The results from the three papers in this thesis revealed great between-individual variation in the underdevelopment of the retina in persons with aniridia. This was characterized by varying grades of foveal hypoplasia (paper I), reduced cone photoreceptor density and mosaic regularity (paper II) and decreased thicknesses of the outer retinal layers within the macular area (paper III), compared with normal healthy controls. High-contrast visual acuity and colour discrimination threshold varied greatly between the participants and was largely associated with the variation in foveal morphology and cone specialization. Great variability was also evident between and within different genotypes. However, detailed genotyping and analysis of the retinal layers showed that the location and extent of the mutation may account for some of the observed variation in retinal phenotype.

Generally, larger genotype-phenotype studies in aniridia aim at describing the whole eye giving a general assessment of the different eye structures [e.g. 9, 160, 161]. This limits the ability to capture large individual variations and detailed characterization of the different affected eye structures. The main focus here has been to contribute with more in-depth knowledge about the retina in aniridia and how variations in foveal morphology affect visual function. The results also contribute to increased knowledge about how loss of one functional copy of the *PAX6* gene affects development of the fovea and alter the cone photoreceptor distribution across the macula in human retinas.

In the following sections, the overall findings of the thesis are discussed with focus on theoretical and clinical implications, methodological considerations and limitations as well as future perspectives.

5.1 Individual differences in retinal structure

An underdeveloped iris is considered a hallmark of aniridia. It is, however, clear from the papers in this thesis that the anterior and posterior segments are affected differently. Thus, the appearance of the iris alone cannot provide information about foveal morphology in aniridia.

Foveal hypoplasia was seen in the majority of the participants with aniridia in whom OCT was possible (92.3%) and underlines that abnormal foveal development is a typical feature in congenital aniridia. The great between-individual variation in phenotype and severity previously described in aniridia is also evident in the retina. Foveal hypoplasia is thus not an “all-or-nothing phenomena”. This variation in foveal hypoplasia grade is consistent with what has been described recently [85, 86]. However, quantitative measurements of the retinal layers and the photoreceptor mosaic revealed large variation also within each grade of foveal hypoplasia, which is vital to be aware of when classifying the fovea in persons with aniridia. Thus, the extent of thickness increase of the central outer retinal layers should be specified in addition to whether a feature is present or not.

It is clear from the slight increase in central foveal cone density relative to the perifovea shown in paper II, that cone packing occurs to some degree in the absence of the foveal pit, supporting previous observations in albinism [46, 74]. For those with the fewest central cones (paper II), the amount of increased foveal cone density matches the initial cone packing prior to foveal pit formation in normal development [63]. The subsequent elongation and inward displacement of cones, thought to result from a combination of mechanical and molecular factors [56], seems to be more and differently affected in persons with aniridia. This supports the theory that the lack of a foveal avascular zone and a foveal pit contribute to the inhibition of optimal cone specialization, and thus causes a lack of the typical high peak in central cone density. Developmental differences in the deep vascular plexus is one factor that plays a role in the large variation in foveal cone packing and elongation [162] observed in aniridia.

Paper II showed and emphasized the importance of imaging the retina for improving understanding of underlying pathophysiology and retinal development and organization in aniridia. While OCT is used in clinical evaluation of aniridia today, AOSLO is not yet widespread clinically or suited for all patients. The majority of the current knowledge about retinal development in aniridia has evolved from the research on mice [126, 127, 133]. Hence, future studies employing single-cell retinal imaging in larger cohorts may

be very important as a part in improving our understanding of retinal development and maturation in aniridia in humans, which in turn may lay foundations for a better clinical management of aniridia patients.

5.2 Relationship between retinal structure and visual function

Despite sharing the same diagnosis, individuals with aniridia present various degrees of vision impairment, and consequently have completely different needs for visual and technical aids. Some need a white stick to navigate while others can drive a car!

Ranges of normal variation in numbers of cells in the retina and in ratios of cell types are often large [29, 30, 149, 163], usually without any obvious subjective effects on visual function. The large variation in photoreceptor density across the macula in aniridia may, however, have larger functional consequences because there is not the same redundancy of cells as is found in most normal healthy retinas. It is not unlikely that low redundancy of cells will also make the retina more vulnerable to other ocular pathology. Hence, knowledge regarding the structure-function relationship in aniridia is essential to better understand visual function in general in this patient group and maximize utilization of their remaining vision.

Vision loss in aniridia is multifactorial, thus it is challenging to predict visual function from foveal structure alone. In paper III, central thickness of the outer retinal layers accounted for approximately 66 % of the variation in visual acuity in aniridia. This analysis excluded the ten participants with the most severe corneal opacities. It is important to note that more severe corneal opacification is likely to cause an additional deterioration of visual function that may progress over time.

At least two other studies, that have used OCT to assess foveal hypoplasia in large aniridia cohorts, have been published during the time course of this project [85, 86]. Casas-Llera *et al*. [86], have recently validated the qualitative foveal hypoplasia grading system [70] to a large cohort of persons with congenital aniridia, although no genetic information is provided. They describe the presence of outer segment lengthening (foveal hypoplasia grade 2) as the breaking point for predicting visual potential, with

significantly better visual acuity in the group with grade 2 compared with grade 3 and 4 foveal hypoplasia [86]. While the grading system is a valuable clinical tool for assessing the degree of foveal hypoplasia in aniridia, it is vital to be aware of the strikingly large variability and overlap in visual acuity within and between the different foveal hypoplasia grades [86]. This has clinical implications because the strong correlation measured between grade of foveal hypoplasia and visual acuity may not be generally true at an individual level. The results reported in paper II and III underscore the large variability in visual acuity within each foveal hypoplasia grade, and further suggests that variable thickness of the outer retinal layers, despite the same OCT grade, is representative of the variation in visual acuity. This indicates the need for a more detailed assessment of foveal structure for predicting visual potential for a given person with aniridia.

The findings in paper II implicates that retinal factors other than foveal cone density plays a role in limiting visual acuity. The reduced parafoveal and perifoveal ganglion cell layer thickness, observed in paper III, indicates that the retina contains a reduced number of ganglion cells. Another possible explanation is that the normal foveal non-convergent wiring of cones to ganglion cells is altered. Hence, the limit of resolution in the fovea is limited by the midget ganglion cell mosaic rather that the Nyquist limit of the cone mosaic. Further, Provis *et al*. [56], have suggested that the elasticity of the foveal region, required for normal foveal formation, is reliant on the non-convergent cone-ganglion cell pathway. Thus, it is reasonable to hypothesize that the midget circuitry is altered in aniridia-associated foveal hypoplasia, as suggested in albinism [46]. This may explain why persons with almost identical cone densities, in paper II, have unequal visual acuity. Convergence of cone inputs to midget ganglion cells predicts decreased, but not an absence of, colour-opponent response, similar to that suggested for the retinal periphery [164, 165]. Hence, an alteration of the foveal “private-line” circuitry may account for reduced red-green colour discrimination, as observed and discussed in paper I. Future histological studies are needed to test this hypothesis. In addition to fewer foveal cones and alterations in associated pathways, reduced

photopigment optical density is another factor that can affect colour discrimination in aniridia, possibly as a consequence of immature and short foveal cones [166, 167].

Knowing the limitations of visual outcome following treatment is of particular significance in aniridia because intraocular surgery and pharmaceutical therapy are associated with adverse side effects and high risk of complications that can lead to worsening of the condition. Intervention may trigger opacification of the cornea [168], presumably as a result of limbal stem cell deficiency [169]. High risk of developing progressive fibrotic membrane in the anterior chamber (aniridic fibrotic membrane) following even standard surgical treatment has also been reported [170]. The large individual differences in retinal structure, both between individual persons with aniridia and within families, underscores that a generalization based on the average of a group is not appropriate when considering the potential treatment benefit.

Currently, there are no treatment options for foveal hypoplasia. On the other hand, future possibilities for treatment raise questions regarding selection of individuals for clinical trials. This emphasizes the importance of understanding the structures of the retina in aniridia for gaining insight about between-individual variation and the potential of visual function. An important observation from this thesis is the indication that the fovea has continued to develop after birth in some persons with aniridia, as supported by the marked increase in cone specialization observed as considerably higher cone density and elongated cones in the foveal center relative to the perifovea (paper II and III). Although this proposed postnatal development seems to occur to a lesser extent than in normal controls, it suggests that development is not completely arrested in all persons with aniridia. This may provide a window of opportunity for therapeutic intervention in children with aniridia, which potentially may help to improve retinal function, stimulate foveal development and optimize vision. Longitudinal studies are needed to confirm this.

A number of potential approaches to treat aniridia have been described. Nonsense suppression is a therapeutic approach that target and overwrite premature stop codons (PTCs) caused by nonsense mutations in *PAX6* mRNA so that partial levels of deficient

protein function can be restored [171]. Promising results have been shown in an aniridia mouse model (*Pax6*$^{Sey/+}$) where postnatal administration of an eye drop formulation of Ataluren ("START" therapy) reversed abnormalities in the cornea, lens and retina, increased retinal function and prevented disease progression [172, 173]. In the retina, the gene therapy increased the photoreceptor density and the thickness of all retinal layers in the aniridia mice [173]. Currently, there is an ongoing trial for aniridia (NCT02647359; ClinicalTrials.Gov) that is testing the safety and efficacy of oral nonsense suppression (Ataluren®) in persons with aniridia.

5.3 *PAX6* in central retinal development

Most of the knowledge about the role of *PAX6* in retinal development comes from studies of animal models with absence of a foveal structure [126, 127, 131], although green anole (*Anolis carolinensis*, a foveated lizard) has recently been suggested as a new model to study foveal development [174]. Conditions associated with abnormal or arrested retinal and foveal development, like aniridia, offer a good opportunity to increase our understanding of foveal development and possible components of the foveal developmental pathway.

The findings in this thesis suggests that loss of one functional copy of *PAX6* alters the number of cells in the inner and outer retina, which reflects the critical role of *PAX6* in early embryonic retinal development [105]. Furthermore, the strong association between having a *PAX6* mutation and foveal hypoplasia clearly indicates that *PAX6* is crucial for foveal formation that starts around mid-gestation [55] and for increasing the number of cones in the fovea [105]. No current literature has determined the mechanism/molecular basis of foveal hypoplasia in *PAX6* mutations.

Paper III discussed a possible role of *PAX6* in foveal formation through regulation of anti-angiogenic factors in the RPE and retinal ganglion cells that in turn affect formation of the foveal avascular zone [56, 175]. This suggests that *PAX6* activity is required prior to foveal pit formation. Other ocular conditions are also commonly associated with altered foveal development. The reduced foveal cone density in aniridia described in paper II, is

for example, similar to that described in previous *in-vivo* studies in albinism [46, 73], which is also associated with different degrees of foveal hypoplasia. Albinism is characterized by absent or reduced melanin pigment in the eye and associated with mutations in the *TYR, OCA2* or *TYRP1* gene, among others [176]. Though the underlying mechanisms differ, the impaired foveal development in both conditions suggest that there can be a common link in that the RPE may have a contributing role in FAZ formation and foveal development. This is supported by a study that found that PAX6 is involved in the initiation of the pigmentation program by regulating expression of downstream genes such as *Mitf* and *Tyr* either directly or indirectly [130]. Moreover, the role of *PAX6* in RPE pigment production is also likely to explain the light or hypopigmented fundus observed in many of the participants with aniridia [177].

PAX6 continues to be expressed in the retina during adulthood, specifically in the inner retinal layers: the ganglion cell, bipolar cell layers and the amacrine cells [134]. Since PAX6 might have a functional role in the maintenance and protection of the aging retina, one can speculate on whether decreased *PAX6* expression is the most likely reason for the low cone density and irregular cone mosaic observed in the oldest participant with aniridia in paper II.

5.4 Genetic variability and correlations between genotype and phenotype

There is a large diversity in the genetic mutations causing aniridia in this cohort, as also described in other aniridia cohorts [9, 121, 122, 161, 178, 179]. An increasing number of studies have emphasized the role of non-coding *PAX6* regions and regulatory regions in aniridia [93, 95, 96, 116, 118, 180]. The increased mutation detection rate (~97%) in paper III compared with paper I (~76%) underscores this importance of including non-coding *PAX6* regions and flanking regions containing known *PAX6* regulatory elements as well as combining different analysis methods. A wide variety of *PAX6* gene mutations identified here have already been described, but paper III identified three new mutations not previously reported. Hence, this thesis contributes to expanding the

genetic spectrum associated with aniridia. See figure 6 in paper III for an overview, location and frequency of the identified variants in this cohort.

Knowledge about genotype-phenotype correlations is crucial to assist in the clinical diagnosis, to determine when a possible intervention is advisable, and in development of individualized treatments and rehabilitation. Genotype-phenotype correlations in aniridia have, however, been difficult to establish due to a number of possible reasons, such as the high number of different mutations [8] and the large phenotypic variability associated with the same mutation [120, 181] – both among patients from the same family and among those from unrelated families. This great variation is also apparent in retinal organization and function in this cohort. Additional complexities of the *PAX6* gene include the impact of other associated genes, presence of multiple alternative promoters and transcripts [105, 107, 182], mosaicism [183] and epigenetic factors [50].

Previous studies have tried grouping mutations within the *PAX6* coding regions in a variety of ways (for example by protein domain or mutation type) but haven't found a clear relationship between genotype and phenotype (reviewed in [113]). The early work in the field assumed that the protein domain affected would play a role in disease severity, but now it is a general consensus that that is not the case because most of the mutations will ultimately cause haploinsufficiency [113]. An exception is missense mutations which tends to be associated with a variable severity but also some milder aniridia and non-aniridia phenotypes [9, 115]. Surprisingly, no missense mutations were found in this study despite about 12 % of the intragenic mutations reported in *PAX6* are missense mutations [92].

Despite all the potential confounding factors, paper III shows that when considering the whole *PAX6* region, including untranslated regions (non-coding regions) and its flanking regions (regulatory regions), the location and extent of the mutation may still provide valuable information that can help in predicting retinal phenotype. These findings also show the potential benefit of applying more detailed imaging, testing and analysis methods to capture the individual differences and gain more in-depth understanding of the different structures that contributes to the variable phenotypes.

An interesting finding in paper III was the marked phenotypic differences between deletions where haploinsufficiency was predicted due to NMD of non-functional protein and deletions where a complete absence of the gene product was expected. Variability in NMD efficiency is suggested as a plausible explanation for these variable clinical presentations [184]. However, more studies are required to confirm these findings. Regardless, this is a novel observation in aniridia that may also provide new knowledge about the large between-individual differences in phenotype.

The large between-individual variation in foveal hypoplasia, iris hypoplasia and corneal involvement within family #2, observed in paper II, suggests that factors other than the identified splice site mutation also play a role in defining the phenotype. Total iris hypoplasia, but near normal foveal morphology and otherwise mild anterior segment changes were seen in the *ELP4-DCDC1* deletion (family #11, paper III). These findings underscore that changes in the retina correlate poorly with the degree of iris hypoplasia. It is therefore likely that molecular factors causing variation in phenotype in the retina differ from those at play in the iris. Hence, better knowledge about *PAX6* dosage sensitivity and requirements in the different affected tissues may be of great importance to understand phenotypic outcomes.

5.5 Methodological considerations and study limitations

5.5.1 Study design and sample

This project was designed as a cross-sectional, observational study with a main aim of exploring retinal phenotype and genotype in congenital aniridia, which is a rare disease. The cross-sectional design was appropriate as it allows for detailed characterization of important features of the disorder, multiple outcomes, comparisons between groups, assessment of the relationship between variables as well as identifying possible predictors of outcomes which are essential for answering the research questions. However, one cannot provide any causal effects from the results [185].

Recruiting research participants via an organization may introduce selection bias. One could argue that members of patient organizations may have other characteristics than non-members. For instance, they may have experienced more challenges with their disorder or represent a greater proportion of those with more severe phenotypes, although these are just speculations. Statistically speaking, on the other hand, the study participants present a representative sample: they represent more than half of the persons known to have aniridia in Norway and their age range and geographic spread among the participants constitute a strength. The sample represents a large range of phenotypes, similar to the range of previously characterized phenotypes [e.g. 9], although those with the most severe anterior segment disease where excluded from the OCT and AOSLO analyses. The study sample also represents a large range of genotypes associated with aniridia. However, there are few participants in the groups with CTE mutations and mutations in regulatory regions, which make robust conclusions about phenotype-genotype correlations difficult. On the other hand, the low frequencies of these mutations are in line with previously reported frequencies [92].

5.5.2 Measurements and procedures

The chart used for measuring visual acuity limited the quantification of visual acuity poorer than 1.8 logMAR. Both computer-based and plate tests intended for testing spatial vision in severe visual impairment have been developed [186, 187]. These tests could have been applied to obtain a more precise acuity measurement in the participants with profound low vision in these studies.

Different aspects of vision may be tested by several different methods. High-contrast visual acuity is expected to be linked to the resolving power of the visual system. However, the visual function includes far more than the ability to see fine details of high contrast. In daily life we use vision to perceive visual stimuli that are of different sizes, varying brightness, colours and movement, but the stimuli are not necessarily of high contrast. A decrease in visual acuity is also likely to reduce the ability to distinguish details with low contrast [188]. Moreover, contrast sensitivity can be strongly affected

by light scatter [189] and would therefore be an important measure to assess functional vision in aniridia.

Many of those with aniridia are very sensitive to light and commonly wear filter glasses. This raises the question on whether lingering filter effects could have affected the colour vision testing if they usually wore coloured filters. However, the vast majority of the participants that have filter glasses reports that they mostly use them outdoors and only sporadically indoors. With such non-constant wear, a relatively rapid adaptation is expected [190, 191]. All the participants were indoors for at least one hour before colour vision testing, thus lingering filter effects are expected to have very little or no impact on the results.

One of the challenges in obtaining reliable posterior segment images is related to anterior segment opacities and nystagmus which may result in degraded image quality, poorer contrast and resolution. This limited the number of participants that were imageable. To minimize this limitation, individual adjustments of head position and OCT imaging acquisition mode were permitted. One of these adjustments meant changing from a high-resolution to a high-speed mode, which halves the number of A-scans per B-scan and thus reduced resolution. However, the difference in the number of A-scans would only affect the lateral resolution and have minimal influence on thickness measurements [192]. A strength of these studies is that individual retinal magnification factors were calculated based on ocular biometry measurements and accounted for in the image analyses, providing a more accurate lateral image scaling. Good tolerance to speckle noise is one main advantage of using an active contour approach to retinal layer segmentation [148].

The measurements of the outer nuclear layer in paper II and III can be confounded by the presence of the Henle fiber layer, hence the correct designation of this layer is ONL + HFL. These two layers cannot be differentiated easily without capturing directional OCT [193]. It is likely that the HFL orientation and thickness differs in aniridia compared to normal, as recently shown in albinism where the foveal HFL was thicker [194]. If the HFL contribute more to central ONL thickness in aniridia than in controls, as can be

expected if some amount of centripetal cone migration has occurred, the decrease in ONL thickness in aniridia compared with normal controls would be even larger than measured in paper II and III.

Besides nystagmus and poor optical media, AOSLO imaging is particularly sensitive to monochromatic aberrations that arise from irregular tear film, cornea and lens, which is commonly observed in aniridia. Seven persons from one family were originally included in imaging of the photoreceptor mosaic, but cones were reliably identified in only five of these participants. Even so, they represent different grades of foveal hypoplasia (grade 2–4). Ideally, a larger number of participants, especially those with different genotypes, should be imaged with AOSLO to assess the full range of photoreceptor structure changes associated with *PAX6* mutations. Nevertheless, the thinning of the outer retinal layers across the macula (paper III) clearly indicates reduced foveal cone density also across the different mutations. The challenge nystagmus poses to imaging quality could be improved with the use of eye tracking [195], that may be available in the near future.

5.6 Future perspectives

Through doing this research and in working with persons who have aniridia and their families, it is clear that more research is required. There is a need for research, not only on the eye, but also to understand the consequences of the fact that *PAX6* is also expressed outside the eye, for example in terms of auditive processing [196], sleep [197, 198] and metabolic issues [199]. Further to this, aniridia is not only a congenital rare disorder that causes vision impairment, it has also great impact on people, their lives and their families. A qualitative study with semi-structured interviews of persons with aniridia was conducted in a small subset of the present aniridia cohort [200]. This revealed a need for more attention in the future to provide reliable and scientifically grounded information about individual experiences of living with aniridia [200]. Since the focus of this thesis is the retina and visual function, a few specific perspectives that have surfaced through this work will be mentioned.

(1) A better understanding of inter- and intra-individual variability in how vision develops and changes as persons with aniridia grow and age, is needed. There is a need to understand to what degree foveal development continues after birth, the consequence of the observed lack of or reduced amount of macular pigment [177], and to what degree this is related to the genotype. Longitudinal assessment and further evaluation of foveal development would be essential to understand whether and how therapeutic strategies and early visual optimization could influence foveal development.

(2) A better understanding of rod and cone function is needed, not only to understand the central retina, but also how the peripheral retina is affected. As a part of the work in the "Aniridia and Vision" project, measurements of dark adaptation were performed. Preliminary results indicate a normal time to rod-cone break in aniridia, but an overall reduction in both dark adapted cone and rod sensitivity [201]. Completion of these analyses is important to increase our understanding of rod function in persons with aniridia and their ability to adapt to changing light levels.

Because of the progressive nature of ocular surface disease, such as aniridia-associated keratopathy, this is one of the key priorities of treatment. In addition to limbal stem cell deficiency, meibomian gland dysfunction, loss of meibomian glands and increased tear film osmolarity are factors that are associated with worsening keratopathy [79, 80]. In addition, inflammatory mediators play a role [137]. Thus, continued focus on the multifaceted nature of AAK is crucial to develop novel diagnostics and treatments.

Recently, an EU COST (European Cooperation in Science and Technology) Action (ANIRIDIA-NET CA18116; 2019-2023) was established, with an aim to share knowledge, build networks and stimulate aniridia-related research across Europe, which gives a great opportunity to make progress in our understanding and treatment of the disease.

6 Conclusion

The research in this thesis aimed to characterize retinal structure and foveal morphology, its importance to visual performance, and genotype-phenotype correlations in congenital aniridia. High-resolution imaging of the retina shows that persons with aniridia have varying degrees of foveal hypoplasia, decreased thicknesses and altered topography of the outer and inner retinal layers. This underscores the key role of *PAX6* in retinal development. Moreover, the cone photoreceptor density and mosaic regularity are reduced across the macula, relative to normal healthy controls. This variation in foveal morphology and cone specialization is associated with variation in high-contrast visual acuity and red-green colour discrimination. However, the between-individual variation is large, both between and within different genotypes, thus outcomes cannot be generalized based on an average aniridia population.

Despite the large phenotypic variation, detailed genotyping and analyses of the retinal layers showed that the position and extent of the mutation, within non-coding, coding or flanking regulatory regions of the *PAX6* gene, may be predictive for the severity of foveal underdevelopment. Further, the results indicate that foveal development is not completely arrested in all persons with aniridia, which underscores the importance of optimal visual stimulation in early childhood and suggests that early administration of therapy, may improve foveal development and optimize vision. Longitudinal studies following the same individuals over time are warranted to document the extent of postnatal development in aniridia and investigate if visual acuity improves accordingly.

This knowledge is of great significance in the clinical management of persons with congenital aniridia to understand limits and potential related to visual function. The large variation in how the retina develops in aniridia underscores that the ability to directly assess the retinal layers is of great value to assist in providing an accurate and early diagnosis, prognosis and subsequent provision of personalized early intervention, facilitation or treatment. As gene therapy may be an option in the future, OCT and AOSLO imaging in conjunction with measures of photoreceptor function could be valuable in selecting individual persons for future trials and measuring the trials' impact.

The genotypic and phenotypic heterogeneity described in this thesis also emphasizes the importance of having a person-centred approach in the clinical management of persons with aniridia to be able to present well-founded individual alternatives of facilitation, rehabilitation or treatment options. The use of colour information may, for example, be of great help in daily life, even if many people who have aniridia experience decreased colour vision. Colours are also central in play and in education, for safety and accessibility, emphasizing the importance of being aware of that some may have challenges with discriminating certain colours. Thus, the use of solid, bright colours could be pivotal.

The close collaboration and contact with the participants were a strength throughout the research in this thesis. Having a good dialog with the participants was by far the main factor contributing to better understanding how the disease impact on persons' daily life, their preferences and concerns, and what is important to each person from their perspective. Such information exchange is also of importance in the clinical management of persons with aniridia and should accommodate for shared decision-making based on each person's preferences.

References

1. Enoch J, McDonald L, Jones L, et al. Evaluating Whether Sight Is the Most Valued Sense. *JAMA Ophthalmol*. 2019.
2. World Health Organization. World report on vision. Geneva: WHO; 2019.
3. Nasjonal kompetansetjeneste for sjeldne diagnoser. Hva er en sjelden diagnose? : Helsenorge.no; 2019 [updated 09.08.2019. Available from: https://helsenorge.no/sjeldne-diagnoser/hva-er-en-sjelden-diagnose.
4. Edén U, Iggman D, Riise R, et al. Epidemiology of aniridia in Sweden and Norway. *Acta Ophthalmologica*. 2008;86(7):727-9.
5. Poli B, Sánches de Vega R, Teofili C. European/International Guidelines on Aniridia: The Patients' Point of View. In: Parekh M, Poli B, Ferrari S, et al., editors. Aniridia Recent Developments in Scientific and Clinical Research. Switzerland: Springer International Publishing; 2015. p. 167-71.
6. Kokotas H, Petersen MB. Clinical and molecular aspects of aniridia. *Clin Genet*. 2010;77(5):409-20.
7. Lee H, Khan R, O'Keefe M. Aniridia: current pathology and management. *Acta Ophthalmol*. 2008;86(7):708-15.
8. Landsend ES, Utheim OA, Pedersen HR, et al. The genetics of congenital aniridia-a guide for the ophthalmologist. *Surv Ophthalmol*. 2018;63(1):105-13.
9. Hingorani M, Williamson KA, Moore AT, et al. Detailed ophthalmologic evaluation of 43 individuals with PAX6 mutations. *Invest Ophthalmol Vis Sci*. 2009;50(6):2581-90.
10. Bredrup C, Knappskog PM, Rodahl E, et al. Clinical manifestation of a novel PAX6 mutation Arg128Pro. *Arch Ophthalmol*. 2008;126(3):428-30.
11. Holmstrom G, Eriksson U, Hellgren K, et al. Optical coherence tomography is helpful in the diagnosis of foveal hypoplasia. *Acta Ophthalmol*. 2010;88(4):439-42.
12. Gregory-Evans K, Cheong-Leen R, George SM, et al. Non-invasive anterior segment and posterior segment optical coherence tomography and phenotypic characterization of aniridia. *Can J Ophthalmol*. 2011;46(4):337-44.
13. Thomas S, Thomas MG, Andrews C, et al. Autosomal-dominant nystagmus, foveal hypoplasia and presenile cataract associated with a novel PAX6 mutation. *Eur J Hum Genet*. 2014;22(3):344-9.
14. Dowling JE. The retina : an approachable part of the brain. Rev. ed. ed: Cambridge; 2012.
15. Rodieck RW. The first steps in seeing. Massachusetts: Sinauer Associates; 1998.
16. Schnapf JL, Kraft TW, Baylor DA. Spectral sensitivity of human cone photoreceptors. *Nature*. 1987;325(6103):439-41.
17. Dartnall HJ, Bowmaker JK, Mollon JD. Human visual pigments: microspectrophotometric results from the eyes of seven persons. *Proc R Soc Lond B Biol Sci*. 1983;220(1218):115-30.
18. Neitz M, Neitz J. Molecular genetics of color vision and color vision defects. *Arch Ophthalmol*. 2000;118(5):691-700.

19. Merbs SL, Nathans J. Absorption spectra of human cone pigments. *Nature*. 1992;356(6368):433-5.
20. Neitz J, Neitz M. The genetics of normal and defective color vision. *Vision Res*. 2011;51(7):633-51.
21. Wassle H. Parallel processing in the mammalian retina. *Nat Rev Neurosci*. 2004;5(10):747-57.
22. Dacey DM, Lee BB. The 'blue-on' opponent pathway in primate retina originates from a distinct bistratified ganglion cell type. *Nature*. 1994;367(6465):731-5.
23. Gegenfurtner KR, Kiper DC. Color vision. *Annu Rev Neurosci*. 2003;26:181-206.
24. Strauss O. The retinal pigment epithelium in visual function. *Physiol Rev*. 2005;85(3):845-81.
25. Curcio CA, Allen KA. Topography of ganglion cells in human retina. *J Comp Neurol*. 1990;300(1):5-25.
26. Masland RH. The neuronal organization of the retina. *Neuron*. 2012;76(2):266-80.
27. Curcio CA, Allen KA, Sloan KR, et al. Distribution and morphology of human cone photoreceptors stained with anti-blue opsin. *J Comp Neurol*. 1991;312(4):610-24.
28. Curcio CA, Sloan KR. Packing geometry of human cone photoreceptors: variation with eccentricity and evidence for local anisotropy. *Vis Neurosci*. 1992;9(2):169-80.
29. Curcio CA, Sloan KR, Kalina RE, et al. Human photoreceptor topography. *J Comp Neurol*. 1990;292(4):497-523.
30. Dees EW, Dubra A, Baraas RC. Variability in parafoveal cone mosaic in normal trichromatic individuals. *Biomed Opt Express*. 2011;2(5):1351-8.
31. Chui TY, Song H, Burns SA. Adaptive-optics imaging of human cone photoreceptor distribution. *J Opt Soc Am A Opt Image Sci Vis*. 2008;25(12):3021-9.
32. Elsner AE, Chui TYP, Feng L, et al. Distribution differences of macular cones measured by AOSLO: Variation in slope from fovea to periphery more pronounced than differences in total cones. *Vision Research*. 2017;132:62-8.
33. Sawides L, de Castro A, Burns SA. The organization of the cone photoreceptor mosaic measured in the living human retina. *Vision research*. 2017;132:34-44.
34. Jackson K, Vergilio GK, Cooper RF, et al. A 2-Year Longitudinal Study of Normal Cone Photoreceptor Density. *Invest Ophthalmol Vis Sci*. 2019;60(5):1420-30.
35. Wells-Gray EM, Choi SS, Bries A, et al. Variation in rod and cone density from the fovea to the mid-periphery in healthy human retinas using adaptive optics scanning laser ophthalmoscopy. *Eye*. 2016;30(8):1135-43.
36. Cooper RF, Wilk MA, Tarima S, et al. Evaluating Descriptive Metrics of the Human Cone Mosaic. *Invest Ophthalmol Vis Sci*. 2016;57(7):2992-3001.
37. Dubra A, Sulai Y, Norris JL, et al. Noninvasive imaging of the human rod photoreceptor mosaic using a confocal adaptive optics scanning ophthalmoscope. *Biomed Opt Express*. 2011;2(7):1864-76.
38. Scoles D, Sulai YN, Langlo CS, et al. In vivo imaging of human cone photoreceptor inner segments. *Invest Ophthalmol Vis Sci*. 2014;55(7):4244-51.

39. Roorda A, Metha AB, Lennie P, et al. Packing arrangement of the three cone classes in primate retina. *Vision Res*. 2001;41(10-11):1291-306.
40. Hofer H, Carroll J, Neitz J, et al. Organization of the Human Trichromatic Cone Mosaic. *The Journal of Neuroscience*. 2005;25(42):9669-79.
41. Roorda A, Williams DR. The arrangement of the three cone classes in the living human eye. *Nature*. 1999;397(6719):520-2.
42. Carroll J, Neitz J, Neitz M. Estimates of L:M cone ratio from ERG flicker photometry and genetics. *J Vis*. 2002;2(8):531-42.
43. Zhang T, Godara P, Blanco ER, et al. Variability in Human Cone Topography Assessed by Adaptive Optics Scanning Laser Ophthalmoscopy. *Am J Ophthalmol*. 2015;160(2):290-300.e1.
44. Wilk MA, Dubis AM, Cooper RF, et al. Assessing the spatial relationship between fixation and foveal specializations. *Vision Res*. 2016.
45. Pedersen HR, Neitz M, Gilson SJ, et al. The Cone Photoreceptor Mosaic in Aniridia: Within-Family Phenotype-Genotype Discordance. *Ophthalmol Retina*. 2019;3(6):523-34.
46. Wilk MA, McAllister JT, Cooper RF, et al. Relationship between foveal cone specialization and pit morphology in albinism. *Invest Ophthalmol Vis Sci*. 2014;55(7):4186-98.
47. Baraas RC, Pedersen HR, Hagen LA. Single-cone imaging in inherited and acquired colour vision deficiencies. *Current Opinion in Behavioral Sciences*. 2019;30:55-9.
48. Sinn R, Wittbrodt J. An eye on eye development. *Mech Dev*. 2013;130(6-8):347-58.
49. Cepko CL, Austin CP, Yang X, et al. Cell fate determination in the vertebrate retina. *Proc Natl Acad Sci U S A*. 1996;93(2):589-95.
50. Aldiri I, Xu B, Wang L, et al. The Dynamic Epigenetic Landscape of the Retina During Development, Reprogramming, and Tumorigenesis. *Neuron*. 2017;94(3):550-68.e10.
51. Young RW. Cell differentiation in the retina of the mouse. *Anat Rec*. 1985;212(2):199-205.
52. Hendrickson A, Zhang C. Development of cone photoreceptors and their synapses in the human and monkey fovea. *J Comp Neurol*. 2017.
53. Hendrickson A. Development of Retinal Layers in Prenatal Human Retina. *Am J Ophthalmol*. 2016;161:29-35.e1.
54. Amini R, Rocha-Martins M, Norden C. Neuronal Migration and Lamination in the Vertebrate Retina. *Front Neurosci*. 2017;11:742.
55. Hendrickson A, Possin D, Vajzovic L, et al. Histologic development of the human fovea from midgestation to maturity. *Am J Ophthalmol*. 2012;154(5):767-78.e2.
56. Provis JM, Dubis AM, Maddess T, et al. Adaptation of the central retina for high acuity vision: cones, the fovea and the avascular zone. *Prog Retin Eye Res*. 2013;35:63-81.
57. Bassett EA, Wallace VA. Cell fate determination in the vertebrate retina. *Trends in Neurosciences*. 2012;35(9):565-73.

58. Gregory-Evans CY, Gregory-Evans K. Foveal hypoplasia: the case for arrested development. *Expert Review of Ophthalmology*. 2011;6(5):565.
59. Dacey DM. The mosaic of midget ganglion cells in the human retina. *J Neurosci*. 1993;13(12):5334-55.
60. Neveu MM, von dem Hagen E, Morland AB, et al. The fovea regulates symmetrical development of the visual cortex. *J Comp Neurol*. 2008;506(5):791-800.
61. Hoshino A, Ratnapriya R, Brooks MJ, et al. Molecular Anatomy of the Developing Human Retina. *Dev Cell*. 2017;43(6):763-79.e4.
62. Springer AD, Hendrickson AE. Development of the primate area of high acuity, 3: temporal relationships between pit formation, retinal elongation and cone packing. *Vis Neurosci*. 2005;22(2):171-85.
63. Diaz-Araya C, Provis JM. Evidence of photoreceptor migration during early foveal development: a quantitative analysis of human fetal retinae. *Vis Neurosci*. 1992;8(6):505-14.
64. Packer O, Hendrickson AE, Curcio CA. Development redistribution of photoreceptors across the Macaca nemestrina (pigtail macaque) retina. *J Comp Neurol*. 1990;298(4):472-93.
65. Yuodelis C, Hendrickson A. A qualitative and quantitative analysis of the human fovea during development. *Vision Res*. 1986;26(6):847-55.
66. Hendrickson A, Zhang C. Development of cone photoreceptors and their synapses in the human and monkey fovea. *J Comp Neurol*. 2019;527(1):38-51.
67. Lee H, Purohit R, Patel A, et al. In Vivo Foveal Development Using Optical Coherence Tomography. *Invest Ophthalmol Vis Sci*. 2015;56(8):4537-45.
68. Vajzovic L, Hendrickson AE, O'Connell RV, et al. Maturation of the human fovea: correlation of spectral-domain optical coherence tomography findings with histology. *Am J Ophthalmol*. 2012;154(5):779-89.e2.
69. Knoblauch K, Vital-Durand F, Barbur JL. Variation of chromatic sensitivity across the life span. *Vision Res*. 2001;41(1):23-36.
70. Thomas MG, Kumar A, Mohammad S, et al. Structural grading of foveal hypoplasia using spectral-domain optical coherence tomography a predictor of visual acuity? *Ophthalmology*. 2011;118(8):1653-60.
71. Provis JM, Diaz CM, Dreher B. Ontogeny of the primate fovea: a central issue in retinal development. *Prog Neurobiol*. 1998;54(5):549-80.
72. Langlo CS, Patterson EJ, Higgins BP, et al. Residual Foveal Cone Structure in CNGB3-Associated Achromatopsia. *Invest Ophthalmol Vis Sci*. 2016;57(10):3984-95.
73. McAllister JT, Dubis AM, Tait DM, et al. Arrested development: high-resolution imaging of foveal morphology in albinism. *Vision Res*. 2010;50(8):810-7.
74. Marmor MF, Choi SS, Zawadzki RJ, et al. Visual insignificance of the foveal pit: reassessment of foveal hypoplasia as fovea plana. *Arch Ophthalmol*. 2008;126(7):907-13.
75. Wilk MA, Wilk BM, Langlo CS, et al. Evaluating outer segment length as a surrogate measure of peak foveal cone density. *Vision Res*. 2017;130:57-66.

76. Baratta G. Osservazioni pratiche sulle principali malattie degli occhi (Practical observations on the main diseases of the eye). Milano1818.
77. Brandt JD, Casuso LA, Budenz DL. Markedly increased central corneal thickness: an unrecognized finding in congenital aniridia. *Am J Ophthalmol*. 2004;137(2):348-50.
78. McCulley TJ, Mayer K, Dahr SS, et al. Aniridia and optic nerve hypoplasia. *Eye (Lond)*. 2005;19(7):762-4.
79. Landsend ECS, Pedersen HR, Utheim OA, et al. Meibomian gland dysfunction and keratopathy are associated with dry eye disease in aniridia. *Br J Ophthalmol*. 2019;103(1):119-24.
80. Landsend ECS, Utheim ØA, Pedersen HR, et al. Dry Eye Disease in a Norwegian-Danish Cohort of Congenital Aniridia. *Investigative Ophthalmology & Visual Science*. 2016;57(12):5701-.
81. Gramer E, Reiter C, Gramer G. Glaucoma and frequency of ocular and general diseases in 30 patients with aniridia: a clinical study. *Eur J Ophthalmol*. 2012;22(1):104-10.
82. Eden U, Lagali N, Dellby A, et al. Cataract development in Norwegian patients with congenital aniridia. *Acta Ophthalmol*. 2014;92(2):e165-7.
83. Lagali N, Wowra B, Fries FN, et al. PAX6 Mutational Status Determines Aniridia-Associated Keratopathy Phenotype. *Ophthalmology*. 2020;127(2):273-5.
84. Seefelder R. Die Aniridie als eine Entwicklungshemmung der Retina. *Albrecht von Graefes Archiv für Ophthalmologie*. 1909;70(1):65-87.
85. Sannan NS, Gregory-Evans CY, Lyons CJ, et al. Correlation of novel PAX6 gene abnormalities in aniridia and clinical presentation. *Can J Ophthalmol*. 2017;52(6):570-7.
86. Casas-Llera P, Siverio A, Esquivel G, et al. Spectral-domain optical coherence tomography foveal morphology as a prognostic factor for vision performance in congenital aniridia. *Eur J Ophthalmol*. 2018:1120672118818352.
87. Tremblay F, Gupta SK, De Becker I, et al. Effects of PAX6 mutations on retinal function: an electroretinographic study. *Am J Ophthalmol*. 1998;126(2):211-8.
88. Hood MP, Kerr NC, Smaoui N, et al. Abnormal cone ERGs in a family with congenital nystagmus and photophobia harboring a p.X423Lfs mutation in the PAX6 gene. *Doc Ophthalmol*. 2015;130(2):157-64.
89. Wu L, Ma Q, Chen Y, et al. Abnormalities of ERG in congenital aniridia. *Yan Ke Xue Bao*. 1991;7(3):151-2, 19.
90. Weber U, Petersen J. [Morphological and functional findings in a family with aniridia (author's transl)]. *Klin Monbl Augenheilkd*. 1981;178(6):439-45.
91. Nelson LB, Spaeth GL, Nowinski TS, et al. Aniridia. A review. *Surv Ophthalmol*. 1984;28(6):621-42.
92. Lima Cunha D, Arno G, Corton M, et al. The Spectrum of PAX6 Mutations and Genotype-Phenotype Correlations in the Eye. *Genes (Basel)*. 2019;10(12).
93. Bhatia S, Bengani H, Fish M, et al. Disruption of autoregulatory feedback by a mutation in a remote, ultraconserved PAX6 enhancer causes aniridia. *Am J Hum Genet*. 2013;93(6):1126-34.

94. Lauderdale JD, Wilensky JS, Oliver ER, et al. 3' deletions cause aniridia by preventing PAX6 gene expression. *Proc Natl Acad Sci U S A*. 2000;97(25):13755-9.
95. Plaisancié J, Tarilonte M, Ramos P, et al. Implication of non-coding PAX6 mutations in aniridia. *Human Genetics*. 2018;137(10):831-46.
96. Ansari M, Rainger J, Hanson IM, et al. Genetic Analysis of 'PAX6-Negative' Individuals with Aniridia or Gillespie Syndrome. *PLoS One*. 2016;11(4):e0153757.
97. Fischbach BV, Trout KL, Lewis J, et al. WAGR syndrome: a clinical review of 54 cases. *Pediatrics*. 2005;116(4):984-8.
98. Gillespie FD. Aniridia, Cerebellar Ataxia, and Oligophrenia in Siblings. *Archives of Ophthalmology*. 1965;73(3):338-41.
99. Hill RE, Favor J, Hogan BL, et al. Mouse small eye results from mutations in a paired-like homeobox-containing gene. *Nature*. 1991;354(6354):522-5.
100. Quiring R, Walldorf U, Kloter U, et al. Homology of the eyeless gene of Drosophila to the Small eye gene in mice and Aniridia in humans. *Science*. 1994;265(5173):785-9.
101. Ton CC, Hirvonen H, Miwa H, et al. Positional cloning and characterization of a paired box- and homeobox-containing gene from the aniridia region. *Cell*. 1991;67(6):1059-74.
102. Glaser T, Walton DS, Maas RL. Genomic structure, evolutionary conservation and aniridia mutations in the human PAX6 gene. *Nat Genet*. 1992;2(3):232-9.
103. Hever AM, Williamson KA, van Heyningen V. Developmental malformations of the eye: the role of PAX6, SOX2 and OTX2. *Clin Genet*. 2006;69(6):459-70.
104. Cvekl A, Callaerts P. PAX6: 25th anniversary and more to learn. *Exp Eye Res*. 2017;156:10-21.
105. Shaham O, Menuchin Y, Farhy C, et al. Pax6: a multi-level regulator of ocular development. *Prog Retin Eye Res*. 2012;31(5):351-76.
106. Schedl A, Ross A, Lee M, et al. Influence of PAX6 gene dosage on development: overexpression causes severe eye abnormalities. *Cell*. 1996;86(1):71-82.
107. Kim J, Lauderdale JD. Analysis of Pax6 expression using a BAC transgene reveals the presence of a paired-less isoform of Pax6 in the eye and olfactory bulb. *Dev Biol*. 2006;292(2):486-505.
108. Azuma N, Tadokoro K, Asaka A, et al. The Pax6 isoform bearing an alternative spliced exon promotes the development of the neural retinal structure. *Human Molecular Genetics*. 2005;14(6):735-45.
109. Kleinjan DA, Seawright A, Mella S, et al. Long-range downstream enhancers are essential for Pax6 expression. *Dev Biol*. 2006;299(2):563-81.
110. Kleinjan DA, Seawright A, Childs AJ, et al. Conserved elements in Pax6 intron 7 involved in (auto)regulation and alternative transcription. *Dev Biol*. 2004;265(2):462-77.
111. Kleinjan DA, Seawright A, Schedl A, et al. Aniridia-associated translocations, DNase hypersensitivity, sequence comparison and transgenic analysis redefine the functional domain of PAX6. *Human Molecular Genetics*. 2001;10(19):2049-59.

112. Kammandel B, Chowdhury K, Stoykova A, et al. Distinct cis-essential modules direct the time-space pattern of the Pax6 gene activity. *Dev Biol*. 1999;205(1):79-97.
113. Tzoulaki I, White IM, Hanson IM. PAX6 mutations: genotype-phenotype correlations. *BMC Genet*. 2005;6:27.
114. Frischmeyer PA, Dietz HC. Nonsense-mediated mRNA decay in health and disease. *Hum Mol Genet*. 1999;8(10):1893-900.
115. Gronskov K, Rosenberg T, Sand A, et al. Mutational analysis of PAX6: 16 novel mutations including 5 missense mutations with a mild aniridia phenotype. *Eur J Hum Genet*. 1999;7(3):274-86.
116. Bayrakli F, Guney I, Bayri Y, et al. A novel heterozygous deletion within the 3' region of the PAX6 gene causing isolated aniridia in a large family group. *J Clin Neurosci*. 2009;16(12):1610-4.
117. Blanco-Kelly F, Palomares M, Vallespin E, et al. Improving molecular diagnosis of aniridia and WAGR syndrome using customized targeted array-based CGH. *PLoS One*. 2017;12(2):e0172363.
118. Syrimis A, Nicolaou N, Alexandrou A, et al. Aniridia due to a novel microdeletion affecting PAX6 regulatory enhancers: case report and review of the literature. *J Genet*. 2018;97(2):555-62.
119. Crolla JA, van Heyningen V. Frequent chromosome aberrations revealed by molecular cytogenetic studies in patients with aniridia. *Am J Hum Genet*. 2002;71(5):1138-49.
120. Yokoi T, Nishina S, Fukami M, et al. Genotype-phenotype correlation of PAX6 gene mutations in aniridia. *Hum Genome Var*. 2016;3:15052.
121. Robinson DO, Howarth RJ, Williamson KA, et al. Genetic analysis of chromosome 11p13 and the PAX6 gene in a series of 125 cases referred with aniridia. *Am J Med Genet A*. 2008;146a(5):558-69.
122. Bobilev AM, McDougal ME, Taylor WL, et al. Assessment of PAX6 alleles in 66 families with aniridia. *Clinical genetics*. 2016;89(6):669-77.
123. Hingorani M, Hanson I, van Heyningen V. Aniridia. *Eur J Hum Genet*. 2012;20(10):1011-7.
124. Law SK, Sami M, Piri N, et al. Asymmetric phenotype of Axenfeld-Rieger anomaly and aniridia associated with a novel PITX2 mutation. *Mol Vis*. 2011;17:1231-8.
125. Ito YA, Footz TK, Berry FB, et al. Severe molecular defects of a novel FOXC1 W152G mutation result in aniridia. *Invest Ophthalmol Vis Sci*. 2009;50(8):3573-9.
126. Klimova L, Kozmik Z. Stage-dependent requirement of neuroretinal Pax6 for lens and retina development. *Development*. 2014;141(6):1292-302.
127. Oron-Karni V, Farhy C, Elgart M, et al. Dual requirement for Pax6 in retinal progenitor cells. *Development*. 2008;135(24):4037-47.
128. Nishina S, Kohsaka S, Yamaguchi Y, et al. PAX6 expression in the developing human eye. *Br J Ophthalmol*. 1999;83(6):723-7.
129. Terzic J, Saraga-Babic M. Expression pattern of PAX3 and PAX6 genes during human embryogenesis. *Int J Dev Biol*. 1999;43(6):501-8.

130. Raviv S, Bharti K, Rencus-Lazar S, et al. PAX6 regulates melanogenesis in the retinal pigmented epithelium through feed-forward regulatory interactions with MITF. *PLoS Genet*. 2014;10(5):e1004360.
131. Marquardt T, Ashery-Padan R, Andrejewski N, et al. Pax6 is required for the multipotent state of retinal progenitor cells. *Cell*. 2001;105(1):43-55.
132. Philips GT, Stair CN, Young Lee H, et al. Precocious retinal neurons: Pax6 controls timing of differentiation and determination of cell type. *Dev Biol*. 2005;279(2):308-21.
133. Remez LA, Onishi A, Menuchin-Lasowski Y, et al. Pax6 is essential for the generation of late-born retinal neurons and for inhibition of photoreceptor-fate during late stages of retinogenesis. *Dev Biol*. 2017;432(1):140-50.
134. Stanescu D, Iseli HP, Schwerdtfeger K, et al. Continuous expression of the homeobox gene Pax6 in the ageing human retina. *Eye (Lond)*. 2007;21(1):90-3.
135. Gregory-Evans CY, Wallace VA, Gregory-Evans K. Gene networks: dissecting pathways in retinal development and disease. *Prog Retin Eye Res*. 2013;33:40-66.
136. Baraas RC, Hagen LA, Dees EW, et al. Substitution of isoleucine for threonine at position 190 of S-opsin causes S-cone-function abnormalities. *Vision Res*. 2012;73:1-9.
137. Landsend ECS, Utheim OA, Pedersen HR, et al. The Level of Inflammatory Tear Cytokines is Elevated in Congenital Aniridia and Associated with Meibomian Gland Dysfunction. *Invest Ophthalmol Vis Sci*. 2018;59(5):2197-204.
138. Baraas RC, Hagen LA, Pedersen HR, et al. Doing eye and vision research in a person-centred way. In: McCormack B, van Dulmen S, Eide H, et al., editors. Person-centred healthcare research. 1st ed. Chichester: Willey Blackwell; 2017. p. 183-9.
139. EURORDIS-Rare Diseases Europe. Rare disease patients' participation in research2018. Available from: https://www.eurordis.org/publication/rare-disease-patients-participation-research
140. World Medical Association. World Medical Association Declaration of Helsinki: ethical principles for medical research involving human subjects. *Jama*. 2013;310(20):2191-4.
141. Richards S, Aziz N, Bale S, et al. Standards and guidelines for the interpretation of sequence variants: a joint consensus recommendation of the American College of Medical Genetics and Genomics and the Association for Molecular Pathology. *Genet Med*. 2015;17(5):405-24.
142. Redeker EJ, de Visser AS, Bergen AA, et al. Multiplex ligation-dependent probe amplification (MLPA) enhances the molecular diagnosis of aniridia and related disorders. *Mol Vis*. 2008;14:836-40.
143. Schouten JP, McElgunn CJ, Waaijer R, et al. Relative quantification of 40 nucleic acid sequences by multiplex ligation-dependent probe amplification. *Nucleic Acids Res*. 2002;30(12):e57.
144. Bailey IL, Bullimore MA, Raasch TW, et al. Clinical grading and the effects of scaling. *Invest Ophthalmol Vis Sci*. 1991;32(2):422-32.

145. Bailey IL, Lovie-Kitchin JE. Visual acuity testing. From the laboratory to the clinic. *Vision Res*. 2013;90:2-9.
146. Hendrickson AE, Yuodelis C. The morphological development of the human fovea. *Ophthalmology*. 1984;91(6):603-12.
147. Kass M, Witkin A, Terzopoulos D. Snakes: Active contour models. *International Journal of Computer Vision*. 1988;1(4):321-31.
148. Mishra A, Wong A, Bizheva K, et al. Intra-retinal layer segmentation in optical coherence tomography images. *Opt Express*. 2009;17(26):23719-28.
149. Miller DT, Williams DR, Morris GM, et al. Images of cone photoreceptors in the living human eye. *Vision Res*. 1996;36(8):1067-79.
150. Roorda A. Adaptive optics ophthalmoscopy. *J Refract Surg*. 2000;16(5):S602-7.
151. Dubra A, Sulai Y. Reflective afocal broadband adaptive optics scanning ophthalmoscope. *Biomed Opt Express*. 2011;2(6):1757-68.
152. Delori FC, editor The ANSI 2014 Standard for Safe Use of Lasers. Frontiers in Optics 2014; 2014 2014/10/19; Tucson, Arizona: Optical Society of America.
153. Delori FC, Webb RH, Sliney DH. Maximum permissible exposures for ocular safety (ANSI 2000), with emphasis on ophthalmic devices. *J Opt Soc Am A Opt Image Sci Vis*. 2007;24(5):1250-65.
154. Scoles D, Sulai YN, Dubra A. In vivo dark-field imaging of the retinal pigment epithelium cell mosaic. *Biomed Opt Express*. 2013;4(9):1710-23.
155. Cooper RF, Sulai YN, Dubis AM, et al. Effects of Intraframe Distortion on Measures of Cone Mosaic Geometry from Adaptive Optics Scanning Light Ophthalmoscopy. *Transl Vis Sci Technol*. 2016;5(1):10.
156. Dubra A, Harvey Z. Registration of 2D Images from Fast Scanning Ophthalmic Instruments. In: Fischer B, Dawant BM, Lorenz C, editors. Biomedical Image Registration: 4th International Workshop, WBIR 2010, Lübeck, Germany, July 11-13, 2010 Proceedings. Berlin, Heidelberg: Springer Berlin Heidelberg; 2010. p. 60-71.
157. Liou HL, Brennan NA. Anatomically accurate, finite model eye for optical modeling. *J Opt Soc Am A Opt Image Sci Vis*. 1997;14(8):1684-95.
158. Li KY, Roorda A. Automated identification of cone photoreceptors in adaptive optics retinal images. *J Opt Soc Am A Opt Image Sci Vis*. 2007;24(5):1358-63.
159. Garrioch R, Langlo C, Dubis AM, et al. The Repeatability of In Vivo Parafoveal Cone Density and Spacing Measurements. *Optom Vis Sci*. 2012;89(5):632-43.
160. Souzeau E, Rudkin AK, Dubowsky A, et al. PAX6 molecular analysis and genotype-phenotype correlations in families with aniridia from Australasia and Southeast Asia. *Mol Vis*. 2018;24:261-73.
161. Dubey SK, Mahalaxmi N, Vijayalakshmi P, et al. Mutational analysis and genotype-phenotype correlations in southern Indian patients with sporadic and familial aniridia. *Mol Vis*. 2015;21:88-97.
162. Pakzad-Vaezi K, Keane PA, Cardoso JN, et al. Optical coherence tomography angiography of foveal hypoplasia. *Br J Ophthalmol*. 2017;101(7):985-8.
163. Hofer H, Carroll J, Neitz J, et al. Organization of the human trichromatic cone mosaic. *J Neurosci*. 2005;25(42):9669-79.

164. Hansen T, Pracejus L, Gegenfurtner KR. Color perception in the intermediate periphery of the visual field. *J Vis*. 2009;9(4):26.1-12.
165. Wool LE, Crook JD, Troy JB, et al. Nonselective Wiring Accounts for Red-Green Opponency in Midget Ganglion Cells of the Primate Retina. *J Neurosci*. 2018;38(6):1520-40.
166. Banks MS, Bennett PJ. Optical and photoreceptor immaturities limit the spatial and chromatic vision of human neonates. *J Opt Soc Am A*. 1988;5(12):2059-79.
167. Renner AB, Knau H, Neitz M, et al. Photopigment optical density of the human foveola and a paradoxical senescent increase outside the fovea. *Vis Neurosci*. 2004;21(6):827-34.
168. Eden U, Riise R, Tornqvist K. Corneal involvement in congenital aniridia. *Cornea*. 2010;29(10):1096-102.
169. Lagali N, Eden U, Utheim TP, et al. In vivo morphology of the limbal palisades of vogt correlates with progressive stem cell deficiency in aniridia-related keratopathy. *Invest Ophthalmol Vis Sci*. 2013;54(8):5333-42.
170. Tsai JH, Freeman JM, Chan CC, et al. A progressive anterior fibrosis syndrome in patients with postsurgical congenital aniridia. *Am J Ophthalmol*. 2005;140(6):1075-9.
171. Wang X, Gregory-Evans CY. Nonsense suppression therapies in ocular genetic diseases. *Cell Mol Life Sci*. 2015;72(10):1931-8.
172. Wang X, Gregory-Evans K, Wasan KM, et al. Efficacy of Postnatal In Vivo Nonsense Suppression Therapy in a Pax6 Mouse Model of Aniridia. *Mol Ther Nucleic Acids*. 2017;7:417-28.
173. Gregory-Evans CY, Wang X, Wasan KM, et al. Postnatal manipulation of Pax6 dosage reverses congenital tissue malformation defects. *J Clin Invest*. 2014;124(1):111-6.
174. Sannan NS, Shan X, Gregory-Evans K, et al. Anolis carolinensis as a model to understand the molecular and cellular basis of foveal development. *Exp Eye Res*. 2018;173:138-47.
175. Kozulin P, Natoli R, Bumsted O'Brien KM, et al. The cellular expression of antiangiogenic factors in fetal primate macula. *Invest Ophthalmol Vis Sci*. 2010;51(8):4298-306.
176. Gronskov K, Ek J, Brondum-Nielsen K. Oculocutaneous albinism. *Orphanet J Rare Dis*. 2007;2:43.
177. Landsend ECS, Pedersen HR, Utheim OA, et al. Characteristics and Utility of Fundus Autofluorescence in Congenital Aniridia Using Scanning Laser Ophthalmoscopy. *Invest Ophthalmol Vis Sci*. 2019;60(13):4120-8.
178. Gronskov K, Olsen JH, Sand A, et al. Population-based risk estimates of Wilms tumor in sporadic aniridia. A comprehensive mutation screening procedure of PAX6 identifies 80% of mutations in aniridia. *Hum Genet*. 2001;109(1):11-8.
179. Vasilyeva TA, Voskresenskaya AA, Kasmann-Kellner B, et al. Molecular analysis of patients with aniridia in Russian Federation broadens the spectrum of PAX6 mutations. *Clin Genet*. 2017;92(6):639-44.
180. D'Elia AV, Pellizzari L, Fabbro D, et al. A deletion 3' to the PAX6 gene in familial aniridia cases. *Mol Vis*. 2007;13:1245-50.

181. Wang GM, Prasov L, Al-Hasani H, et al. Phenotypic Variation in a Four-Generation Family with Aniridia Carrying a Novel PAX6 Mutation. *J Ophthalmol*. 2018;2018:5978293.
182. Epstein JA, Glaser T, Cai J, et al. Two independent and interactive DNA-binding subdomains of the Pax6 paired domain are regulated by alternative splicing. *Genes Dev*. 1994;8(17):2022-34.
183. Tarilonte M, Morin M, Ramos P, et al. Parental Mosaicism in PAX6 Causes Intra-Familial Variability: Implications for Genetic Counseling of Congenital Aniridia and Microphthalmia. *Front Genet*. 2018;9:479.
184. Nguyen LS, Wilkinson MF, Gecz J. Nonsense-mediated mRNA decay: inter-individual variability and human disease. *Neurosci Biobehav Rev*. 2014;46 Pt 2:175-86.
185. Mann CJ. Observational research methods. Research design II: cohort, cross sectional, and case-control studies. *Emerg Med J*. 2003;20(1):54-60.
186. Lange C, Feltgen N, Junker B, et al. Resolving the clinical acuity categories "hand motion" and "counting fingers" using the Freiburg Visual Acuity Test (FrACT). *Graefes Arch Clin Exp Ophthalmol*. 2009;247(1):137-42.
187. Bailey IL, Jackson AJ, Minto H, et al. The Berkeley Rudimentary Vision Test. *Optom Vis Sci*. 2012;89(9):1257-64.
188. Marmor MF. Contrast sensitivity versus visual acuity in retinal disease. *The British journal of ophthalmology*. 1986;70(7):553-9.
189. Patterson EJ, Bargary G, Barbur JL. Understanding disability glare: light scatter and retinal illuminance as predictors of sensitivity to contrast. *J Opt Soc Am A Opt Image Sci Vis*. 2015;32(4):576-85.
190. Tregillus KEM, Engel SA. Long-term adaptation to color. *Current Opinion in Behavioral Sciences*. 2019;30:116-21.
191. Engel SA, Wilkins AJ, Mand S, et al. Habitual wearers of colored lenses adapt more rapidly to the color changes the lenses produce. *Vision Research*. 2016;125:41-8.
192. Serbecic N, Beutelspacher SC, Aboul-Enein FC, et al. Reproducibility of high-resolution optical coherence tomography measurements of the nerve fibre layer with the new Heidelberg Spectralis optical coherence tomography. *Br J Ophthalmol*. 2011;95(6):804-10.
193. Lujan BJ, Roorda A, Croskrey JA, et al. Directional optical coherence tomography provides accurate nuclear layer and Henle fiber layer measurements. *Retina*. 2015;35(8):1511-20.
194. Lee DJ, Woertz EN, Visotcky A, et al. The Henle Fiber Layer in Albinism: Comparison to Normal and Relationship to Outer Nuclear Layer Thickness and Foveal Cone Density. *Invest Ophthalmol Vis Sci*. 2018;59(13):5336-48.
195. Sheehy CK, Tiruveedhula P, Sabesan R, et al. Active eye-tracking for an adaptive optics scanning laser ophthalmoscope. *Biomed Opt Express*. 2015;6(7):2412-23.
196. Bamiou DE, Free SL, Sisodiya SM, et al. Auditory interhemispheric transfer deficits, hearing difficulties, and brain magnetic resonance imaging abnormalities in children with congenital aniridia due to PAX6 mutations. *Arch Pediatr Adolesc Med*. 2007;161(5):463-9.

197. Hanish AE, Butman JA, Thomas F, et al. Pineal hypoplasia, reduced melatonin and sleep disturbance in patients with PAX6 haploinsufficiency. *J Sleep Res*. 2016;25(1):16-22.
198. Berntsson SG, Kristoffersson A, Daniilidou M, et al. Aniridia with PAX6 mutations and narcolepsy. *J Sleep Res*. 2020:e12982.
199. Netland PA, Scott ML, Boyle JWt, et al. Ocular and systemic findings in a survey of aniridia subjects. *J AAPOS*. 2011;15(6):562-6.
200. Bjørgum R. Å leve med en usynlig og uforutsigbar funksjonsnedsettelse: erfaringer og opplevelser knyttet til å leve med aniridi [Unpublished Master Thesis]. Kongsberg: University of South-Eastern Norway; 2019.
201. Pedersen HR, Hagen LA, Landsend ES, et al. Color vision, dark adaptation and retinal structure in Aniridia. *Investigative Ophthalmology & Visual Science*. 2016;57(12):623-.

Paper I

Pedersen, H. R., Hagen, L. A., Landsend, E. C. S., Gilson, S. J., Utheim, Ø. A., Utheim, T. P., Neitz M., & Baraas, R. C. (2018). Color Vision in Aniridia. *Investigative Ophthalmology & Visual Science, 59*(5), 2142-2152. doi:10.1167/iovs.17-23047

Color Vision in Aniridia

Hilde R. Pedersen,[1] Lene A. Hagen,[1] Erlend C. S. Landsend,[2] Stuart J. Gilson,[1] Øygunn A. Utheim,[2,3] Tor P. Utheim,[1–4] Maureen Neitz,[5] and Rigmor C. Baraas[1]

[1]National Centre for Optics, Vision and Eye Care, Faculty of Health and Social Sciences, University College of Southeast Norway, Kongsberg, Norway
[2]Department of Ophthalmology, Oslo University Hospital, Oslo, Norway
[3]Department of Medical Biochemistry, Oslo University Hospital, Oslo, Norway
[4]Department of Ophthalmology, Drammen Hospital, Drammen, Norway
[5]Department of Ophthalmology, University of Washington, Seattle, Washington, United States

Correspondence: Rigmor C. Baraas, National Centre for Optics, Vision and Eye Care, Faculty of Health and Social Sciences, University College of Southeast Norway, Kongsberg, Norway;
rigmor.baraas@usn.no.

Submitted: September 25, 2017
Accepted: March 27, 2018

Citation: Pedersen HR, Hagen LA, Landsend ECS, et al. Color vision in aniridia. *Invest Ophthalmol Vis Sci*. 2018;59:2142–2152. https://doi.org/10.1167/iovs.17-23047

Purpose. To assess color vision and its association with retinal structure in persons with congenital aniridia.

Methods. We included 36 persons with congenital aniridia (10–66 years), and 52 healthy, normal trichromatic controls (10–74 years) in the study. Color vision was assessed with Hardy-Rand-Rittler (HRR) pseudo-isochromatic plates (4th ed., 2002); Cambridge Color Test and a low-vision version of the Color Assessment and Diagnosis test (CAD-LV). Cone-opsin genes were analyzed to confirm normal versus congenital color vision deficiencies. Visual acuity and ocular media opacities were assessed. The central 30° of both eyes were imaged with the Heidelberg Spectralis OCT2 to grade the severity of foveal hypoplasia (FH, normal to complete: 0–4).

Results. Five participants with aniridia had cone opsin genes conferring deutan color vision deficiency and were excluded from further analysis. Of the 31 with aniridia and normal opsin genes, 11 made two or more red-green (RG) errors on HRR, four of whom also made yellow-blue (YB) errors; one made YB errors only. A total of 19 participants had higher CAD-LV RG thresholds, of which eight also had higher CAD-LV YB thresholds, than normal controls. In aniridia, the thresholds were higher along the RG than the YB axis, and those with a complete FH had significantly higher RG thresholds than those with mild FH ($P = 0.038$). Additional increase in YB threshold was associated with secondary ocular pathology.

Conclusions. Arrested foveal formation and associated alterations in retinal processing are likely to be the primary reason for impaired red-green color vision in aniridia.

Keywords: aniridia, color vision, foveal hypoplasia, retinal development

The reported prevalence of congenital aniridia in Norway and Sweden is about 1:72,000.[1] Characteristic features in aniridia include absence or hypoplasia of the iris, foveal hypoplasia (FH) and nystagmus, while optic nerve hypoplasia (ONH) occurs but is less common.[2,3] Aniridia may lead to severe visual impairment, although there is considerable phenotypic variation between and within families.[4,5] Secondary progressive ocular complications, such as aniridia associated keratopathy (AAK), cataract, and glaucoma, are common from adolescence and onward.[4,6,7]

Aniridia-like phenotypes may be caused by mutations in genes such as *FOXC1* and *PITX2*,[8] but typically (>85%) it is caused by loss of one functional copy of the *PAX6* gene,[9] with about one-third of cases being sporadic and two-thirds being inherited as an autosomal-dominant trait.[10] The *PAX6* gene is located on chromosome band 11p13 and regulates transcription of other genes important for ocular development. Gene dysfunction may affect multiple ocular structures.[11] Aniridia phenotypes caused by *PAX6* mutations are associated with different degrees of foveal hypoplasia, most commonly to a degree of no foveal avascular zone (FAZ) and no foveal depression.[12,13] It is known that *Pax6* acts on several target genes required for retinal ganglion cell development and retina neurogenesis.[14,15] *PAX6/Pax6* dosage expression varies during normal development,[16–18] and animal studies show that abnormal *PAX6/Pax6* expression affects the distribution, development, and the balance of different types of retinal cells.[17,19]

Normal foveal development depends on a high ganglion cell count within the central retina[20] and is characterized by formation of a FAZ before the foveal depression is formed, displacement of the inner retinal layers and postnatal elongation and migration of cones toward the center of the fovea.[21–23] Trichromatic color vision requires a normally developed healthy functioning retina containing cone photoreceptors with three different opsins (L, M, and S cones),[24] including specialized postreceptoral interaction with other retinal neurons (bipolar, amacrine, horizontal, and ganglion cells).[25] During human fetal retinal development, S cones appear earlier than L and M cones,[26] with S cones present around the start of FAZ development and before the foveal depression develops.[27] Disruptions in foveal development that occur around this time may therefore affect L and M cone development, density and its associated retinal circuitry, limiting the number of bipolar and horizontal cell contacts needed for normal red-green vision, more so than for blue-yellow vision. Thus, it is

reasonable to hypothesize that foveal hypoplasia associated with aniridia could affect red-green color discrimination.

Here, results are reported from experiments using computerized color vision tests together with retinal imaging (OCT and color fundus photo) to examine color vision and retinal layer structure in persons with congenital aniridia. These experiments provide insight into the association between the degree of arrested foveal formation in aniridia and impairment of red-green color vision and how this is accompanied by impairment of yellow-blue color vision when secondary pathology is advanced.

Methods

Participants

We recruited 36 participants previously diagnosed with congenital aniridia (15 males), aged between 9 and 72 years, and 52 healthy, normal trichromatic controls (21 males), aged between 10 and 74 years, to the study. Participants with aniridia were recruited through the Norwegian Association of Aniridia, whereas normal controls were recruited through the National Centre for Optics, Vision and Eye Care, University College of Southeast Norway. The study was conducted in accordance with the tenets of the Declaration of Helsinki and was approved by the Regional Committee for Medical and Health Research Ethics (Southern Norway Regional Health Authority). All participants and/or their guardians signed informed consent after full explanation of the study's purpose and procedures.

Clinical Assessment

The participants underwent an eye examination including subjective refraction, slit-lamp biomicroscopy, and color fundus photography (Topcon TRC-NW6S nonmydriatic fundus camera; Topcon Corp., Tokyo, Japan). Monocular visual acuity (logMAR) was measured with a digital high-contrast chart at 6 m (TestChart 2000; Thomson Software Solutions, London, UK). The test distance was reduced to 3 or 1 m if a reliable measurement could not be obtained at the longer distance. Color vision was screened binocularly with the Hardy-Rand-Rittler 4th edition (HRR; Richmond Products, Albuquerque, NM, USA) pseudoisochromatic plates using previously described methods.[28] Those who made two or more errors on red-green (RG) screening plates on the second sitting were tested with the RG diagnostic plates and classified to have mild, medium, or strong RG deficiency depending on errors made on these plates. Those who made one or more errors on the yellow-blue (YB) screening plates on the second sitting were classified as mild, and if errors were made on the YB diagnostic plates, they were classified to have medium or strong YB deficiency depending on errors made on these plates.

The clarity of the lens was evaluated using the Lens Opacities Classification System III (LOCS III).[29] AAK was graded 0 to 3 where stage 0 indicated that the cornea was not affected; stage 1 indicated a partially affected corneal limbus; stage 2 indicated a totally affected limbus, without central corneal involvement; and stage 3 indicated a totally affected limbus with central corneal opacification.[30] ONH was evaluated as present or not based on funduscopy, estimated by the ratio of disc-to-fovea distance and disc diameter (average of horizontal and vertical), and confirmed by measurements on color fundus photographs.[31,32] ONH was defined as present when the ratio was >3.5, meaning that >3.5 optic discs could be apposed between the expected foveal center and the border of the optic disc. Borderline cases were also evaluated based on appearance of the optic disc, and ONH was defined as present if the optic nerve head was obviously small or if the disc showed a typical double ring sign. Glaucoma was noted as present or not based on previous ocular history and treatment.

Foveal Hypoplasia

Foveal hypoplasia was assessed by analyzing structural alterations on spectral domain optical coherence tomography (SD-OCT) images acquired with an OCT2 device (Spectralis; Heidelberg Engineering GmbH, Heidelberg, Germany). Volumetric scans, either $20^\circ \times 20^\circ$ or $30^\circ \times 10^\circ$ (consisting of 49 B-scans and 512–1536 A-scans/B-scan) were centered at the expected foveal center. Between 5 and 20 B-scans (frames) were averaged during acquisition to improve signal-to-noise ratio and compensate for eye motion (TruTrack; Heidelberg Engineering GmbH). Horizontal line scans, with a nominal scan length of 30°, were obtained in eyes where macular volumes could not be obtained. Multiple scans were acquired in the region of the expected foveal location to look for signs of foveal specialization.[21,33,34] The lateral scale of all OCT scans was corrected for individual retinal magnification factor by multiplying the nominal scan length with the ratio between each individual's axial length, obtained with the IOL Master (Carl Zeiss Meditec AG, Jena, Germany), and the OCT default axial length (24 mm).

Horizontal line scans were segmented at the inner limiting membrane (ILM); posterior boundary of the outer plexiform layer (OPL); center of the external limiting membrane (ELM); center of the ellipsoid zone (EZ); center of the interdigitation zone (IZ); and the retinal pigment epithelium-Bruch's Membrane (RPE-BrM) band, using custom software implementing a method similar to that used by Park et al.[35] The foveal center was defined as the section with the minimal foveal thickness (ILM to RPE-BrM) within the foveal depression. When no pit was present, the maximum widening of the outer nuclear layer (OPL to ELM) and/or lengthening of the photoreceptor outer segments (EZ to IZ) was used to identify the expected foveal center. Individual OCT line scans through the foveal center were used to grade foveal hypoplasia in participants with aniridia following the criteria suggested by Thomas et al.[36]: absence of extrusion of plexiform layers (grade 1); grade 1 plus absence of foveal depression (grade 2); grade 2 plus absence of outer segment lengthening (grade 3); and grade 3 plus absence of outer nuclear layer widening (grade 4).

Color Vision

Color vision was examined with a low vision version of the Color Assessment and Diagnosis (CAD-LV) test (City Occupational Ltd., London, UK). The CAD test has been used to examine both congenital[37] and acquired color vision deficiencies,[38,39] and is validated with a reported high test-retest reliability.[40] To ascertain the degree of noncongenital deficiencies and elucidate if it was receptoral or postreceptoral in origin, some participants were invited to do the Cambridge Color Test (CCT; Cambridge Research Systems Ltd., Cambridge, UK), and anomaloscope (HMC Oculus Anomaloscope MR, Type 47700; Oculus Optikgeräte GmbH, Wetzlar, Germany). All participants wore the appropriate refractive correction as determined during the initial clinical assessment.

Color Assessment and Diagnosis Test

The normal controls and 31 of the participants with aniridia were tested with the CAD. The CAD test measures red-green (RG) and yellow-blue (YB) color detection thresholds with a chromatic, moving isoluminant stimulus embedded in a

background of dynamic luminance contrast noise.[41–43] Chromatic thresholds were measured using a 4-alternative-forced-choice method along 16 hue directions in the CIE 1931 (x, y) chromaticity diagram.[44] The test conditions were altered to compensate for low vision (LV) in aniridia—the stimulus was double its default size and moved slower to compensate for reduced visual acuity. That is, the stationary achromatic square array of 15×15 checkers subtended $5.7° \times 5.7°$ in visual angle and the smaller moving chromatic square array of 5×5 checkers subtended $1.8° \times 1.8°$ visual angle at a distance of 140 cm. The temporal frequency was 50% lower than the default setting, and random luminance modulation was increased by 100% to mask the detection of rod-mediated signals that might be introduced by the larger stimulus. Background luminance was 24 cd/m^2. The monitor (SpectraView PA241W; NED Display Solutions, Itasca, IL, USA) was calibrated daily using a photometer (Gossen Mavo Monitor USB, CO Ltd., Nürnberg, Germany).

Median RG and YB thresholds, represented as chromatic difference (CD) from the background chromaticity ($x = 0.305$, $y = 0.323$), were computed.[45] The test was performed binocularly to minimize nystagmus and to indicate overall functional performance, and took 10–12 minutes to complete. As a control, RG and YB thresholds were also measured at a lower luminance level (2.4 cd/m^2; a 1.0 spectrally calibrated neutral density filter was added in front of each eye) for a subset of normal controls ($n = 38$, age 10–67 years).

Cambridge Color Test

The normal controls and 16 of the participants with aniridia (age 11–66 years, logMAR 0.00–0.90) were tested with the CCT Trivector test following standard procedures.[46,47] The test was performed binocularly and took 3 to 4 minutes to complete. Participants were tested twice, and average thresholds were used for analysis. The CCT is a computer-based pseudo-isochromatic test and the stimuli were generated via a graphics system (VSG ViSaGe; Cambridge Research Systems Ltd., Rochester, UK) and presented on a 22-inch CRT monitor (LaCie Electron 22blueIV; LaCie Group, Paris, France). The luminance and chromaticity of the monitor were checked daily with a colorimeter (PR650 Spectra; Photo Research, Inc., Chatsworth, MA, USA). The target was a Landolt-C with inner and outer diameters of 2.2° and 4.3°, respectively, and a gap size of 1° visual angle presented at a test distance of 305 cm. The gap position varied randomly from trial to trial (up, down, left, right), and the observer's task was to indicate the position of the gap by pushing the correct button on a response box within 3 seconds. The test employed a staircase method (11 reversals) for measuring color-discrimination thresholds in three directions along the protan, deutan, and tritan confusion axes in the CIE 1976 (u', v') chromaticity diagram. The maximum color-vector length was set to 0.1600 units. The mean of the last six reversals was taken as the threshold.

Rayleigh Color Match

Ten participants with aniridia performed the Rayleigh color match (Oculus Optikgeräte GmbH) using their best eye. The Rayleigh stimulus is a 2° circular field divided in two semicircles. The upper part is the color-mixture field with a mixture of green (545 nm) and red (671 nm) light, and the lower part is the reference field with yellow light (589 nm). Using the procedure suggested by Linksz,[48] the participant's first task was to find the metameric match between the upper and lower fields by adjusting the luminance of the monochromatic yellow reference field and the relative amounts of red and green light in the mixture field. Theoretically, this is the match that produces the same set of quantum catches at the level of the photoreceptors.[49] This first match was used as the starting point for finding the matching range. Several different relative amounts of red and green light in the mixture field were set by the operator using a staircase procedure, and the participant's task was to judge whether each of them appeared uniform or not by adjusting the luminance of the reference field. The matching range was taken as the difference between the highest and the lowest red/green ratio that the participant would accept after making his/her own luminance adjustments. The mean match midpoint ± SD and matching range for color normal observers for this particular instrument is 40.3 ± 1.91 and 2.01 ± 1.09.[50] A person with a protan deficiency requires more red to match the yellow reference field resulting in a higher than normal match midpoint, whereas someone with a deutan deficiency requires more green resulting in a lower than normal match midpoint. Larger than normal matching ranges signify poorer discrimination, with dichromats accepting all mixture ratios as metameric if the luminance is adjusted appropriately.

Genetic Analysis

All participants, with the exception of participants 5119 and 5124, gave saliva samples (Oragene-DNA, OG-500, DNA Self-Collection Kit; DNA Genotek, Inc., Ottawa, ON, Canada) for genetic analysis of cone opsin gene mutations known to be associated with congenital color vision deficiencies.[24,51] In order to detect genetic evidence of a red-green color vision deficiency, DNA was isolated from saliva samples, and a genotyping performed using a previously described assay.[51] DNA was also used in the PCR to amplify exons 2 through 5 of the L and M opsin genes separately, and exons 2, 3, and 4 were directly sequenced.[28] To identify/confirm the genetic cause of aniridia for each participant, the *PAX6* gene was amplified and sequenced using PCR primers and conditions that were described previously.[52] Fluorescent DNA sequencing was performed on both DNA strands. For participants who were negative for *PAX6* mutations, exons and intron/exon junctions of the *PITX2* and *FOXC1* genes were amplified and sequenced using the PCR primers described by Ansari et al.[53]

Data Analysis

Statistical analysis were performed with R (v3.3.2), R Foundation for Statistical Computing, Vienna, Austria.[54] The data for the aniridia group was found to be nonnormally distributed, as verified by histograms and q-q plots. The nonparametric Mann-Whitney U test was applied for independent samples and the Wilcoxon signed-rank test for paired samples. Correlations were assessed with Spearman correlation coefficients (r_s). Between-group differences were examined with Kruskal-Wallis 1-way ANOVA. The significance level was set to $P \leq 0.05$. Bonferroni-corrected P values are reported for multiple comparisons. Bland-Altman plots were used to compare the CAD and CCT measurements with the nonparametric limits of agreement estimated as the 2.5 and 97.5 quantiles of the differences and the average bias estimated as the median of the differences. The statistical normal limits for the CAD-LV test were computed based on the median color discrimination threshold and the 2.5% quantile and 97.5% quantile (giving a 95% interquantile range) for the normal controls in the study. A quantile regression was conducted to estimate and plot a curve to the median, 2.5% and 97.5% quantiles as a function of age using the quantreg v5.33 package for R.[55] CAD-LV units were calculated to assess the severity of color vision loss in aniridia, dividing the aniridia thresholds by the normal median RG and YB thresholds (based on data from

Table 1. Age Distribution and Number of Participants in Each Age Group

	Aniridia			Normal Controls		
Age Group	*n*	Median Age	Age Range	*n*	Median Age	Age Range
<20	7	12	9–19	11	14	10–19
20–29	9	24	20–29	15	23	20–27
30–49	9	40	31–49	11	41	32–47
50–59	3	51	50–56	5	55	51–58
>60	3	66	64–67	10	67.5	62–74

our 52 controls), respectively. Both thresholds represented as CD $\times 10^4$ and thresholds expressed as CAD-LV units were used for analysis.

Results

Clinical Assessment and Genetics

A total of 31 of 36 participants with aniridia (aged 10–67 years, 12 males) had cone opsin genes known to be associated with normal color vision, including four female carriers of deutan color vision deficiency. Five males with aniridia were excluded from further analysis as they were confirmed to have cone opsin genes conferring congenital deutan color vision deficiency. Table 1 shows the age distribution for all the study participants.

Those with normal opsin genes had corrected visual acuity 0.00 to 1.76 logMAR in their best eye; 11 (35.5%) of these made two or more RG errors on the HRR, four (12.9%) of which also made YB errors, while one (3.2%) made YB errors only. Summary of clinical findings and color vision test results for the participants with aniridia are presented in Tables 2 and 3. The participants who were negative for *PAX6* mutations, were also negative for disease-causing mutations in both the *PITX2* and *FOXC1* genes.

All 52 normal controls had cone opsin genes known to be associated with normal color vision, including five female carriers of deutan color vision deficiency. None of the normal controls made more than one error on the HRR; only two made one error on plate 7 (the most difficult RG screening plate). Their corrected visual acuity was 0.16 logMAR or better in their dominant eye. The controls were healthy with no known systemic disease or ocular abnormalities. Clinical assessment, color fundus photography, and OCT imaging were performed on each participant, and all controls were found to be healthy and free of eye disease. Nuclear opalescence, nuclear color grade, cortical- and posterior subcapsular cataract were graded

Table 2. Summary of Clinical Findings for the Participants With Aniridia*

ID	Age	Genetic Mutation	Visual Acuity,† logMAR	Nystagmus	Aniridia Associated Keratopathy, Grade	Foveal Hypoplasia, Grade	Optic Nerve Hypoplasia	Glaucoma	Lens Status
5124	23	N/A	0.40	N	0	0	N	N	Phakic
5139	15	Unknown	0.00	N	0	0	N	N	Phakic
5132	64	Unknown	0.56	N	0	1	N	Y	Pseudophakic
5134	49	Unknown	0.18	N	1	1	N	N	Pseudophakic
5116	66	*PAX6*	0.40	N	2	2	N	N	Pseudophakic
5120	42	*PAX6*	0.22	N	1	2	N	N	Phakic
5123	24	*PAX6*	0.50	N	2	2	N	N	Phakic
5154	24	Unknown	0.72	Y	1	2	N	N	Phakic
5114	56	*PAX6*	0.86	Y	1	3	Y	Y	Aphakic
5125	15	*PAX6*	0.74	Y	1	3	N	Y	Phakic
5126	12	*PAX6*	0.80	Y	1	3	N	Y	Phakic
5135	40	*PAX6*	0.70	Y	1	3	Y	Y	Phakic
5137	20	*PAX6*	0.70	Y	1	3	N	N	Phakic
5144	32	*PAX6*	0.74	Y	2	3	N	Y	Pseudophakic
5147	11	Unknown	0.50	Y	2	3	N	N	Phakic
5148	49	*PAX6*	0.60	N	2	3	N	Y	Pseudophakic
5113	32	*PAX6*	0.80	Y	2	4	N	N	Phakic
5117	20	Unknown	1.00	Y	2	4	N	Y	Pseudophakic
5119	9	N/A	1.00	Y	1	4	N	Y	Phakic
5127	41	*PAX6*	1.20	Y	2	4	N	Y	Pseudophakic
5131	29	*PAX6*	1.30	Y	1	4	Y	Y	Aphakic
5138	11	*PAX6*	0.90	Y	1	4	N	N	Phakic
5140	19	*PAX6*	0.70	Y	2	4	N	N	Phakic
5141	23	*PAX6*	1.00	Y	2	4	N	N	Phakic
5149	31	*PAX6*	0.90	Y	2	4	N/A	N	Phakic
5110	50	*PAX6*	1.00	Y	3	N/A	Y	Y	Pseudophakic
5118	25	*PAX6*	0.74	Y	3	N/A	N	Y	Pseudophakic
5121	51	*PAX6*	CF	Y	3	N/A	N	N	Phakic
5129	67	*PAX6*	1.30	Y	3	N/A	N	Y	Aphakic
5145	36	*PAX6*	1.76	Y	3	N/A	N/A	N	Pseudophakic
5152	26	Unknown	1.30	Y	3	N/A	N/A	Y	Phakic

CF, counting fingers at 0.5 m; N, no; Y, yes; N/A, not applicable.
* The participants are ordered by the grade of foveal hypoplasia.
† Measured with their best eye.

Table 3. Summary of Color Vision Test Results for the Participants With Aniridia*

		CAD-LV Threshold (CD × 10^4), $n = 27$		CCT, $n = 16$			Rayleigh Match, $n = 10$		HRR, $n = 31$	
ID	Age	RG	YB	Protan	Deutan	Tritan	Midpoint	Range	RG	YB
5124	23	N/A	N/A	–	–	–	–	–	Normal	Normal
5139	15	84	134	50	64	62	–	–	Normal	Normal
5132	64	183	327	296	328	1186	46.2	6.0	Mild	Normal
5134	49	93	193	–	–	–	–	–	Normal	Normal
5116	66	116	170	146	131	133	45.7	4.9	Normal	Normal
5120	42	50	113	84	81	92	41.0	5.1	Normal	Normal
5123	24	118	221	79	86	168	40.2	4.2	Normal	Normal
5154	24	110	167	41	54	72	–	–	Normal	Normal
5114	56	434	1198	320	407	1398	–	–	Medium	Mild
5125	15	196	317	73	74	103	–	–	Normal	Normal
5126	12	94	159	130	121	117	42.6	4.3	Normal	Normal
5135	40	123	187	153	218	286	42.2	6.6	Normal	Normal
5137	20	93	166	136	142	737	44.9	4.0	Normal	Normal
5144	32	104	144	–	–	–	–	–	Normal	Normal
5147	11	143	216	132	128	210	44.4	7.4	Mild	Normal
5148	49	192	497	96	149	1076	44.1	11.4	Mild	Mild
5113	32	154	177	128	120	115	–	–	Mild	Normal
5117	20	186	231	–	–	–	–	–	Normal	Normal
5119	9	N/A	N/A	–	–	–	–	–	Normal	Normal
5127	41	239	210	–	–	–	–	–	Mild	Normal
5131	29	197	154	–	–	–	–	–	Medium	Normal
5138	11	80	141	182	157	192	–	–	Normal	Normal
5140	19	133	213	–	–	–	–	–	Normal	Normal
5141	23	231	238	–	–	–	–	–	Normal	Normal
5149	31	181	277	–	–	–	–	–	Normal	Normal
5110	50	119	213	–	–	–	–	–	Normal	Normal
5118	25	220	848	141	154	739	40.5	7.8	Normal	Mild
5121	51	N/A	N/A	–	–	–	–	–	Mild	Strong
5129	67	621	1292	–	–	–	–	–	Medium	Mild
5145	36	124	196	–	–	–	–	–	Mild	Normal
5152	26	N/A	N/A	–	–	–	–	–	Mild	Normal

N/A, not applicable; RG, red-green; YB, yellow-blue.
* The participants are ordered by the grade of foveal hypoplasia (as in Table 2).

and found to be lower than NO2, NC4, C2, and P0 (LOCS III), respectively. None of the normal controls had undergone cataract surgery.

Color Vision

Figure 1 shows RG and YB CAD-LV thresholds for 27 participants with aniridia (circles) and 52 normal controls (squares) as a function of age. Four participants with aniridia were unable to complete the CAD-LV test, either because of too poor vision ($n = 2$) or of other reasons ($n = 2$; one child and one with cerebral palsy).

RG and YB CAD-LV thresholds for normal controls decreased with increasing age from 10 to 20 years, and YB CAD-LV thresholds increased with increasing age from about 50 years. The median (2.5–97.5% quantile) CAD-LV RG and YB thresholds for the normal controls were 72.7 (45.7–112.4) CD × 10^4 and 163.2 (104.2–256.3) CD × 10^4, respectively. CAD-LV RG and YB thresholds were higher when measured at the mesopic light level (2.4 cd/m^2), with a median (2.5%–97.5% quantile) difference between the two tests of 27.8 (5.3–71.8) and 49.1 (–1.0 to 265.4) CD×10^4, respectively. The median (2.5%–97.5% quantile) thresholds along the protan, deutan and tritan confusion axes for the CCT were 58.5 (31.0–118.6), 56.0 (31.7–99.3) and 83.5 (39.0–257.5) respectively for normal controls.

RG and YB CAD-LV thresholds were significantly higher for those with aniridia compared with age-matched normal controls (Mann-Whitney U test: RG: $P < 0.001$, YB: $P = 0.002$). A total of 19 participants with aniridia had RG thresholds that were higher than the 97.5% quantile that was defined as the upper normal limit based our normal control data, of whom seven also had YB thresholds higher than the 97.5% quantile. None had higher YB threshold than the upper normal limit only. Figure 2 shows CAD-LV YB thresholds as a function of RG thresholds; both calculated as CAD-LV standard units. CAD-LV RG thresholds were significantly higher than the CAD-LV YB thresholds ($Z = 3.1$, $P = 0.001$) in aniridia (Fig. 2).

CCT RG threshold was calculated as the mean of the protan and deutan thresholds. There was good agreement between the CAD-LV and the CCT test, but both RG and YB median CAD-LV were higher than the median CCT thresholds. The median RG difference (CAD-CCT threshold) was 12.2 and 19.7 for normal controls and participants with aniridia, respectively (Fig. 3). The median YB differences in thresholds were 69.5 and 28.9, respectively. However, for three of the participants with aniridia, the CCT tritan thresholds were more than twice as high as their CAD-LV YB threshold.

Ten of those with aniridia agreed to be measured with Rayleigh anomaloscopy. The median matching midpoint was 43.3 (range, 40.2–46.2), with a median matching range of 5.6 (range, 4.0–11.4).

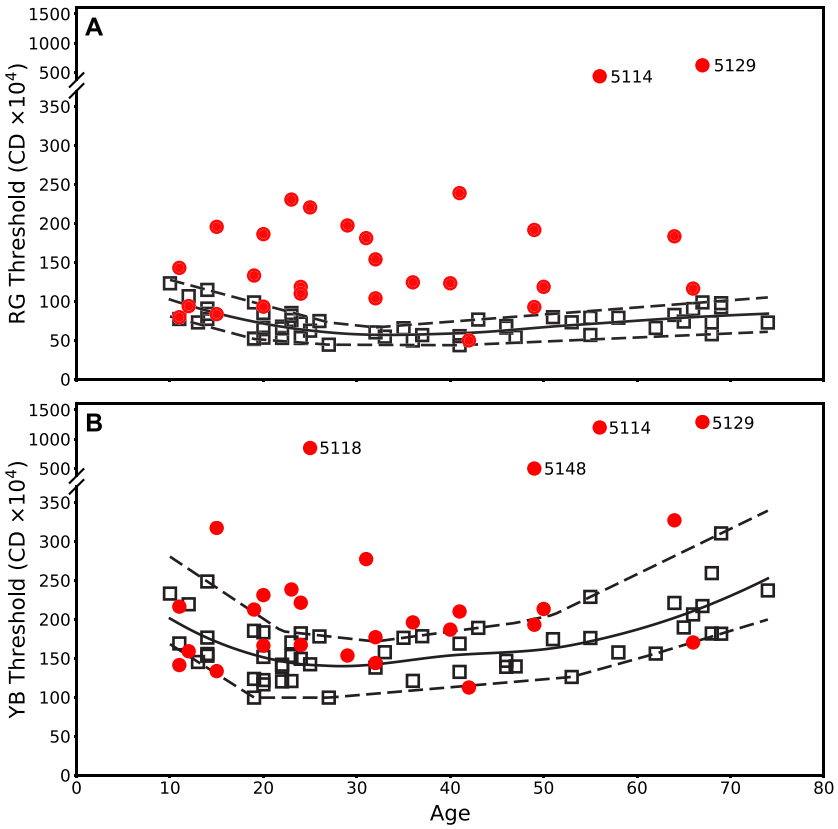

FIGURE 1. (**A**) CAD-LV RG and (**B**) YB thresholds as a function of age for each observer with aniridia (*filled circles*) and normal controls (*open squares*). The *solid line* shows the fitted median and the *dotted lines* represent the 2.5% and 97.5% quantile estimated with a quantile regression for the normal controls. For clarity, observers with extremely high thresholds (*labeled*) are shown on an extended *y*-axis.

Foveal Hypoplasia and Color Vision in Aniridia

Figure 4 shows OCT scans from five participants with aniridia and foveal hypoplasia grade from 0 to 4. Foveal hypoplasia was observed in 23 of the 25 participants with aniridia imaged with OCT (six had too severe nystagmus and/or ocular media opacities to allow imaging). Two participants had grade 1, four grade 2, eight grade 3 and nine grade 4. One participant had intermediate age-related macular degeneration (which made correct foveal grading difficult) and was, therefore, excluded from the analysis which included structural changes and visual function.

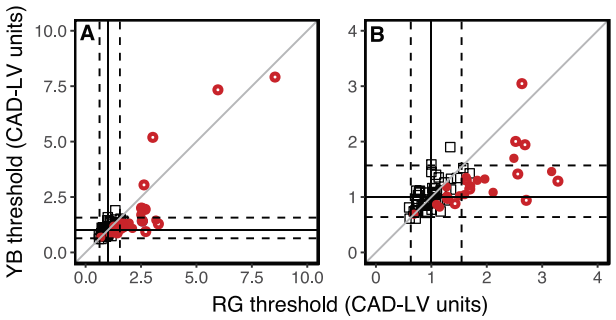

FIGURE 2. CAD-LV RG and YB threshold for participants with aniridia (*filled circles*), aniridia and secondary glaucoma (*open circles*) and normal controls (*open squares*). Median, 2.5% and 97.5% quantiles for the normal controls are marked. Thresholds are presented in CAD-LV standard units, calculated by dividing the thresholds by the normal median values for RG and YB threshold, respectively. (**A**) All data included, (**B**) Only CV-LV units < 4 units included for better visualization of the individual data points.

There was a strong correlation between the grade of foveal hypoplasia and visual acuity ($r_s = 0.859$, $P < 0.001$). A positive correlation was found between grade of foveal hypoplasia and CAD-LV RG threshold ($r_s = 0.558$, $P = 0.007$), but not for CAD-LV YB threshold ($r_s = 0.255$, $P = 0.252$). Those with foveal hypoplasia grade 0–2 (mild) were grouped and compared with those with grade 3 (moderate) and grade 4 (complete) for between-group comparisons (Fig. 5). Kruskal-Wallis ANOVA revealed a significant difference in CAD-LV RG thresholds between the grades of FH ($\chi^2 = 6.876$, $df = 2$, $P = 0.032$). Those with complete FH (grade 4) had significantly higher CAD-LV RG thresholds than those with mild FH (grade 0–2; $P = 0.038$) (Fig. 5A).

Secondary Pathology and Color Vision in Aniridia

Thirteen of the 27 (48%) participants with aniridia who performed the CAD-LV test had previously been diagnosed with glaucoma and/or ocular hypertension. Six of these had higher than normal thresholds for both CAD-LV RG and YB. Five of these six were also tested on the CCT, and four had higher than normal thresholds for both CCT RG and YB (ID: 5132, 5114, 5148, 5118). The only person without glaucoma who had higher than normal thresholds for both CAD-LV RG and YB (5149) had severe cortical and posterior subcapsular opacification of the lens. The participants with aniridia and the highest thresholds for both CAD-LV RG and YB had either ONH in addition to glaucoma (5114) or high-grade keratopathy in addition to glaucoma (5129, 5118). The other three with ONH had only increased RG threshold.

Kruskal-Wallis ANOVA indicated a difference in CAD-LV YB thresholds between the three AAK severity groups (mild: grade 0–1; moderate: grade 2; severe: grade 3; $\chi^2 = 6.749$, $df = 2$, $P =$

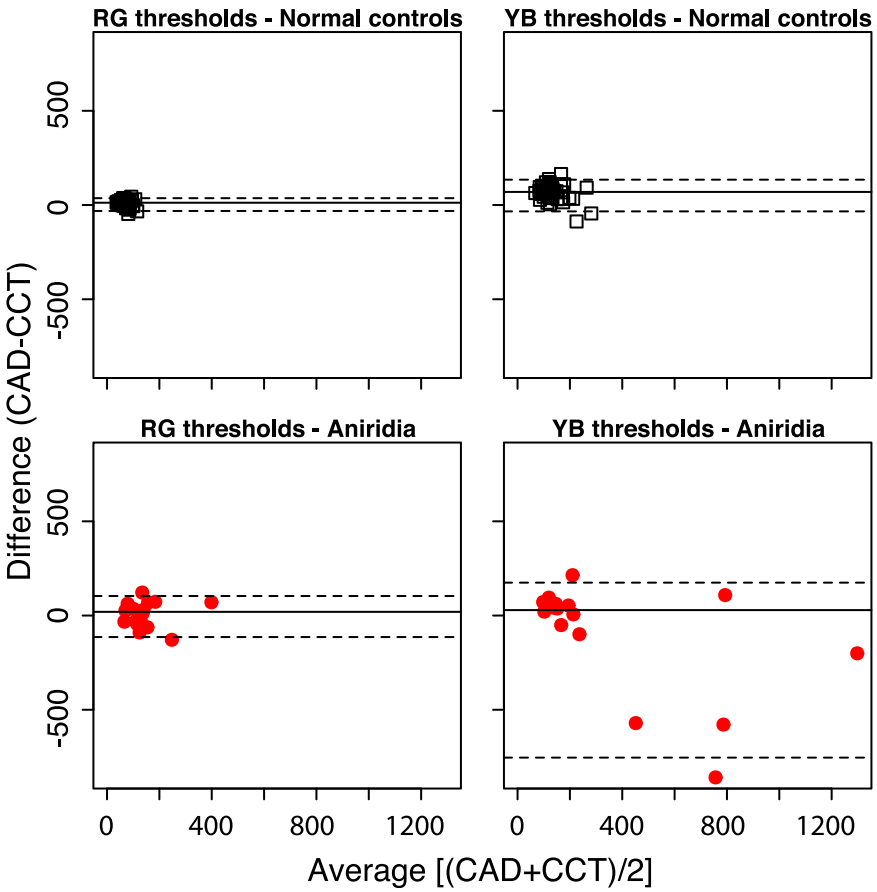

FIGURE 3. Bland-Altman plots that show the agreement between CAD and CCT. The average [(CAD+CCT/2)] is plotted against the differences (CAD-CCT) for each color discrimination axis for normal controls (*upper row*, *open squares*) and observers with aniridia (*bottom row*, *filled circles*). The *black solid line* represents the median difference, and the *dotted lines* are 2.5% and 97.5% quantiles of the difference.

0.034), but post hoc pairwise comparisons failed to reveal any significant differences (mild/moderate: $P = 0.167$, mild/severe: $P = 0.079$) (Fig. 5D). Note that 12 of 13 with glaucoma also had AAK, and if the 13 with glaucoma were removed from the analysis, only one of the remaining with AAK (5149) had higher than normal CAD-LV YB threshold. The person with glaucoma and no AAK (5132) had higher than normal CAD-LV YB threshold. There were no significant differences in CAD-LV RG thresholds between any of the AAK severity groups (mild/moderate and mild/severe: $P = 0.23$) (Fig. 5C).

Evaluation of lens opacities based on LOCS III grading was only applicable for persons with at least one phakic eye ($n = 18$). Total grading score showed no significant correlation with either RG or YB CAD-LV thresholds ($r_s = 0.296$, $P = 0.305$ and $r_s = 0.252$, $P = 0.384$, respectively).

DISCUSSION

The results presented here show that persons with aniridia exhibit a quantifiable loss of color vision. The greatest loss was in RG color discrimination, which was positively correlated with the grade of foveal hypoplasia. Additional loss was observed in YB color discrimination, but this was associated with secondary ocular pathology, usually glaucoma. Color vision is known to vary as a function of age with maximum sensitivity around 20 years of age, thought to reflect normal healthy development and maturation of the visual system.[56–58] The gradual increase in color discrimination from childhood until early adulthood can be observed for the normal controls in this study, but not for those with aniridia. These findings suggest that a likely reason for loss of red-green color vision in aniridia is arrested foveal formation and associated alterations in retinal structure and processing.

Loss of color vision has been described on one occasion previously, in a family with 11 members with congenital aniridia.[59] We show that loss of RG and YB color vision is frequent in aniridia but cannot always be detected with the HRR pseudoisochromatic plates. Computerized tests, that allow for more accurate measures of chromatic discrimination such as the CAD-LV or the CCT, are required to quantify the loss. General loss in red-green discrimination was also observed for the Rayleigh match, with matching midpoints within normal limits for all except two, but matching ranges more than 2 standard deviations larger than for normal trichromats.[50]

The majority of persons with aniridia ($n = 23$) in this study exhibited the same variation in the degree of foveal hypoplasia (grades 1–4) as previously described for aniridia caused by *PAX6* mutations.[13,36,60] Only two participants had grade 0, both with clearly defined FAZ and RG thresholds within the normal range. Those with complete FH had significantly higher RG thresholds than those with mild FH. There was no association between age, RG thresholds, and FH grade. The degree of FH is most likely associated with the timing of arrested foveal formation,[22,26] resulting in a lower number of L and M cones in the fovea, and foveal cones that are more similar to the peripheral cones with shorter cone outer segments[26] and decreased cone photopigment optical densi-

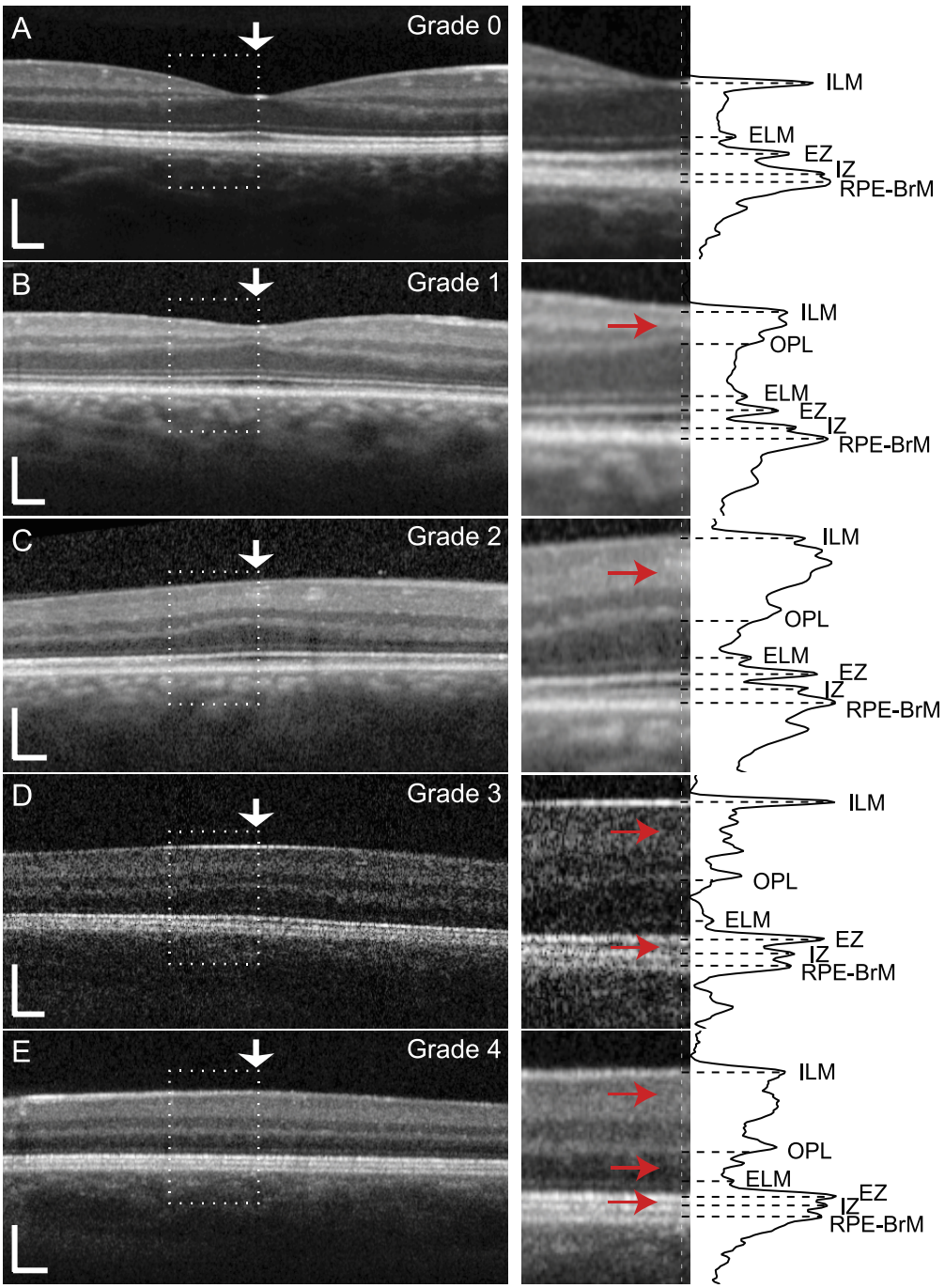

Figure 4. OCT scans from the central 10° of five participants with aniridia (**A–E**) showing the grades (0–4) of foveal hypoplasia.[36] The *dotted rectangle* delineates the ×2 magnified area represented on the right. The marked retinal layers were segmented and analyzed using longitudinal reflectivity profiles averaged over a 5-pixel wide region positioned at the foveal center (*vertical arrows* in *left column*). The distance between the ELM and the posterior boundary of OPL was defined as the outer nuclear layer thickness and the cone outer segments are bounded by the hyperreflective peaks corresponding to IZ and EZ. (**B**) Grade 1 is defined as absence of extrusion of plexiform layers (marked with *arrow* in magnified section on *right*). (**C**) Grade 2 is defined as grade 1 plus absence of foveal depression (marked with *arrow*). (**D**) Grade 3 is defined as grade 2 plus absence of outer segment lengthening (marked with *arrows*). (**E**) Grade 4 is defined as grade 3 plus absence of outer nuclear layer widening (marked with *arrows*). *Scale bars*: 200 μm.

ty.[61] Those who have anirida and associated FH because of *PAX6* mutations may also have a lower ganglion cell density[14,15] and lesser developed cone to midget circuitry (predominance of connections from a single cone to a single midget bipolar cell and a single ganglion cell),[17,19,26] normally located within the FAZ.[20,22] Thus, we argue that altered spatial organization of cone photoreceptors and associated circuitry of the central retina in aniridia is the most likely cause of poorer than normal red-green color discrimination. This is supported by the reduction in cortical volume in the region where the fovea is represented, previously reported in aniridia.[62] We cannot rule out that unstable fixation and

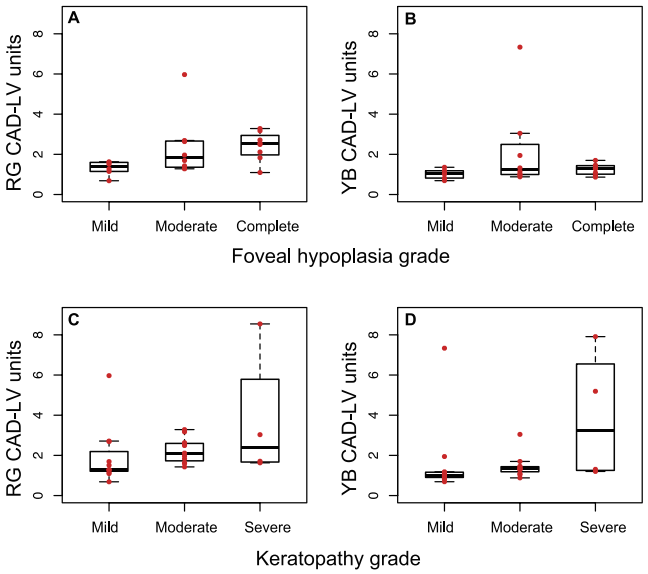

Figure 5. Comparison of CAD-LV RG and YB threshold units between (**A**, **B**) three grades of foveal hypoplasia (mild, grade 0–2; moderate, grade 3; complete, grade 4) and (**C**, **D**) aniridia associated keratopathy. Note that the four participants with severe AAK (**C**, **D**) are not included in any of the FH groups because of insufficient OCT image quality.

nystagmus may also play a role in that a larger part of the retina will be used for sampling a scene, more akin to perifoveal sampling in normal controls.[63,64]

Secondary pathology may aggravate both spatial and color vision function early on in aniridia, because with FH there are most likely far fewer cones and possibly not the same redundancy of cells within the macular region as that observed in normally developed retinas.[65] This is corroborated by previously reported correlations between high contrast achromatic visual acuity and the degree of retinal development as ascertained by the grades of FH.[36] It is known from studies on other retinal degenerative diseases that visual acuity may remain within normal limits even when cone density is less than half of what is observed in normal controls.[66–68]

The RG thresholds were significantly higher than YB thresholds in persons with aniridia, with loss of YB color vision in addition to loss of RG vision appearing to be most strongly associated with glaucoma. Both RG and YB color vision loss have previously been reported in glaucoma,[69–71] with higher thresholds being associated with severity of the disease.[71] The two with aniridia who had the highest RG and YB thresholds, have had glaucoma for more than 20 years (assumed to reflect severity of glaucoma). Loss of YB color vision is also commonly associated with media opacities and a reduction in retinal illuminance caused by increased absorption of short wavelength light.[57,58] There was no significant correlation between YB color vision loss and grade of media opacity here, perhaps because only four participants who performed the CAD test had stage 3 AAK (central corneal involvement), and because of the younger age in the phakic group. The pattern of cataract development in aniridia is also different from typical age-related changes.[6] Combined media opacities (AAK and cataract) in anirida may result in a general reduction of retinal illuminance. But, as measured with an added ND filter (to simulate reduced retinal illuminance) in normal controls, this resulted in an almost uniform increase in both RG and YB CAD-LV thresholds, as opposed to the significantly higher RG thresholds in aniridia.

Both normal and impaired color discrimination has been reported in other disorders associated with foveal hypoplasia,[63,72–75] but it is not known if other pathophysiologic mechanisms that cause FH also affect color discrimination. In aniridia, we surmise that *PAX6* mutation dosage expression is likely to be directly correlated with the degree of FH and the degree of impaired red-green color discrimination. Future work including more detailed *PAX6* genotyping and additional measurement techniques, such as multimodal AOSLO imaging,[76–78] may enable us to test this hypothesis.

Conclusions

In conclusion, visual function loss in aniridia is not limited to loss of visual acuity. Additional loss of color vision appears to be a combined consequence of the timing of arrested foveal formation and secondary ocular pathology. It is a reminder that persons with aniridia are equally likely to inherit congenital color vision deficiencies as others.

Acknowledgments

Supported by the Norwegian Association of Aniridia (Aniridi Norge). The genetic analysis portion of this work was conducted by the University of Washington and was supported by Research to Prevent Blindness, and National Institutes of Health/National Eye Institute Grant P30EY001730. HRP holds a PhD position funded by the Norwegian Ministry of Education and Research.

Disclosure: **H.R. Pedersen**, None; **L.A. Hagen**, None; **E.C.S. Landsend**, None; **S.J. Gilson**, None; **Ø.A. Utheim**, None; **T.P. Utheim**, None; **M. Neitz**, None; **R.C. Baraas**, None

References

1. Edén U, Iggman D, Riise R, Tornqvist K. Epidemiology of aniridia in Sweden and Norway. *Acta Ophthalmol*. 2008;86:727–729.
2. Hingorani M, Williamson KA, Moore AT, van Heyningen V. Detailed ophthalmologic evaluation of 43 individuals with PAX6 mutations. *Invest Ophthalmol Vis Sci*. 2009;50:2581–2590.
3. McCulley TJ, Mayer K, Dahr SS, Simpson J, Holland EJ. Aniridia and optic nerve hypoplasia. *Eye (Lond)*. 2005;19:762–764.
4. Hingorani M, Hanson I, van Heyningen V. Aniridia. *Eur J Hum Genet*. 2012;20:1011–1017.
5. Lee H, Khan R, O'Keefe M. Aniridia: current pathology and management. *Acta Ophthalmol*. 2008;86:708–715.
6. Eden U, Lagali N, Dellby A, et al. Cataract development in Norwegian patients with congenital aniridia. *Acta Ophthalmol*. 2014;92:e165–e167.
7. Netland PA, Scott ML, Boyle JWT, Lauderdale JD. Ocular and systemic findings in a survey of aniridia subjects. *J AAPOS*. 2011;15:562–566.
8. Landsend ES, Utheim OA, Pedersen HR, Lagali N, Baraas RC, Utheim TP. The genetics of congenital aniridia—a guide for the ophthalmologist. *Surv Ophthalmol*. 2018;63:105–113.
9. Vincent MC, Pujo AL, Olivier D, Calvas P. Screening for PAX6 gene mutations is consistent with haploinsufficiency as the main mechanism leading to various ocular defects. *Eur J Hum Genet*. 2003;11:163–169.
10. Shaw MW, Falls HF, Neel JV. Congenital aniridia. *Am J Hum Genet*. 1960;12:389–415.
11. Tzoulaki I, White IM, Hanson IM. PAX6 mutations: genotype-phenotype correlations. *BMC Genet*. 2005;6:27.
12. Holmstrom G, Eriksson U, Hellgren K, Larsson E. Optical coherence tomography is helpful in the diagnosis of foveal hypoplasia. *Acta Ophthalmol*. 2010;88:439–442.

13. Gregory-Evans K, Cheong-Leen R, George SM, et al. Non-invasive anterior segment and posterior segment optical coherence tomography and phenotypic characterization of aniridia. *Can J Ophthalmol*. 2011;46:337–344.
14. Riesenberg AN, Le TT, Willardsen MI, Blackburn DC, Vetter ML, Brown NL. Pax6 regulation of Math5 during mouse retinal neurogenesis. *Genesis*. 2009;47:175–187.
15. Marquardt T, Ashery-Padan R, Andrejewski N, Scardigli R, Guillemot F, Gruss P. Pax6 is required for the multipotent state of retinal progenitor cells. *Cell*. 2001;105:43–55.
16. Schedl A, Ross A, Lee M, et al. Influence of PAX6 gene dosage on development: overexpression causes severe eye abnormalities. *Cell*. 1996;86:71–82.
17. Hsieh YW, Yang XJ. Dynamic Pax6 expression during the neurogenic cell cycle influences proliferation and cell fate choices of retinal progenitors. *Neural Dev*. 2009;4:32.
18. Philips GT, Stair CN, Young Lee H, et al. Precocious retinal neurons: Pax6 controls timing of differentiation and determination of cell type. *Dev Biol*. 2005;279:308–321.
19. Manuel M, Pratt T, Liu M, Jeffery G, Price DJ. Overexpression of Pax6 results in microphthalmia, retinal dysplasia and defective retinal ganglion cell axon guidance. *BMC Dev Biol*. 2008;8:59.
20. Leventhal AG. Evidence that retinal ganglion cell density affects foveal development. *Perspect Dev Neurobiol*. 1996;3:203–211.
21. Yuodelis C, Hendrickson A. A qualitative and quantitative analysis of the human fovea during development. *Vision Res*. 1986;26:847–855.
22. Provis JM, Dubis AM, Maddess T, Carroll J. Adaptation of the central retina for high acuity vision: cones, the fovea and the avascular zone. *Prog Retin Eye Res*. 2013;35:63–81.
23. Hendrickson A, Possin D, Vajzovic L, Toth CA. Histologic development of the human fovea from midgestation to maturity. *Am J Ophthalmol*. 2012;154:767–778.e2.
24. Neitz J, Neitz M. The genetics of normal and defective color vision. *Vision Res*. 2011;51:633–651.
25. Solomon SG, Lennie P. The machinery of colour vision. *Nat Rev Neurosci*. 2007;8:276–286.
26. Xiao M, Hendrickson A. Spatial and temporal expression of short, long/medium, or both opsins in human fetal cones. *J Comp Neurol*. 2000;425:545–559.
27. Cornish EE, Hendrickson AE, Provis JM. Distribution of short-wavelength-sensitive cones in human fetal and postnatal retina: early development of spatial order and density profiles. *Vision Res*. 2004;44:2019–2026.
28. Dees EW, Gilson SJ, Neitz M, Baraas RC. The influence of L-opsin gene polymorphisms and neural ageing on spatio-chromatic contrast sensitivity in 20–71 year olds. *Vision Res*. 2015;116:13–24.
29. Chylack LT Jr, Wolfe JK, Singer DM, et al. The lens opacities classification system III. The longitudinal study of Cataract Study Group. *Arch Ophthalmol*. 1993;111:831–836.
30. Mackman G, Brightbill FS, Optiz JM. Corneal changes in aniridia. *Am J Ophthalmol*. 1979;87:497–502.
31. Barr DB, Weir CR, Purdie AT. An appraisal of the disc-macula distance to disc diameter ratio in the assessment of optic disc size. *Ophthalmic Physiol Opt*. 1999;19:365–375.
32. Sato KI. Reference interval for the disc-macula distance to disc diameter ratio in a large population of healthy Japanese adults: a prospective, observational study. *Medicine (Baltimore)*. 2017;96:e6613.
33. Dubis AM, Costakos DM, Subramaniam CD, et al. Evaluation of normal human foveal development using optical coherence tomography and histologic examination. *Arch Ophthalmol*. 2012;130:1291–1300.
34. Hendrickson AE, Yuodelis C. The morphological development of the human fovea. *Ophthalmology*. 1984;91:603–612.
35. Park JC, Collison FT, Fishman GA, et al. Objective analysis of hyperreflective outer retinal bands imaged by optical coherence tomography in patients with Stargardt disease. *Invest Ophthalmol Vis Sci*. 2015;56:4662–4667.
36. Thomas MG, Kumar A, Mohammad S, et al. Structural grading of foveal hypoplasia using spectral-domain optical coherence tomography a predictor of visual acuity? *Ophthalmology*. 2011;118:1653–1660.
37. Konstantakopoulou E, Rodriguez-Carmona M, Barbur JL. Processing of color signals in female carriers of color vision deficiency. *J Vis*. 2012;12(2):11.
38. O'Neill-Biba M, Sivaprasad S, Rodriguez-Carmona M, Wolf JE, Barbur JL. Loss of chromatic sensitivity in AMD and diabetes: a comparative study. *Ophthalmic Physiol Opt*. 2010;30:705–716.
39. Vemala R, Sivaprasad S, Barbur JL. Detection of early loss of color vision in age-related macular degeneration – with emphasis on drusen and reticular pseudodrusen. *Invest Ophthalmol Vis Sci*. 2017;58:BIO247–BIO254.
40. Seshadri J, Christensen J, Lakshminarayanan V, Bassi CJ. Evaluation of the new web-based "Colour Assessment and Diagnosis" test. *Optom Vis Sci*. 2005;82:882–885.
41. Barbur JL, Rodriguez-Carmona M, Harlow JA, Mancuso K, Neitz J, Neitz M. A study of unusual Rayleigh matches in deutan deficiency. *Vis Neurosci*. 2008;25:507–516.
42. Barbur JL. 'Double-blindsight' revealed through the processing of color and luminance contrast defined motion signals. *Prog Brain Res*. 2004;144:243–259.
43. Barbur JL, Harlow AJ, Plant GT. Insights into the different exploits of colour in the visual cortex. *Proc Biol Sci*. 1994;258:327–334.
44. Rodriguez-Carmona M, Harlow A, Walker G, Barbur J. The variability of normal trichromatic vision and the establishment of the "normal" range. In: Nieves JL, Hernández-Andrés J, eds. *Proceedings of 10th Congress of the International Colour Association*. Granada, Spain: Association Internationale de la Couleur; 2005:979–982.
45. Barbur JL, Rodriguez-Carmona M, Harlow AJ. Establishing the statistical limits of 'normal' chromatic sensitivity. In: *Proceedings of the ISCC/CIE Expert Symposium 2006: 75 Years of the CIE Standard Colorimetric Observer*. Vienna, Austria: International Commission on Illumination; 2006.
46. Regan BC, Reffin JP, Mollon JD. Luminance noise and the rapid determination of discrimination ellipses in colour deficiency. *Vision Res*. 1994;34:1279–1299.
47. Baraas RC, Hagen LA, Dees EW, Neitz M. Substitution of isoleucine for threonine at position 190 of S-opsin causes S-cone-function abnormalities. *Vision Res*. 2012;73:1–9.
48. Linksz A. *An Essay on Color Vision and Clinical Color-Vision Tests*. New York: Grune and Stratton; 1964.
49. Rushton WAH. Review Lecture. Pigments and signals in colour vision. *J Physiol*. 1972;220:1P–31P.
50. Dees EW, Baraas RC. Performance of normal females and carriers of color-vision deficiencies on standard color-vision tests. *J Opt Soc Am A Opt Image Sci Vis*. 2014;31:A401–A409.
51. Davidoff C, Neitz M, Neitz J. Genetic testing as a new standard for clinical diagnosis of color vision deficiencies. *Trans Vis Sci Tech*. 2016;5(5):2.
52. Yokoi T, Nishina S, Fukami M, et al. Genotype-phenotype correlation of PAX6 gene mutations in aniridia. *Hum Genome Var*. 2016;3:15052.
53. Ansari M, Rainger J, Hanson IM, et al. Genetic analysis of 'PAX6-negative' individuals with Aniridia or Gillespie syndrome. *PLoS One*. 2016;11:e0153757.

Investigative Ophthalmology & Visual Science

54. R Core Team. *R: A Language and Environment For Statistical Computing*. Vienna: R Foundation for Statistical Computing; 2016.
55. Koenker R. Quantreg: Quantile Regression. R Package Version 5.33. Available at: https://cran.r-project.org/package=quantreg.
56. Knoblauch K, Vital-Durand F, Barbur JL. Variation of chromatic sensitivity across the life span. *Vision Res*. 2001;41:23–36.
57. Paramei GV, Oakley B. Variation of color discrimination across the life span. *J Opt Soc Am A Opt Image Sci Vis*. 2014;31: A375–A384.
58. Barbur JL, Rodriguez-Carmona M. Color vision changes in normal aging. In: Elliott AJ, Fairchild MD, Franklin A, eds. *Handbook of Color Psychology*. Cambridge, United Kingdom: Cambridge University Press; 2015:180–196.
59. Weber U, Petersen J. Morphological and functional findings in a family with aniridia [in German]. *Klin Monbl Augenheilkd*. 1981;178:439–445.
60. Bredrup C, Knappskog PM, Rodahl E, Boman H. Clinical manifestation of a novel PAX6 mutation Arg128Pro. *Arch Ophthalmol*. 2008;126:428–430.
61. Renner AB, Knau H, Neitz M, Neitz J, Werner JS. Photopigment optical density of the human foveola and a paradoxical senescent increase outside the fovea. *Vis Neurosci*. 2004;21: 827–834.
62. Neveu MM, von dem Hagen E, Morland AB, Jeffery G. The fovea regulates symmetrical development of the visual cortex. *J Comp Neurol*. 2008;506:791–800.
63. Lourenço PE, Fishman GA, Anderson RJ. Color vision in albino subjects. *Doc Ophthalmol*. 1983;55:341–350.
64. Hansen T, Pracejus L, Gegenfurtner KR. Color perception in the intermediate periphery of the visual field. *J Vis*. 2009;9(4): 26.
65. Dees EW, Dubra A, Baraas RC. Variability in parafoveal cone mosaic in normal trichromatic individuals. *Biomed Opt Express*. 2011;2:1351–1358.
66. Carroll J, Baraas RC, Wagner-Schuman M, et al. Cone photoreceptor mosaic disruption associated with Cys203Arg mutation in the M-cone opsin. *Proc Natl Acad Sci U S A*. 2009;106:20948–20953.
67. Michaelides M, Rha J, Dees EW, et al. Integrity of the cone photoreceptor mosaic in oligocone trichromacy. *Invest Ophthalmol Vis Sci*. 2011;52:4757–4764.
68. Ratnam K, Carroll J, Porco TC, Duncan JL, Roorda A. Relationship between foveal cone structure and clinical measures of visual function in patients with inherited retinal degenerations. *Invest Ophthalmol Vis Sci*. 2013;54:5836–5847.
69. Papaconstantinou D, Georgalas I, Kalantzis G, et al. Acquired color vision and visual field defects in patients with ocular hypertension and early glaucoma. *Clin Ophthalmol*. 2009;3: 251–257.
70. Niwa Y, Muraki S, Naito F, Minamikawa T, Ohji M. Evaluation of acquired color vision deficiency in glaucoma using the Rabin cone contrast test. *Invest Ophthalmol Vis Sci*. 2014;55: 6686–6690.
71. Rauscher FG, Chisholm CM, Edgar DF, Barbur JL. Assessment of novel binocular colour, motion and contrast tests in glaucoma. *Cell Tissue Res*. 2013;353:297–310.
72. Vincent A, Kemmanu V, Shetty R, Anandula V, Madhavarao B, Shetty B. Variable expressivity of ocular associations of foveal hypoplasia in a family. *Eye (Lond)*. 2009;23:1735–1739.
73. Oliver MD, Dotan SA, Chemke J, Abraham FA. Isolated foveal hypoplasia. *Br J Ophthalmol*. 1987;71:926–930.
74. Grønskov K, Ek J, Brondum-Nielsen K. Oculocutaneous albinism. *Orphanet J Rare Dis*. 2007;2:43.
75. Ilia M, Jeffery G. Retinal cell addition and rod production depend on early stages of ocular melanin synthesis. *J Comp Neurol*. 2000;420:437–444.
76. Scoles D, Sulai YN, Langlo CS, et al. In vivo imaging of human cone photoreceptor inner segments. *Invest Ophthalmol Vis Sci*. 2014;55:4244–4251.
77. Dubra A, Sulai Y. Reflective afocal broadband adaptive optics scanning ophthalmoscope. *Biomed Opt Express*. 2011;2: 1757–1768.
78. Pedersen HR, Gilson SJ, Dubra A, Munch IC, Larsen M, Baraas RC. Multimodal imaging of small hard retinal drusen in young healthy adults. *Br J Ophthalmol*. 2018;102:146–152.

Investigative Ophthalmology & Visual Science

Paper II

Pedersen, H. R., Neitz M., Gilson, S. J., Landsend, E. C. S., Utheim, Ø. A., Utheim, T. P., & Baraas, R. C. (2019). The cone photoreceptor mosaic in aniridia: within-family phenotype-genotype discordance. *Ophthalmology Retina* 3:523-534. https://doi.org/10.1016/j.oret.2019.01.020

AMERICAN ACADEMY OF OPHTHALMOLOGY®

The Cone Photoreceptor Mosaic in Aniridia

Within-Family Phenotype–Genotype Discordance

Hilde R. Pedersen, MSc,[1] Maureen Neitz, PhD,[2] Stuart J. Gilson, PhD,[1] Erlend C.S. Landsend, MD,[3] Øygunn Aas Utheim, MD, PhD,[4] Tor Paaske Utheim, MD, PhD,[1,3] Rigmor C. Baraas, PhD[1]

Purpose: Investigate in vivo cone photoreceptor structure in familial aniridia caused by deletion in the *PAX6* gene to elucidate the complexity of between-individual variation in retinal phenotype.

Design: Descriptive case-control study.

Participants: Eight persons with congenital aniridia (40–66 yrs) from 1 family and 33 normal control participants (14–69 yrs), including 7 unaffected family members (14–53 yrs).

Methods: DNA was isolated from saliva samples and used in polymerase chain reaction analysis to amplify and sequence exons and intron or exon junctions of the *PAX6* gene. High-resolution retinal images were acquired with OCT and adaptive optics scanning light ophthalmoscopy. Cone density (CD; in cones per square millimeter) and mosaic regularity were estimated along nasal–temporal meridians within the central 0° to 5° eccentricity. Horizontal spectral-domain OCT line scans were segmented to analyze the severity of foveal hypoplasia (FH) and to measure retinal layer thicknesses.

Main Outcomes and Measures: Within-family variability in macular retinal layer thicknesses, cone photoreceptor density, and mosaic regularity in aniridia compared with normal control participants.

Results: DNA sequencing revealed a known *PAX6* mutation (IV2-2delA). Those with aniridia showed variable iris phenotype ranging from almost normal appearance to no iris. Four participants with aniridia demonstrated FH grade 2, 2 demonstrated grade 3 FH, and 1 demonstrated grade 4 FH. Visual acuity ranged from 0.20 to 0.86 logarithm of the minimum angle of resolution. Adaptive optics scanning light ophthalmoscopy images were acquired from 5 family members with aniridia. Foveal CD varied between 19 899 and 55 128 cones/mm^2 with overlap between the foveal hypoplasia grades. Cone density was 3 standard deviations (SDs) or more less than the normal mean within 0.5°, 2 SDs less than the normal mean at 0.5° to 4°, and more than 1 SD less than the normal mean at 5° retinal eccentricity.

Conclusions: The results showed considerable variability in foveal development within a family carrying the same *PAX6* mutation. This, together with the structural and functional variability within each grade of foveal hypoplasia, underlines the importance of advancing knowledge about retinal cellular phenotype in aniridia. *Ophthalmology Retina 2019;3:523-534 © 2019 by the American Academy of Ophthalmology*

Supplemental material available at www.ophthalmologyretina.org.

Congenital aniridia usually causes significant visual impairment. Bilateral hypoplasia of the iris and fovea are characteristic findings. Persons with aniridia are at high risk of early-onset cataract, keratopathy, and glaucoma development. Based on population studies in Norway, Sweden, Denmark, and the United States, the prevalence of aniridia is estimated to be 1:64 000 to 1:96 000.[1,2] Heterozygous mutations in *paired box gene 6* (*PAX6*)[3] primarily are responsible for aniridia. Most known mutations introduce premature termination codons into the PAX6 open reading frame that lead to haploinsufficiency of the PAX6 transcription factor, either by mutations within the *PAX6* gene or its regulatory elements, or more rarely by chromosomal deletions of band 11p13.[4,5] Inheritance typically is autosomal dominant.[6] The phenotypic spectrum associated with *PAX6* mutations is extensive, and aniridia is associated with considerable variability in phenotype and severity.[7]

The *PAX6* gene is a key regulator for normal eye development and interacts with many other genes and proteins. A network of transcription factors including PAX6 is expressed in retinal progenitor cells to control differentiation of multiple early-born (i.e., retinal ganglion cells, cone photoreceptors) and late-born (glycinergic amacrine cells, bipolar cells) retinal nerve cell types.[8] Normal foveal development is characterized by formation of a foveal avascular zone before the foveal depression is formed and displacement of the inner retinal layers. Postnatal elongation and migration of cones toward the center of the fovea lead to a pronounced increase in cone photoreceptor density.[9–11] Aniridia-associated mutations within the *PAX6* gene are known to alter retinal cell composition and

https://doi.org/10.1016/j.oret.2019.01.020
ISSN 2468-6530/19

subsequent postreceptoral organization, including arrested formation of the fovea.[12–14] It is not known whether the degree of *PAX6* haploinsufficiency correlates with the degree of foveal hypoplasia[15] and impaired migration of cone photoreceptors toward the fovea center.[9–11]

Few studies have used high-resolution imaging to investigate retinal layer structure in aniridia,[13,16] and none have investigated the cone photoreceptor mosaic. Herein, spectral-domain OCT and adaptive optics scanning light ophthalmoscopy (AOSLO) were combined to advance the understanding of foveal hypoplasia in familial aniridia through in vivo examinations of retinal layers and photoreceptors at single-cell resolution. This allowed detailed evaluation of retinal phenotypic variability within a family with aniridia.

Methods

Participants

Eight persons from 1 family with congenital aniridia (5 males 40–66 years of age) and 33 normal control participants (14 males 14–69 years of age), including 7 unaffected family members (3 males 14–53 years of age), were recruited through the Norwegian Association of Aniridia, via family members, or through the National Centre for Optics, Vision and Eye Care, University of South-Eastern Norway. The study was conducted in accordance with the tenets of the Declaration of Helsinki and approved by the Regional Committee for Medical and Health Research Ethics (Southern Norway Regional Health Authority). All participants or their guardians gave written informed consent after the purpose, procedures, and possible consequences of the study were explained.

Genetic Analysis

DNA was extracted from saliva samples collected with the Oragene-DNA Self-Collection Kit, OG-500 (DNA Genotek, Inc, Ottawa, Canada) from all 41 participants. The *PAX6* gene was amplified, and exon and intron or exon junctions were sequenced using polymerase chain reaction primers and conditions described previously.[17] Fluorescent DNA sequencing was performed on both DNA strands. One family member with aniridia and 3 unaffected family members who provided saliva samples for genotyping were unable to participate in any further studies.

Clinical Assessment

Seven of 8 family members with aniridia, 4 unaffected family members, and 26 nonrelated normal control participants underwent an eye examination including refraction, evaluation of the anterior and posterior segment, and ocular biometry (IOL Master; Carl Zeiss Meditec AG, Jena, Germany), as well as OCT (details follow). Visual acuity (VA; in logarithm of the minimum angle of resolution units) was measured with a digital high-contrast chart at 6 m (TestChart 2000; Thompson Software Solutions, London, United Kingdom). The Lens Opacities Classification System III[18] was used to evaluate the clarity of the lens. Aniridia-associated keratopathy was graded based on a previously described grading scale.[19]

OCT

High-resolution volumetric spectral-domain OCT images were acquired with the Heidelberg Spectralis OCT2 (Heidelberg Engineering GmbH, Heidelberg, Germany). The scans were 30° × 10°, consisted of 49 B-scans (1536 A-scans/B-scan), and were centered at the assumed foveal center. To improve signal-to-noise ratio and to compensate for eye motion (TruTrack; Heidelberg Engineering), 20 B-scans (frames) were averaged during acquisition. One eye, for which macular volumes could not be obtained because of severe nystagmus, was imaged using horizontal line scans with a nominal scan length of 30°. Multiple scans were acquired in the foveal region to identify signs of foveal specialization.[9,20,21] The lateral scale of all OCT scans was corrected for retinal magnification factor based on individual ocular biometry, calculated with optical design software (Zemax EE; Radiant Zemax, Redmond, WA) using the eye model of Liou and Brennan.[22]

Spectral-domain OCT-derived measures were obtained semi-automatically with custom software. An automatic active contour method,[23] using the Python implementation by van der Walt et al,[24] was used first to segment the anterior edge at the inner limiting membrane in a similar fashion as that described by Mishra et al.[25] Successive layers then were segmented at the posterior boundary of the outer plexiform layer; the center of the external limiting membrane, ellipsoid zone, and interdigitation zone; and the posterior boundary of the retinal pigment epithelium–Bruch's membrane band using the contour of the previous layer as a seed. The foveal center was defined as the section with maximum outer segment (OS) length (ellipsoid zone to interdigitation zone) and minimum foveal thickness (internal limiting membrane to retinal pigment epithelium–Bruch's membrane) within the foveal pit. When no pit was present, the maximum lengthening of the photoreceptor OSs (ellipsoid zone to interdigitation zone), widening of the outer nuclear layer (outer plexiform layer to external limiting membrane), or both were used to identify the expected foveal center. The B-scan through the defined foveal center was used for analysis.

The thickness values for each segmented layer were extracted and averaged at 5-pixel (approximately 28.3 μm) increments from the expected foveal center out to 10° temporal, and nasal eccentricity and the thickness of each retinal layer were calculated. Definition of the retinal layers are presented in Figure 1A. Outer nuclear layer (ONL) and Henle's fiber layer (HFL) were defined as 1 layer because the HFL could not be differentiated easily from the ONL without capturing directional OCT.[26] The relative foveal-to-perifoveal lengthening of the photoreceptor OS, inner segment, and ONL plus HFL was calculated by dividing their foveal thickness values by the average of their thickness at 5° nasal and temporal to the fovea.

Adaptive Optics Scanning Light Ophthalmoscopy

The Kongsberg AOSLO[27,28] was used to obtain images of the photoreceptor mosaic in 5 participants with aniridia (4 men 40–66 years of age) and 30 age-matched normal control participants, including 4 unaffected family members. Ocular media opacities and nystagmus precluded imaging of the photoreceptor mosaic in participants 5114 and 5135. Before imaging, 1 drop of cyclopentolate 1% or tropicamide 0.5% was used to dilate the pupil and control accommodation in participants without severe iris hypoplasia. Confocal[29] and nonconfocal split-detector[30] images with 1° fields of view were acquired simultaneously within 1° of the foveal location and along the temporal and nasal meridians out to 5° eccentricity sampled at 0.5° or 1° intervals. Individual raw image sequences contained 150 frames. Image analyses and registration were performed as described previously.[28] Registered images from each retinal location were stitched together manually into a montage aligned with the corresponding en face

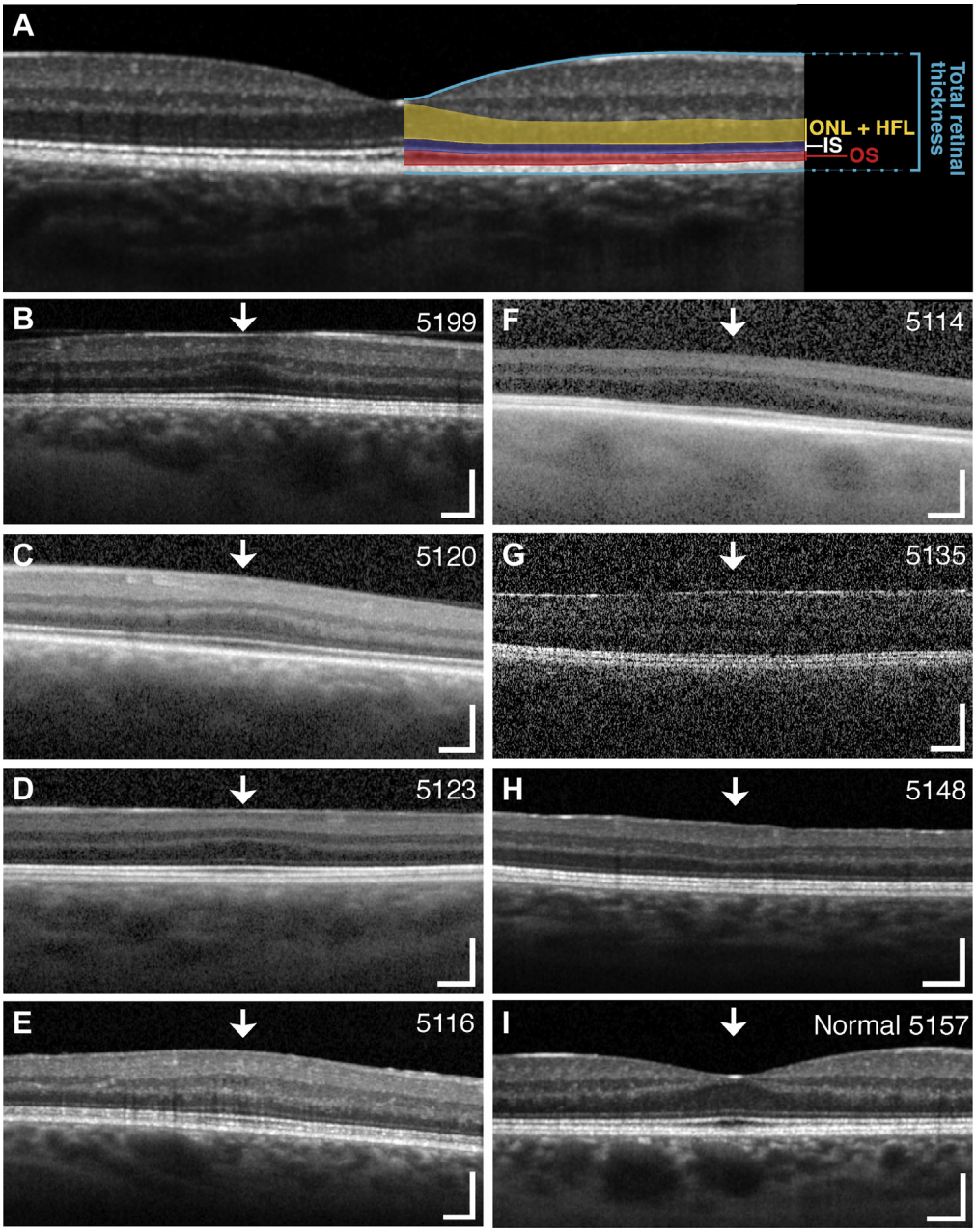

Figure 1. Spectral-domain OCT images showing different degrees of foveal hypoplasia. **A**, Horizontal transfoveal OCT scan of a normal healthy 23-year-old including a graphical illustration of the definition of the segmented retinal layers used in (**B**–**I**). Foveal hypoplasia was graded according to the scale proposed by Thomas et al[15] as (**B**–**E**) grade 2, (**F**, **G**) grade 3, (**H**) grade 4, and (**I**) normal. Variation in foveal hypoplasia in (**B**–**H**) 7 family members with aniridia and (**I**) 1 unaffected family member. Arrows mark the location of the foveal center. This corresponds to the foveal location in the cone mosaics shown in Figure 4. Scale bars = 200 μm. HFL = Henle's fiber layer; IS = inner segment; ONL = outer nuclear layer; OS = outer segment.

infrared image acquired by the OCT using selected blood vessel landmarks. These steps ensured that the AOSLO images were scaled correctly and were positioned regardless of the individual participant's fixation skill and uncontrolled eye movements. The image montages were cross-referenced with the OCT scans to confirm that the location of the foveal center corresponded in both methods. This allowed us to estimate the location of the foveal center in the AOSLO montage also when the most central cones could not be resolved reliably.

Cone Density and Mosaic Regularity

Individual cones in the confocal images were identified via a semiautomatic algorithm as described previously.[28,31] Non-confocal split-detection images were used to disambiguate cones from rods in the perifovea. Cone density was estimated over 50×50-μm sampling windows at the foveal center out to 5° eccentricity along the horizontal and nasal meridian. Voronoi analysis[32] was performed to measure intercell distance (ICD; the

Table 1. Summary of Clinical Phenotype in the Family Members with a *PAX6* IV2-2delA Mutation

Patient Identification No.	Age (yrs)	Gender	Visual Acuity*	Axial Length	Iris Hypoplasia	Lens Status	Nystagmus	Aniridia-Associated Keratopathy Grade	Glaucoma	Optic Nerve Hypoplasia	Foveal Hypoplasia Grade	Red–Green Threshold†	Foveal Cone Density (cones/mm^2)	Symbol
5120	42	M	0.22	23.80	Thin rim of iris	N2, C1, P1	No	1	No	No	2	50	55 128	○
5199	40	M	0.20	25.55	Bright iris, eccentric pupil	N0, C2, P0	No	1	No	No	2	78	51 826	✳
5123	24	M	0.50	22.72	Almost complete	N1, C3, P1	No	2	No	No	2	118	31 837	◇
5116	66	M	0.40	25.66	Thin rim of iris	Pseudophakic	No	2	No	No	2	116	19 899	
5114	56	F	0.86	23.97	Complete	Aphakic	Yes	1	Yes	Yes	3	434	NA	●
5135	40	F	0.70	24.05	Complete	N2, C4, P3	Yes	1	Yes	Yes	3	123	NA	■
5148	49	F	0.60	21.04	Almost complete	Pseudophakic	No	2	Yes	No	4	192	32 713	◀

F = female; M = male; NA = not available.
*In logarithm of the minimum angle of resolution units.
†Low-vision version of the Color Assessment and Diagnosis test. Values derived from data collected by Pedersen et al.[14]

average distance between a cone and all of its neighbors) and the average distance between each cone and its nearest neighbor for all cones whose Voronoi cell was contained completely within the sampling window.[33] The percentage of 6-sided Voronoi cells was calculated to characterize the regularity of the photoreceptor mosaic. The mean (μ) and standard deviation (SD; σ) for each metric were calculated to find the coefficient of variation (CV = σ / μ) to indicate the overall regularity of the ICD and nearest neighbor distance independent of density and distance between the cones. Each participant's dominant eye was used for OCT and AOSLO analysis.

Statistical Analysis

QQ plots, histograms, and the Shapiro-Wilk test were used to assess normality of the variables. Means±SDs are reported for the normal control data and full ranges are reported for the aniridia data. The Wilcoxon rank-sum test (equivalent to the Mann–Whitney *U* test) was applied for independent samples. Correlations were assessed with Spearman correlation coefficients. Linear regression analysis was performed to investigate age-related changes in cone density for the normal control participants. The significance level was set to $P \leq 0.05$. Statistical analyses were performed using R statistical software version 3.5.1, including the package ggplot2 (R Foundation for Statistical Computing, Vienna, Austria).

Intrarater and Interrater Reliability

Intraclass correlation coefficients[34] were computed to assess the intrarater and interrater reliability associated with cone density estimates in images of the foveal, parafoveal, and perifoveal cone mosaic in the participants with aniridia. The CD measurements were repeated by 2 observers (H.R.P. and R.C.B.) at 4 retinal locations (foveal center, 1°, 3°, and 5° retinal eccentricity) from each of the 5 participants with aniridia (total of 20 images). Agreement was assessed between the 2 observers, as well as between 2 measurements made by the same observer (H.R.P.). Analyses were performed using R statistical software version 3.5.1, including the package irr. A 1-way model, in which only the participants are considered as random effects, was considered appropriate.

Access to relevant datasets are available at usn.figshare.com (https://doi.org/10.23642/usn.7605887).

Results

Clinical Findings and Genetics

DNA sequencing revealed an IV2-2delA mutation of the *PAX6* gene in 8 of the family members who previously were diagnosed with aniridia. This mutation is known to cause aniridia and has been reported in the Human PAX6 Allelic Variant Database (Leiden Open Variation Database).[3] It is a deletion of the −2 nucleotide in intron 2, disrupting the canonical splice site sequence at the 3′ splice acceptor site upstream of exon 2. This mutation will affect splicing, most often resulting in exon skipping. However, this is a noncoding exon, and the effect on the protein translation is not known but may lead to loss of functional protein.[35] No *PAX6* abnormality was identified in the 7 unaffected family members, nor in any of the other normal control participants. The inheritance pattern of the mutation is shown in Figure S1 (available at www.ophthalmologyretina.org).

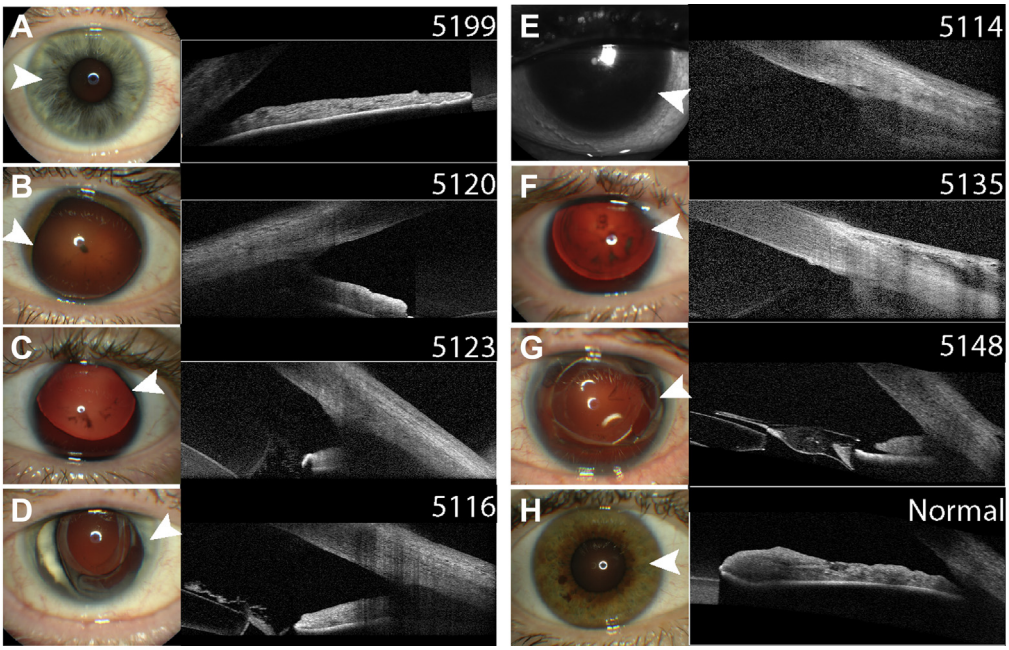

Figure 2. Iris and spectral-domain OCT images showing variation in iris phenotype. **A**–**G**, Iris in participants carrying the *PAX6* mutation. **H**, Iris in a normal control participant. **A**, Iris with an almost normal appearance, but a slightly decentered pupil and thinning of the iris tissue. **B**, **D**, Thin rim of remnant iris. **C**, **G**, Almost total iris hypoplasia with only a small stump of visible remnant iris. **E**, **F**, Total absence of iris. White arrows indicate the location of the iris structure in the corresponding OCT image shown to the right.

Table 1 shows a summary of clinical phenotype in the 7 family members with aniridia who underwent an eye examination (marked with an asterisk in Figure S1). Total or near total iris hypoplasia or a thin rim of iris was observed in 6 of the family members. Participant 5199 initially demonstrated a normal iris, but on closer inspection, the iris was unusually thin and bright gray–pale blue, and the pupil was decentered nasally in both eyes (Fig 2A).

The normal control participants, including the 4 unaffected family members, were healthy with no reported systemic disease or ocular abnormalities and were found to be free of eye disease on clinical assessment, including fundus examination. Visual acuity was 0.10 logarithm of the minimum angle of resolution units or better.

Retinal Layer Thicknesses and Foveal Cone Specialization

Foveal hypoplasia was observed in all participants with aniridia; 4 showed grade 2 (all males), 2 showed grade 3 (both females), and 1 showed grade 4 (female). All, as per grading definition, lacked excavation of inner retinal layers, but ONL and cone OS thickness in the fovea varied considerably between and within each foveal hypoplasia grade (Fig 1).

Total foveal thickness (Fig 3A) ranged from 302.1 to 357.8 μm, compared with normal control participants who showed a mean±SD foveal thickness of 230.3±18.9 μm ($P < 0.001$). The foveal ONL plus HFL thickness (Fig 3B) in aniridia ranged from 49.7 to 99.2 μm and was significantly thinner than in normal control participants (mean, 106.3±14.8 μm; $P < 0.001$). Those with aniridia demonstrated a shorter foveal cone OS (range, 22.2–34.9 μm) compared with normal control participants (mean, 44.1±3.3 μm; $P < 0.001$; Fig 3C). However, relative lengthening (foveal-to-perifoveal length ratio) of the OS was within normal mean ± 2 SD for 3 of them, consistent with specialization of the foveal cones. The ONL plus HFL and OS foveal-to-perifoveal length ratio showed a clear relationship with foveal hypoplasia grade (Fig 3D). Those with aniridia demonstrated shorter inner segment length (range, 26.9–34.6 μm vs. mean ± SD, 33.6±2.4 μm) than the normal control participants, but the difference was not significant ($P = 0.08$).

Retinal Cone Photoreceptor Density and Mosaic Regularity

Images of the foveal cone mosaic for those with aniridia and a normal control are shown in Figure 4 (top), together with confocal and split-detection images of parafovea and perifovea for 1 participant with aniridia (bottom). Peak cone density in aniridia ranged from 19 899 to 55 128 cones/mm^2 (38 280±14 813 cones/mm^2) and was reduced significantly compared with normal control participants, 91 318 to 162 282 cones/mm^2 (122 231±21 572 cones/mm^2; n = 13; $P < 0.001$). Peak cone density was not estimated in the normal control participants in whom cones within the central 50 × 50 μm could not be resolved reliably.

The cone density topographic features among those with aniridia were similar in shape as those seen in the normal control participants but with flatter peaks and reduced cone density at all retinal eccentricities within the central 10° (Fig 5). Cone density varied between family members with aniridia and was more than 3 SD less than the normal mean within 0.5°, more than 2 SD less than the normal mean at 0.5° to 4°, and more than 1 SD less than the normal mean at 5° retinal eccentricity. Estimates of cone density in the participants with aniridia showed a high

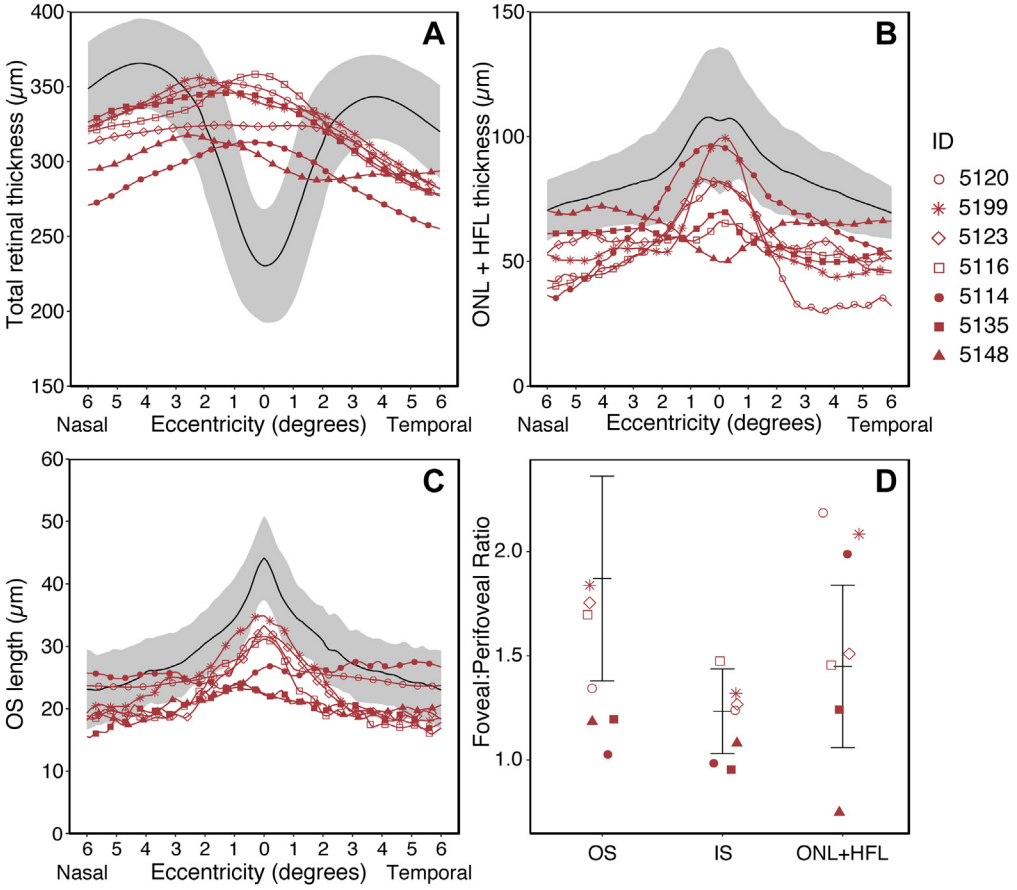

Figure 3. Graphs showing variation in retinal layer thicknesses along the horizontal meridian in aniridia compared with normal control participants. **A**, Total retinal thickness. **B**, Outer nuclear layer (ONL) thickness. **C**, Outer segment (OS) length. Black solid lines and the shaded area represent the normal mean ± 2 standard deviations (SDs). The different filled symbols represent each of the 3 female patients with aniridia and foveal hypoplasia grades 3 to 4 (see Fig 1F–H). Open symbols and asterisks represent the 4 male patients with aniridia and FH grade 2 (see Fig 1B–E). **D**, Relative lengthening of the foveal OS, inner segment (IS), and ONL plus Henle's fiber layer (HFL) represented as the foveal-to-perifoveal ratio. The normal mean is plotted as a horizontal bar with error bars representing ±2 SD.

intrarater agreement (intraclass correlation coefficient, 0.991; 95% confidence interval, 0.977–0.996) and interrater agreement (intraclass correlation coefficient, 0.989; 95% confidence interval, 0.972–0.996).

Cone mosaic regularity was measured by calculating the percentage of cones with 6 Voronoi cell neighbors. Those with aniridia showed a lower mean percentage of Voronoi cells with 6 sides in the parafovea compared with normal control participants (45.9± 10.0% and 55.1±9.9%, respectively; $P < 0.001$), but not in the fovea (49.7% [range, 35.3%–67.0%] vs. 52.0±7.4%; Fig 6A). The eccentricity with comparable cone density to peak density in aniridia varied in normal control participants, but for some it was at approximately 2.5° eccentricity, and the average ± SD percentage of 6-sided cells at this location was the same as that of the fovea: 52.1±7.4%.

There was no difference in coefficients of variation in ICD at the foveal center between participants with aniridia (CV range, 0.091–0.144) and normal control participants (coefficient of variation mean ± SD, 0.107±0.011; $P = 0.57$). However, overall variability in ICD was greater in aniridia (0.107 ±0.022) than in normal retinas (0.086±0.019; $P < 0.001$). This difference in CV was most evident in the parafovea (1°–3° eccentricity; Fig 6B). The same trend also was observed in nearest neighbor distance variability (Fig 6C).

Visual Function and Foveal Cone Specialization

The 3 females with FH grade 3 to 4 showed the shortest OS (Fig 3C, filled symbols) and poorest VA, whereas the 4 males showed FH grade 2, longer OS, and better VA. The 2 males with the best VA and red–green color sensitivity[14] showed the highest cone density, thickest ONL, and longest OS (Fig 7). However, there was an overlap in range of VA and cone density within the OCT grades (Table 1). The oldest participant with aniridia, a man, showed the lowest foveal cone density among all with aniridia, but his foveal cone OSs were clearly elongated. His OS length and foveal-to-perifoveal OS ratio were similar to those of the other participants with FH grade 2 (Fig 3B), but he demonstrated a thinner ONL (Fig 3C). Moreover, there was evidence for cone packing toward the foveal center in the female patient with FH grade 4, even if no ONL or OS lengthening was observed on OCT images.

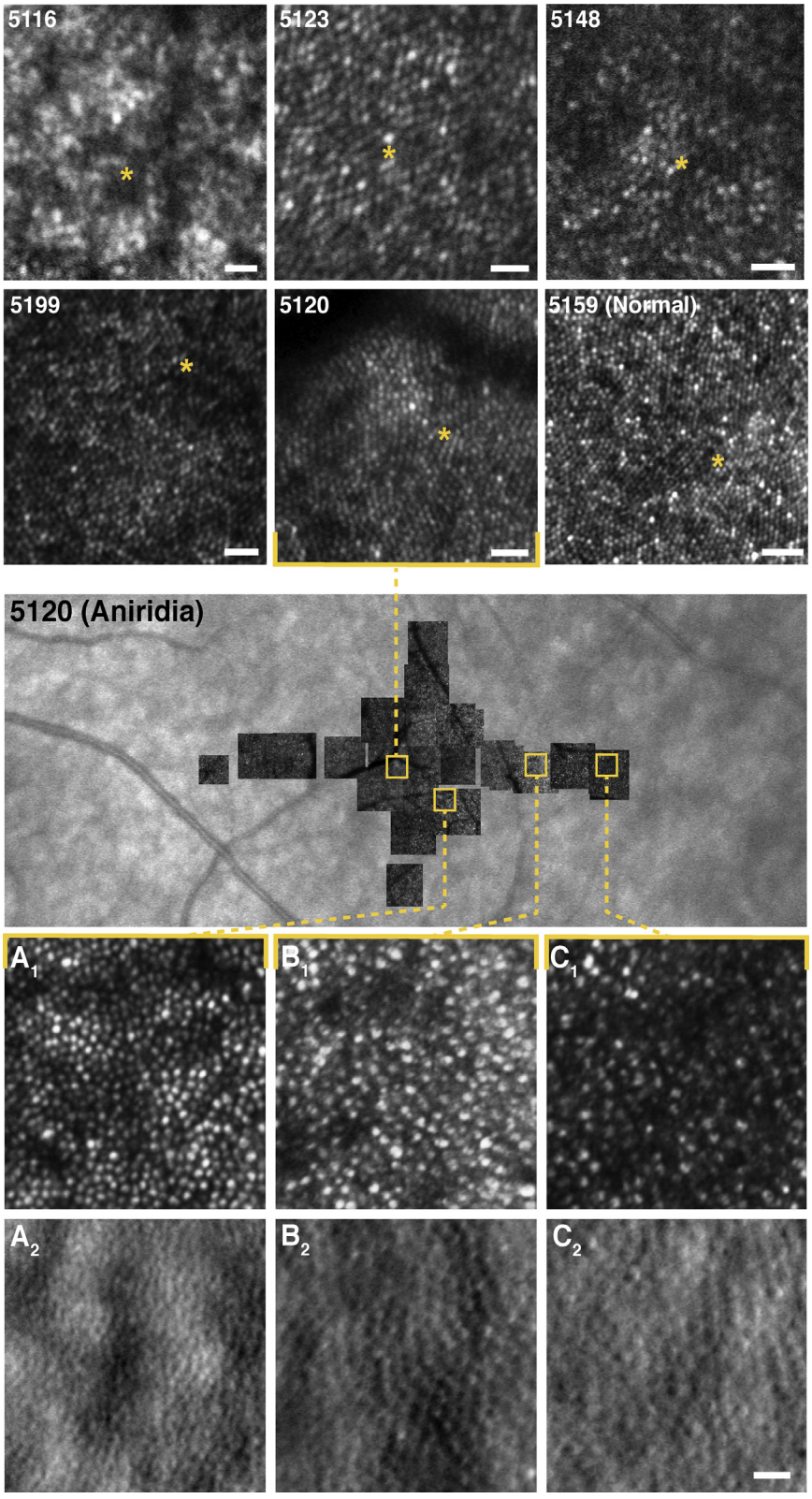

Figure 4. Adaptive optics scanning light ophthalmoscopy (AOSLO) confocal and split-detection images showing variability in foveal cone mosaic within the same aniridia *PAX6* genotype. The top 2 rows show foveal AOSLO images with a 0.5°×0.5° field of view for the 5 family members with aniridia and 1 unaffected family member (5159). Asterisks mark the location of the foveal center for each person. The middle row shows an image montage from the left eye of participant 5120. Nasal is toward the left, and temporal is toward the right. The AOSLO images 5120 and ($\mathbf{A_1}$–$\mathbf{C_1}$) and ($\mathbf{A_2}$–$\mathbf{C_2}$) correspond to the locations indicated by the yellow squares (at approximately 1°, 3°, and 5° temporal eccentricity). $\mathbf{A_1}$, $\mathbf{B_1}$, $\mathbf{C_1}$, Confocal images. $\mathbf{A_2}$, $\mathbf{B_2}$, $\mathbf{C_2}$, Nonconfocal split detection images of the same locations. Scale bars = 20 μm.

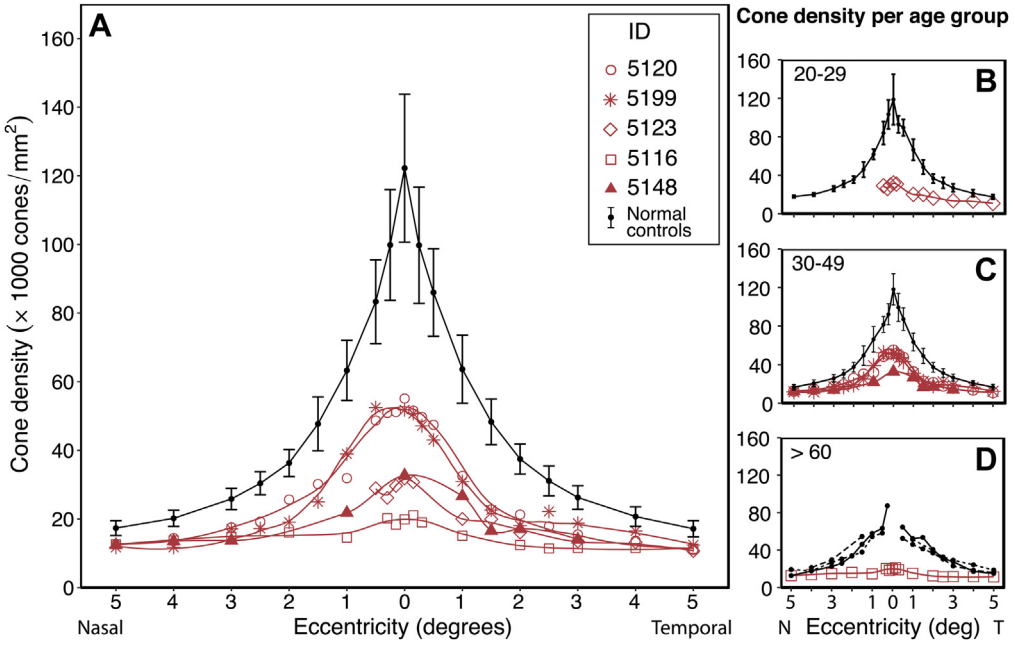

Figure 5. Graphs showing variation in cone density as a function of retinal eccentricity along the nasal and temporal meridian. **A**, Five individuals with aniridia compared with mean ± standard deviation cone density in 30 normal control participants. **B**–**D**, Cone density replotted to show differences between normal control participants and aniridia patients for 3 different age groups.

Gender Differences

The phenotypes observed in the females with aniridia in this family were more severe than those in the males, their degree of foveal hypoplasia was more severe, they had been diagnosed with glaucoma, and 2 of the female patients demonstrated both optic nerve hypoplasia and nystagmus (Table 1). None of the male patients demonstrated glaucoma, optic nerve hypoplasia, or nystagmus. A gender difference also was observed between male and female control participants, with male control participants demonstrating significantly thicker central retinas (241.1±21.1 μm vs. 223.1± 13.6 μm; $P = 0.018$).

Discussion

This study showed the extent of phenotypic variability in familial aniridia through detailed in vivo evaluation of iris and retinal structures of individuals carrying the same *PAX6* mutation. Greater central retinal thickness, shorter OSs, and thinner ONLs were observed in persons with aniridia compared with normal control participants. Cone density was reduced within the central 10°, and the parafoveal cone mosaic was less regular in aniridia than in normal retinas. In this particular family with aniridia, male members were less affected than female members. In addition to differences in severity of foveal hypoplasia, this difference also was evident in degree of iris hypoplasia, with 1 male participant showing an almost normal iris, whereas all female participants showed complete or nearly complete iris hypoplasia. Importantly, the poor association between iris and foveal hypoplasia underscores the importance of a thorough ocular examination for all members of families with aniridia, even those who initially seem unaffected.

The IVS2-delA mutation, found in all 8 participants with aniridia, affects splicing in the 5′ untranslated region of the *PAX6* gene, probably excluding exon 3, but the effect on protein translation is unknown.[35,36] The mutation, reported in the PAX6 Allelic Variant Database, segregates with aniridia in a United Kingdom family and 2 sporadic cases in Russia and Germany.[3] Herein, it was associated with a thinner ONL and lower CD than normal at all the measured eccentricities. Thus, the *PAX6* haploinsufficiency associated with this mutation results in a hypocellular retina, as a consequence of associated loss of propagation of retinal progenitor cells and differentiation into different cell types early in development.[37–39] The lack of a foveal pit in FH grade 2 or more implies that retinal development is arrested before the foveal pit normally starts to form, which is at mid gestation (25–28 fetal weeks).[11,21] Indeed, *PAX6* is thought to have an indirect role on molecular markers that normally are expressed in retinal ganglion cells to prevent vascular ingrowth.[11] Foveal pit formation depends on the presence of a foveal avascular zone as well as an adequate proportion of midget-type ganglion cells to allow displacement of inner retinal layers.[10,11]

The observed thinner outer retinal layers in those with aniridia, as compared with normal control participants, is in line with impaired cone specialization. However, the foveal-to-perifoveal ratio (within normal range) of the ONL thickness and OS length (Fig 3D) suggests that some degree of foveal cone migration and specialization must have occurred even in persons with FH grades 2 and 3. This is evidenced further by similar foveal mosaic regularity in

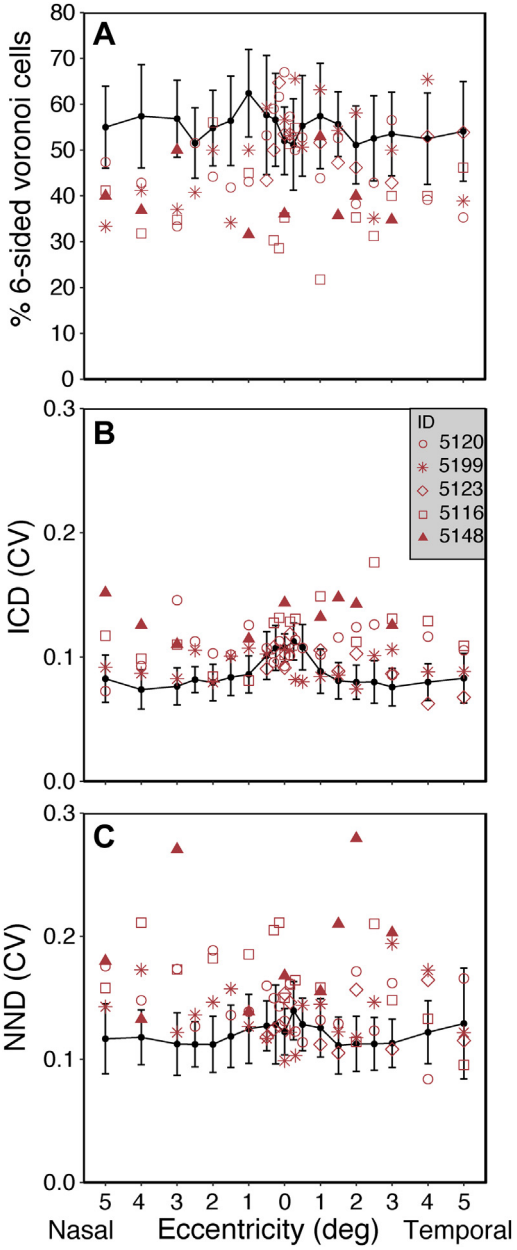

Figure 6. Graphs showing photoreceptor mosaic regularity as a function of retinal eccentricity. **A**, Percentage of 6-sided Voronoi cells. **B**, Variability in intercone distance. **C**, Variability in nearest neighbor distance. Each metric is plotted as a function of retinal eccentricity along the nasal and temporal meridian for 5 individuals with aniridia compared with the mean ± standard deviation of 30 normal control participants. The variability in intercell distance (ICD) and nearest neighbor distance (NND) was calculated as coefficient of variation (CV = σ / μ).

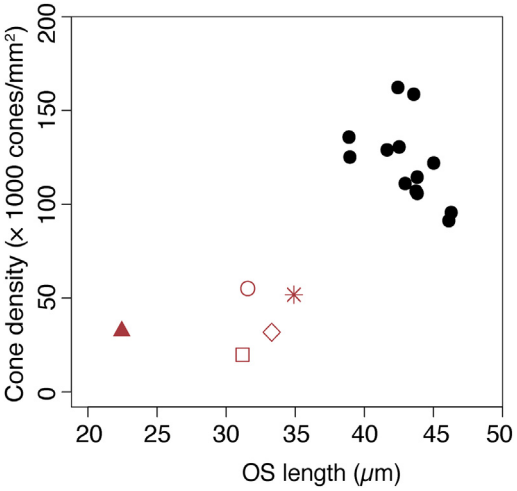

Figure 7. Graph showing the relationship between foveal cone density and cone outer segment (OS) elongation. Peak cone density is plotted as a function of OS length. The different red symbols represent participants with aniridia, and filled black circles are normal control participants.

aniridia and control participants, even if foveal cone density is significantly lower in aniridia. The observation suggests that cone packing has occurred independently of foveal pit formation, which is in line with what Wilk et al[40] propose in albinism; a foveal pit may not be needed for further cone packing but plays a facilitatory role. The parafoveal cone mosaic was less regular in aniridia patients compared with control participants, more akin to that observed for cones at greater eccentricities in normal retinas.

The degree of impaired migration and elongation of cones varied between FH grades as expected, but important differences also were observed within each FH grade. This may be a developmental difference related to the degree of vascularity in the deep foveal capillary plexus. This has been reported to contribute to the inhibition of outer retinal specialization.[41] Development of retinal vasculature in aniridia warrants further investigation. Although the total number of cones in the retina is expected to remain constant after mid gestation,[21] early migration of cones toward the foveal center will increase the foveal cone density to a certain degree.[42] This initial cone migration may be responsible for the cone packing seen in the aniridia patients with lowest peak cone density. However, the visible foveal cone OS elongation, thickening of the ONL, or both observed here in FH grades 2 and 3 suggest that postnatal elongation and migration of cones have occurred in aniridia but to a lesser degree than in normal control participants. The observed cone packing toward the foveal center without ONL or OS lengthening in FH grade 4 may describe a threshold at which increased density will elongate cone OS. We previously reported an association between foveal hypoplasia grade and red−green color discrimination in aniridia.[14] Herein, higher foveal cone density was observed in those with the highest red−green sensitivity (lowest threshold; Table 1). Differences in retinal ganglion cell density, cone−retinal ganglion cell pathways,[43] or both are factors that may explain variation in visual function between persons with the same grade of foveal hypoplasia and the variable relationship among CD, VA, and color vision.

The 2 retinas with highest and the 1 with lowest CD in the aniridia group were graded as FH grade 2. The age of the participant with lowest CD may suggest an age-related decline in CD. A slight, but significant, age-related decline

in CD also was observed at 0.5° and 1° for the normal control participants ($R^2 = 0.30$ and $P = 0.001$, and $R^2 = 0.26$ and $P = 0.002$, respectively); only 3 of the normal control participants were older than 60 years. Presenile aging may play a role in aniridia together with additional factors (like increased vulnerability to retinal diseases resulting from the low redundancy of macular cones in foveal hypoplasia and possible risk for phototoxic damage). Subtle retinal changes and poorer image quality also may decrease the number of reflective cones that are identified in confocal AOSLO,[44] and thus, cone density may be underestimated. Nonconfocal images unfortunately were not available at this location for this participant.

In most cases, the phenotype in aniridia may be explained by the loss of 1 functional copy of the *PAX6* gene (haploinsufficiency), which provides an insufficient level of PAX6 protein.[4,45] Abnormal mRNA is degraded through nonsense-mediated decay, which prevents accumulation of truncated protein products within cells.[46] It is not clear how haploinsufficiency can lead to wide variation in phenotype and severity within a family. However, the complex gene expression associated with *PAX6* that is regulated at multiple levels during different processes of eye development may contribute to large phenotypic variability.[47–49] Differences in genetic background and transcriptional and epigenetic regulation may alter the function of the PAX6 protein further, in turn affecting coactivators, corepressors, and regulation of downstream targets.[47,50,51] In some cases, competition for DNA binding between truncated PAX6 proteins and wild-type PAX6 proteins possibly results in phenotypic variability, so-called dominant-negative effects.[52] It is not known if mutations that lead to abnormal mRNA splicing in the 5′ untranslated region may cause this effect. In conclusion, quantitative analysis of cone elongation and packing within the macular area including the fovea allowed for a more detailed evaluation of retinal phenotypic variability in aniridia than reported previously. The analysis revealed a decreased number of cones within the macular area and considerable variability in foveal development within a family with aniridia carrying the same genetic *PAX6* mutation. This, together with the structural and functional variability within each grade of foveal hypoplasia, underlines the importance of in vivo examinations of retinal layers and photoreceptors at single-cell resolution. Such detailed examinations are essential for improving our understanding of underlying pathophysiology and retinal development in different aniridia *PAX6* mutations. This will aid clinicians and scientists alike in determining prognosis, rehabilitation, and the potential for gene therapy and stem cell replacement strategies.

References

1. Edén U, Iggman D, Riise R, Tornqvist K. Epidemiology of aniridia in Sweden and Norway. *Acta Ophthalmologica*. 2008;86:727–729.
2. Landsend ES, Utheim OA, Pedersen HR, et al. The genetics of congenital aniridia-a guide for the ophthalmologist. *Surv Ophthalmol*. 2018;63:105–113.
3. Human PAX6 allelic variant database (LOVD Database). http://lsdb.hgu.mrc.ac.uk/home.php?select_db=PAX6. Accessed 18.08.18.
4. Vincent MC, Pujo AL, Olivier D, Calvas P. Screening for PAX6 gene mutations is consistent with haploinsufficiency as the main mechanism leading to various ocular defects. *Eur J Hum Genet*. 2003;11:163–169.
5. Kleinjan DA, Seawright A, Schedl A, et al. Aniridia-associated translocations, DNase hypersensitivity, sequence comparison and transgenic analysis redefine the functional domain of PAX6. *Hum Mol Genet*. 2001;10:2049–2059.
6. Shaw MW, Falls HF, Neel JV. Congenital aniridia. *Am J Hum Genet*. 1960;12:389–415.
7. Hingorani M, Williamson KA, Moore AT, van Heyningen V. Detailed ophthalmologic evaluation of 43 individuals with PAX6 mutations. *Invest Ophthalmol Vis Sci*. 2009;50:2581–2590.
8. Remez LA, Onishi A, Menuchin-Lasowski Y, et al. Pax6 is essential for the generation of late-born retinal neurons and for inhibition of photoreceptor-fate during late stages of retinogenesis. *Dev Biol*. 2017;432:140–150.
9. Yuodelis C, Hendrickson A. A qualitative and quantitative analysis of the human fovea during development. *Vision Res*. 1986;26:847–855.
10. Hendrickson A, Possin D, Vajzovic L, Toth CA. Histologic development of the human fovea from midgestation to maturity. *Am J Ophthalmol*. 2012;154:767–778.e762.
11. Provis JM, Dubis AM, Maddess T, Carroll J. Adaptation of the central retina for high acuity vision: cones, the fovea and the avascular zone. *Prog Retin Eye Res*. 2013;35:63–81.
12. Gregory-Evans K, Cheong-Leen R, George SM, et al. Non-invasive anterior segment and posterior segment optical coherence tomography and phenotypic characterization of aniridia. *Can J Ophthalmol*. 2011;46:337–344.
13. Sannan NS, Gregory-Evans CY, Lyons CJ, et al. Correlation of novel PAX6 gene abnormalities in aniridia and clinical presentation. *Can J Ophthalmol*. 2017;52:570–577.
14. Pedersen HR, Hagen LA, Landsend ECS, et al. Color vision in aniridia. *Invest Ophthalmol Vis Sci*. 2018;59:2142–2152.
15. Thomas MG, Kumar A, Mohammad S, et al. Structural grading of foveal hypoplasia using spectral-domain optical coherence tomography a predictor of visual acuity? *Ophthalmology*. 2011;118:1653–1660.
16. Thomas S, Thomas MG, Andrews C, et al. Autosomal-dominant nystagmus, foveal hypoplasia and presenile cataract associated with a novel PAX6 mutation. *Eur J Hum Genet*. 2014;22:344–349.
17. Yokoi T, Nishina S, Fukami M, et al. Genotype-phenotype correlation of PAX6 gene mutations in aniridia. *Hum Genome Var*. 2016;3:15052.
18. Chylack Jr LT, Wolfe JK, Singer DM, et al. The Lens Opacities Classification System III. The Longitudinal Study of Cataract Study Group. *Arch Ophthalmol*. 1993;111:831–836.
19. Landsend ECS, Pedersen HR, Utheim OA, et al. Meibomian gland dysfunction and keratopathy are associated with dry eye disease in aniridia. *Br J Ophthalmol*. 2019;103:119–124.
20. Dubis AM, Costakos DM, Subramaniam CD, et al. Evaluation of normal human foveal development using optical coherence tomography and histologic examination. *Arch Ophthalmol*. 2012;130:1291–1300.
21. Hendrickson AE, Yuodelis C. The morphological development of the human fovea. *Ophthalmology*. 1984;91:603–612.
22. Liou HL, Brennan NA. Anatomically accurate, finite model eye for optical modeling. *J Opt Soc Am A Opt Image Sci Vis*. 1997;14:1684–1695.

23. Kass M, Witkin A, Terzopoulos D. Snakes: active contour models. *Int J Comput Vis*. 1988;1:321–331.
24. van der Walt S, Schonberger JL, Nunez-Iglesias J, et al. scikit-image: image processing in Python. *PeerJ*. 2014;2:e453.
25. Mishra A, Wong A, Bizheva K, Clausi DA. Intra-retinal layer segmentation in optical coherence tomography images. *Opt Express*. 2009;17:23719–23728.
26. Lujan BJ, Roorda A, Croskrey JA, et al. Directional optical coherence tomography provides accurate nuclear layer and Henle fiber layer measurements. *Retina*. 2015;35:1511–1520.
27. Dubra A, Sulai Y. Reflective afocal broadband adaptive optics scanning ophthalmoscope. *Biomed Opt Express*. 2011;2:1757–1768.
28. Pedersen HR, Gilson SJ, Dubra A, et al. Multimodal imaging of small hard retinal drusen in young healthy adults. *Br J Ophthalmol*. 2018;102:146–152.
29. Dubra A, Sulai Y, Norris JL, et al. Noninvasive imaging of the human rod photoreceptor mosaic using a confocal adaptive optics scanning ophthalmoscope. *Biomed Opt Express*. 2011;2:1864–1876.
30. Scoles D, Sulai YN, Langlo CS, et al. In vivo imaging of human cone photoreceptor inner segments. *Invest Ophthalmol Vis Sci*. 2014;55:4244–4251.
31. Li KY, Roorda A. Automated identification of cone photoreceptors in adaptive optics retinal images. *J Opt Soc Am A Opt Image Sci Vis*. 2007;24:1358–1363.
32. Baraas RC, Carroll J, Gunther KL, et al. Adaptive optics retinal imaging reveals S-cone dystrophy in tritan color-vision deficiency. *J Opt Soc Am A Opt Image Sci Vis*. 2007;24:1438–1447.
33. Cooper RF, Wilk MA, Tarima S, Carroll J. Evaluating descriptive metrics of the human cone mosaic. *Invest Ophthalmol Vis Sci*. 2016;57:2992–3001.
34. Bland JM, Altman DG. Measurement error and correlation coefficients. *BMJ*. 1996;313:41–42.
35. Prosser J, van Heyningen V. PAX6 mutations reviewed. *Hum Mutat*. 1998;11:93–108.
36. Axton RA, Hanson IM, Love J, et al. Combined SSCP/heteroduplex analysis in the screening for PAX6 mutations. *Mol Cell Probes*. 1997;11:287–292.
37. Oron-Karni V, Farhy C, Elgart M, et al. Dual requirement for Pax6 in retinal progenitor cells. *Development*. 2008;135:4037–4047.
38. Marquardt T, Ashery-Padan R, Andrejewski N, et al. Pax6 is required for the multipotent state of retinal progenitor cells. *Cell*. 2001;105:43–55.
39. Klimova L, Kozmik Z. Stage-dependent requirement of neuroretinal Pax6 for lens and retina development. *Development*. 2014;141:1292–1302.
40. Wilk MA, McAllister JT, Cooper RF, et al. Relationship between foveal cone specialization and pit morphology in albinism. *Invest Ophthalmol Vis Sci*. 2014;55:4186–4198.
41. Pakzad-Vaezi K, Keane PA, Cardoso JN, et al. Optical coherence tomography angiography of foveal hypoplasia. *Br J Ophthalmol*. 2017;101:985–988.
42. Diaz-Araya C, Provis JM. Evidence of photoreceptor migration during early foveal development: a quantitative analysis of human fetal retinae. *Vis Neurosci*. 1992;8:505–514.
43. Rossi EA, Roorda A. The relationship between visual resolution and cone spacing in the human fovea. *Nat Neurosci*. 2010;13:156–157.
44. Pallikaris A, Williams DR, Hofer H. The reflectance of single cones in the living human eye. *Invest Ophthalmol Vis Sci*. 2003;44:4580–4592.
45. Lee HJ, Colby KA. A review of the clinical and genetic aspects of aniridia. *Semin Ophthalmol*. 2013;28:306–312.
46. Khajavi M, Inoue K, Lupski JR. Nonsense-mediated mRNA decay modulates clinical outcome of genetic disease. *Eur J Hum Genet*. 2006;14:1074.
47. Osumi N, Shinohara H, Numayama-Tsuruta K, Maekawa M. Concise review: Pax6 transcription factor contributes to both embryonic and adult neurogenesis as a multifunctional regulator. *Stem Cells*. 2008;26:1663–1672.
48. Hever AM, Williamson KA, van Heyningen V. Developmental malformations of the eye: the role of PAX6, SOX2 and OTX2. *Clin Genet*. 2006;69:459–470.
49. Cvekl A, Callaerts P. PAX6: 25th anniversary and more to learn. *Exp Eye Res*. 2017;156:10–21.
50. Ashery-Padan R, Marquardt T, Zhou X, Gruss P. Pax6 activity in the lens primordium is required for lens formation and for correct placement of a single retina in the eye. *Genes Dev*. 2000;14:2701–2711.
51. Gregory-Evans CY, Wallace VA, Gregory-Evans K. Gene networks: dissecting pathways in retinal development and disease. *Prog Retin Eye Res*. 2013;33:40–66.
52. Singh S, Tang HK, Lee JY, Saunders GF. Truncation mutations in the transactivation region of PAX6 result in dominant-negative mutants. *J Biol Chem*. 1998;273:21531–21541.

Footnotes and Financial Disclosures

Originally received: September 19, 2018.
Final revision: January 30, 2019.
Accepted: January 30, 2019.
Available online: February 5, 2019. Manuscript no. ORET_2018_472.

[1] National Centre for Optics, Vision and Eye Care, Faculty of Health and Social Sciences, University of South-Eastern Norway, Kongsberg, Norway.

[2] Department of Ophthalmology, University of Washington, Seattle, Washington.

[3] Department of Ophthalmology, Oslo University Hospital, Oslo, Norway.

[4] The Norwegian Dry Eye Clinic, Oslo, Norway.

Presented in part at: Association for Research in Vision and Ophthalmology Annual Meeting, May 2018, Honolulu, Hawaii; and the Fourth European Conference on Aniridia, August 2018, Paris, France.

Financial Disclosure(s):
The author(s) have no proprietary or commercial interest in any materials discussed in this article.

Supported by the Norwegian Association of Aniridia (Aniridi Norge, Sandefjord, Norway; H.R.P., R.C.B.); and the Norwegian Ministry of Education and Research (Oslo, Norway; H.R.P.). The genetic analysis portion of this work was conducted by the University of Washington and was supported by Research to Prevent Blindness, Inc., New York, New York (M.N.), and the National Eye Institute, National Institutes of Health, Bethesda, Maryland (grant no.: P30EY001730; M.N.).

HUMAN SUBJECTS: Human subjects were included in this study. The human ethics committees at the Regional Committee for Medical and Health Research Ethics (Southern Norway Regional Health Authority) approved the study. All research adhered to the tenets of the Declaration of Helsinki. All participants provided informed consent.

No animal subjects were included in this study.

Author Contributions:

Conception and design: Pedersen, Neitz, Gilson, Landsend, Ø.A.Utheim, T.P.Utheim, Baraas

Analysis and interpretation: Pedersen, Neitz, Gilson, Baraas

Data collection: Pedersen, Neitz, Gilson, Baraas

Obtained funding: Pedersen, Neitz, Baraas

Overall responsibility: Pedersen, Neitz, Gilson, Landsend, Ø.A.Utheim, T.P.Utheim, Baraas

Abbreviations and Acronyms:
AOSLO = adaptive optics scanning light ophthalmoscopy; **CD** = cone density; **FH** = foveal hypoplasia; **HFL** = Henle's fiber layer; **ICD** = intercell distance; **ONL** = outer nuclear layer; **OS** = outer segment; **PCR** = polymerase chain reaction; **SD** = standard deviation; **VA** = visual acuity.

Correspondence:
Rigmor C. Baraas, PhD, National Centre for Optics, Vision and Eye Care, University of South-Eastern Norway, Hasbergsvei 36, 3616 Kongsberg, Norway. E-mail: rigmor.baraas@usn.no.

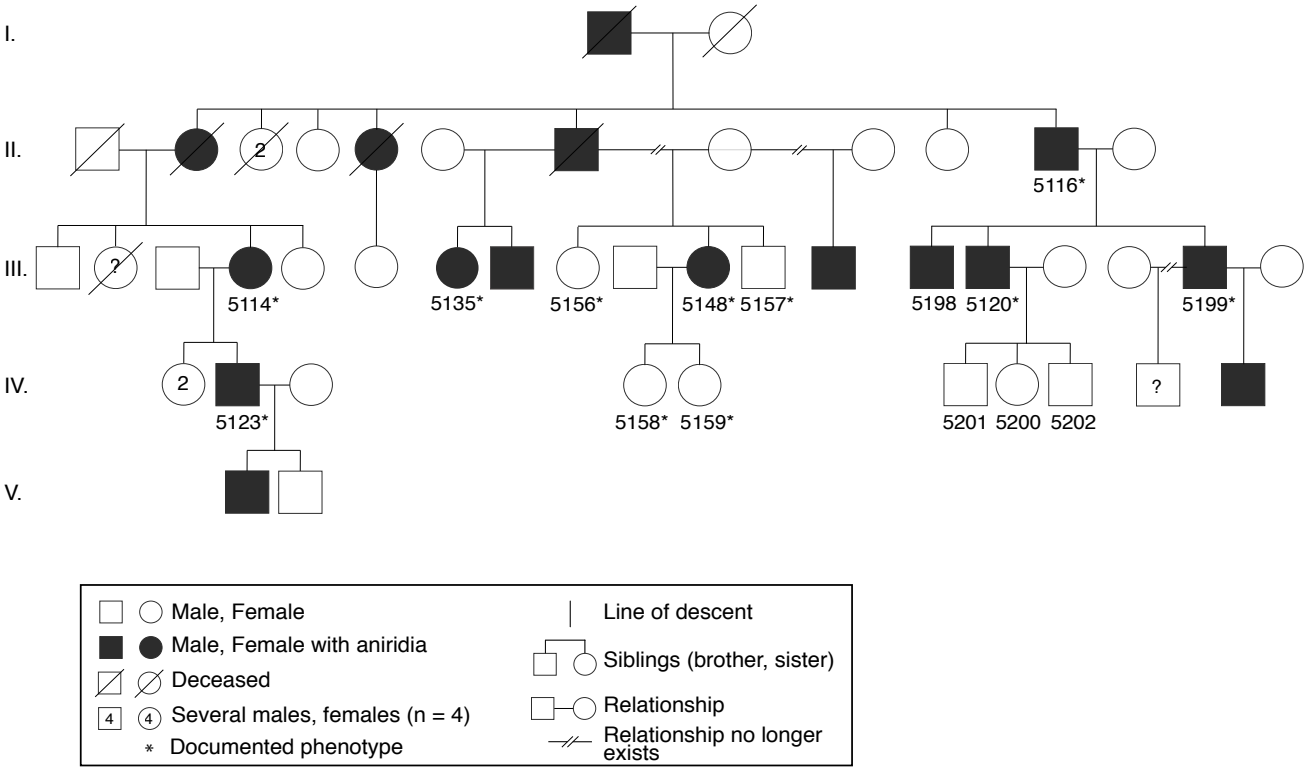

Supplemental Figure 1: Pedigree of the family with a *PAX6* mutation showing an autosomal dominant inheritance pattern. The genotype was analyzed for 15 family members, indicated by their study ID number. The phenotype was documented for family members marked with study ID number followed by *. Written informed consent to publish the pedigree have been obtained from all the study participants and/or their guardians.

Paper III

Pedersen, H. R., Baraas, R. C., Landsend, E. C. S., Utheim, Ø. A., Utheim, T. P., Gilson, S. J., Neitz, M. (Accepted). *PAX6* Genotypic and Retinal Phenotypic Characterization in Congenital Aniridia. *Investigative Ophthalmology & Visual Science.*

PAX6 Genotypic and Retinal Phenotypic Characterization in Congenital Aniridia

Hilde R. Pedersen[1], Rigmor C. Baraas[1], Erlend C. S. Landsend,[3] Øygunn A. Utheim,[3] Tor P. Utheim,[1]

Stuart J. Gilson[1] and Maureen Neitz[2]

[1]National Centre for Optics, Vision and Eye Care, Faculty of Health and Social Sciences, University of South-Eastern Norway, Kongsberg, Norway

[2]Department of Ophthalmology, University of Washington, Seattle, WA, USA

[3]Department of Ophthalmology, Oslo University Hospital, Oslo, Norway

Corresponding authors:
Prof. Rigmor C. Baraas
National Centre for Optics, Vision and Eye Care,
Faculty of Health and Social Sciences, University of South-Eastern Norway, Kongsberg, Norway
E-mail: rigmor.baraas@usn.no
Phone: +47 31 00 89 62

Prof. Maureen Neitz
Department of Ophthalmology, University of Washington, Seattle, WA, USA
E-mail: mneitz@uw.edu

Grant information: The genetic analysis portion of this work was conducted by the University of Washington and was supported by Research to Prevent Blindness, and National Institutes of Health/National Eye Institute Grant NIH P30EY001730. HRP holds a PhD position funded by the Norwegian Ministry of Education and Research.

Word count: 4660

Abstract

Purpose: Investigate the association between *PAX6* genotype and macular morphology in congenital aniridia.

Methods: The study included 37 participants (15 males) with congenital aniridia (10–72 years) and 58 age-matched normal controls (18 males). DNA was isolated from saliva samples. *PAX6* exons, intron/exon junctions, and known regulatory regions were amplified in polymerase chain reaction (PCR) and sequenced. Multiplex ligation-dependent probe amplification (MLPA) was performed to detect larger deletions or duplications in *PAX6* or known cis-regulatory regions. SD-OCT images were acquired and segmented semi-automatically. Mean thicknesses were calculated for inner and outer retinal layers within the macula along nasal and temporal meridians.

Results: Mutations in *PAX6* or regulatory regions were found in 97% of the participants with aniridia. Foveal hypoplasia was observed in all who had a mutation within the *PAX6* gene. Aniridic eyes had thinner outer retinal layers than controls, but with large between-individual variation (mean±SD 156.3±32.3µm vs 210.8±12.3µm, $P<0.001$). Parafoveal and perifoveal inner and outer retinal layers were thinner in aniridia. Participants with mutations in non-coding *PAX6* regions had thicker foveal outer retinal layers than those with mutations in the *PAX6* coding regions ($P=0.04$) and showed signs of postnatal development and maturation. Mutations outside the *PAX6* gene were associated with the mildest retinal phenotypes.

Conclusions: *PAX6* mutations are associated with significant thinning of macular inner and outer retinal layers, consistent with misdirected retinal development resulting in abnormal foveal formation and reduced number of neurons in the macula, with mutations in *PAX6* coding regions giving the worst outcome.

Introduction

Congenital aniridia is a rare genetic disorder disrupting normal development of the eye and affects an estimated 1 in 64,000–72,000 people worldwide.[1, 2] Heterozygous mutations within the *PAX6* gene (*paired box gene 6*; OMIM # 607108) or associated regulatory regions, are the most common cause of aniridia.[3-6] These mutations reduce the expression of the *PAX6* gene and lead to a shortage of functional PAX6 protein which, amongst other effects, disrupts eye development.[7] This can lead to a spectrum of ocular anomalies, including incomplete development of the iris, fovea and optic nerve, severely impaired vision and nystagmus. The progressive nature of aniridia frequently leads to secondary ocular complications such as cataract, glaucoma and aniridia-associated keratopathy (AAK). The clinical phenotype is highly variable among individuals with different genotypes, as well as between individuals with the same genotype.[8-10]

While absence of the iris is considered the hallmark of aniridia, foveal hypoplasia is one of the most common ocular findings, observed even in cases where the iris may appear intact.[8, 11] *PAX6* plays an important role in retinal development,[12] including in cell type specification/differentiation[13] and migration of cones towards the foveal centre.[14] However, little is known about *PAX6*'s specific role in foveal maturation, and the reported variability in visual acuity and foveal hypoplasia in eyes with aniridia[11, 15] may be attributed to different mutations found in or around the *PAX6* gene. It is therefore reasonable to hypothesize that more severe *PAX6* mutations, that has a larger effect on the PAX6 protein dosage, will result in a thinner retina in the perifovea and parafovea, poorer foveal cone specialization and more severe alteration of macular morphology. The current study tested this hypothesis. The aim, therefore, was to assess the contribution of each retinal layer to macular morphology in *PAX6*-associated aniridia, investigate the relationship between foveal cone specialization and visual acuity and to determine any genotype-phenotype relationships.

In addition to employing qualitative grading of foveal hypoplasia using optical coherence tomography (OCT),[16] measures of inner and outer retinal layer thicknesses within the foveal, parafoveal and perifoveal regions were assessed. Such assessment is warranted because of large between-individual variation, both between and within each OCT grade of foveal hypoplasia.[10, 11, 17] This variation indicates that qualitative grading of foveal hypoplasia alone may be insufficient to fully characterize foveal formation in aniridia. Knowledge about individual variations in foveal formation and macular development in aniridia is particularly important for understanding each individual's potential of visual function and for predicting treatment outcomes.

Methods

Thirty-seven persons with congenital aniridia (24 familial, 13 sporadic, 15 males, aged 10–72 [mean ± SD, 35.8 ± 18.6] years) and 58 age-matched normal controls (18 males, aged 10–74 years [35.7 ± 19.0], $P = 0.99$) participated in the study (Table 1). Those with aniridia were recruited through the Norwegian Association of Aniridia or via family members, whereas the normal controls were recruited through the National Centre for Optics, Vision and Eye Care, University of South-Eastern Norway. The study followed the principles in the Helsinki Declaration and was approved by the Regional Committee for Medical and Health Research Ethics (Southern Norway Regional Health Authority). The purpose, procedures and possible consequences of the study were explained to each participant and/or their guardians before data collection and written informed consent was obtained.

The participants underwent a comprehensive eye examination of the anterior and posterior segment as described previously.[17] Best corrected visual acuity was measured with a high-contrast logMAR acuity chart (TestChart 2000, Thomson Software Solutions, London, UK) at 6 meters. If a reliable measurement could not be obtained at the longer distance, the test distance was reduced to 3 or 1 meter and the logMAR value corrected accordingly. Refractive errors were classified based on spherical equivalent refraction (SER = sphere + ½ cylinder). Ocular axial length (AL) was measured with an optical interferometer (IOL Master 700, Carl Zeiss Meditec AG, Jena, Germany). Grading of AAK

have been reported previously.[17, 18]

Table 1. Distribution of participants within each age group

	Normal controls			Aniridia		
Age group	n	Mean age	Age range	n	Mean age	Age range
< 20	14	14.71	10 – 19	8	13.88	9 – 19
20-29	12	22.08	20 – 27	9	23.78	20 – 29
30-39	8	33.62	31 – 37	4	32.75	31 – 36
40-49	8	44.38	41 – 48	6	43.50	40 – 49
50-59	7	52.86	50 – 58	5	54.20	50 – 59
> 60	9	67.44	64 – 74	5	67.00	64 – 72

Genetic Analysis

DNA, isolated from saliva samples (Oragene-DNA, DNA Self-Collection Kit; DNA Genotek, Inc., Ottawa, ON, Canada) from 35 of 37 participants with aniridia, was used in the polymerase chain reaction (PCR) to amplify and sequence the exons (1–13) and intron/exon junctions of the *PAX6* gene using previously described primers and conditions.[9] Fluorescent DNA sequencing was performed on both DNA strands. *PAX6* transcript reference sequence NM_00280.**4** from the National Center for Biotechnology Information (NCBI) was used for nucleotide numbering. Variations were described according to conventional notations.[19] Nucleotide numbering starts with 1 at the A of the ATG translation initiation codon.

For the participants for whom no abnormalities were found by intragenic *PAX6* sequencing, the remote, ultra-conserved *PAX6* enhancer SIMO, located 150 kb downstream from *PAX6* was sequenced.[4, 20] Multiplex ligation-dependent probe amplification (MLPA) was performed using the SALSA MLPA reagent kit P219-B3 (MRC Holland, Amsterdam, the Netherlands) to detect larger deletions or duplications in the *PAX6* genomic region including several known *PAX6* regulatory regions. The MLPA analysis included three control DNA samples. The deletions detected by the MLPA analysis were confirmed by TaqMan Copy Number Assays (Applied Biosystems) using quantitative real-time

PCR to determine gene copy number. Identified *PAX6* mutations were analyzed using online bioinformatics tools (Mutation Taster[21]) to predict their disease-causing potential. Mutations were also checked against entries of the Leiden Open Variation Database (LOVD, https://www.lovd.nl/), ClinVar, ExAC (Exome Aggregation Consortium), HGMD (Human Gene Mutation Database), and a PubMed search.

PITX2 and *FOXC1* genes were amplified and sequenced for participants who were negative for mutations in the *PAX6* genomic region. The primer sequences and PCR conditions have been described previously.[22]

Optical Coherence Tomography

Heidelberg Spectralis OCT2 (Heidelberg Engineering GmbH, Heidelberg, Germany) was used to acquire SD-OCT scans of the macular region as described previously (512–1536 A-scans/B-scan, 49 B-scans over 20°×20° or 30°×10°; 30°×5° for normal controls).[17, 23] The built-in eye-tracking system was used to compensate for eye-motion artifacts and 5–20 horizontal B-scans were averaged during imaging. The participants' head posture and gaze direction were adjusted to minimize the amplitude of nystagmus during OCT imaging. If a reliable volume scan still was unattainable because of nystagmus, a horizontal scan line was moved manually across the macula to look for signs of foveal specialization.[24, 25] Several repetitive horizontal line scans (30° field of view) were acquired at the expected foveal location and above and below the central scan using the optic nerve head as a reference point[26] to increase the probability of scanning through the center of the fovea. The image quality was verified and considered adequate when signal was > 15dB.

Foveal hypoplasia was graded by two separate graders (authors HRP and RCB) according to the grading scheme suggested by Thomas *et al.*[16]: presence of inner layers at the foveal centre (grade 1); absence of a foveal pit (grade 2); absence of outer segment lengthening (grade 3); and absence of outer nuclear layer widening (grade 4). Foveal hypoplasia grade was typically the same in both eyes of each

individual, thus only the dominant eye was included in analysis. The retinal layers were segmented using a semi-automatic active contour method,[27] that sought to follow local image intensity gradients while a thin-plate constraint ensured that segmented contours were smooth and, therefore, robust to local noise. The operator could dynamically modify the contour via an interactive interface to correct for any segmentation errors that may have arisen due to image artefacts or noise (e.g. shadows cast from blood vessels). This method has successfully been applied to OCT image segmentation previously.[10, 28, 29] The horizontal OCT B-scan through the foveal center, defined as the section with maximum photoreceptor layer thickness, was used for analysis (Figure 1). In participants without presence of outer segment (OS) lengthening, the expected foveal location was identified via maximum thickness of the outer nuclear layer (ONL). In those with grade 4 foveal hypoplasia, the expected foveal center was located based on doming of the inner retinal layers (if present), and/or the horizontal and vertical distance between fovea and optic disc as described previously.[26]

Because it is difficult to differentiate ONL and Henle's fiber layer (HFL) without capturing directional OCT,[30] these were defined as one layer. The reflective bands corresponding to the photoreceptor OS – retinal pigment epithelium (RPE) interdigitation zone (IZ) and/or the external limiting membrane (ELM) were not visible or clearly demarcated in seven and ten eyes, respectively. Hence, we used a combined measurement of ONL, photoreceptor inner and outer segment and RPE to provide a more robust thickness measurement of the outer retinal layers. Measurements of the three innermost layers, i.e. the retinal nerve fiber layer (RNFL), ganglion cell layer (GCL) and inner plexiform layer (IPL), were also combined. Thicknesses of all the component layers of the outer and inner retina were also calculated for those where the boundaries between the layers were visible. Mean thicknesses were calculated within five lateral regions: Foveal center (central 50μm), parafoveal region (0.5–1.5mm retinal eccentricity) and perifoveal region (1.5–3.0mm retinal eccentricity) along the nasal and temporal meridians. The lateral scale was corrected for between-individual AL differences by multiplying the lateral scale obtained from the instrument with the ratio between each individual's AL and the OCT AL setting (24 mm for a medium-long eye).

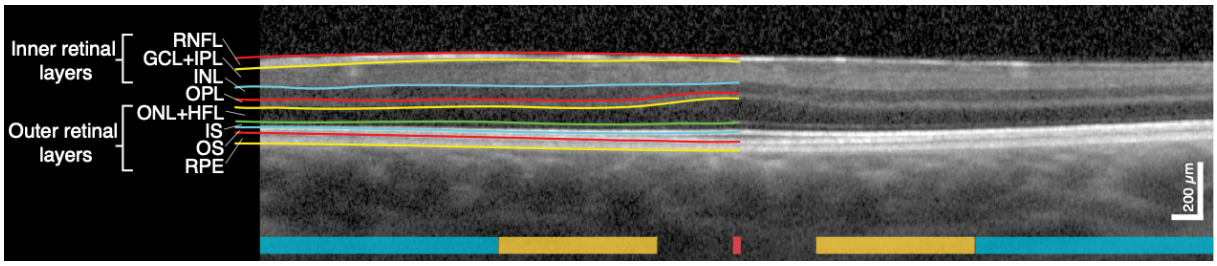

Figure 1. Horizontal SD-OCT scan through the foveal center of a male with *PAX6* related aniridia including an illustration of the segmented retinal layers and definition of the retinal layers. The fovea, parafoveal and perifoveal regions along the nasal and temporal meridians are marked with red, yellow and turquoise, respectively.

Data Analysis

Statistical analyses were performed using R statistical software,[31] version 3.5.1. Normal distribution of the variables was verified using histograms, QQ-plots and the Shapiro-Wilk test. Between-group differences were analyzed using 2-tailed Student's or Welch's independent sample t-tests for equal and unequal variances, respectively. The Wilcoxon rank sum test was applied for non-normal data.

We performed a linear mixed-effects analysis, using the nmle R package,[32] to examine the differences in retinal layer thicknesses between the participants with aniridia and normal controls. A random effect was entered to treat retinal layer as a within-subject variable (random intercept per subject). Weights were added to account for the difference in variance between the groups. Small deviations from homoscedasticity and normality of the residuals, when analyzing the foveal center, were accounted for by applying a square root transformation to the dependent variable. Likelihood ratio tests were performed to compare models. Differences were considered significant when $P \leq 0.05$.

Holm-Bonferroni corrected pairwise t-tests were used to assess differences in outer retinal thickness between the different locations of the *PAX6* mutations. Correlations were assessed using Pearson correlation coefficient (r_p). Multiple linear regression was performed to assess the relationship between logMAR visual acuity, retinal layer thicknesses and AAK grade. Significance level was set at 0.05. Weighted Cohen's Kappa (κ) was calculated to assess interrater agreement in grading of foveal hypoplasia.

Results

Table 2 shows an overview of the clinical phenotypes in aniridia. Iris anomaly severity varied from subtle structural anomalies to complete absence of the iris (more or less symmetrical in both eyes) as observed by slit-lamp examination. Best-corrected visual acuity ranged from logMAR 0.00–1.76 to hand movements at 0.5 m. The mean AL was similar in aniridic eyes (23.27, range 19.48–28.30 mm) and control eyes (23.64, 20.63–26.14 mm, $P = 0.29$), although with a larger range in aniridia. Refractive errors in aniridic eyes ranged from SER -20.50 to +10.00 D. The normal controls were healthy with no systemic or ocular diseases and had visual acuity ≤ 0.10 logMAR.

Aniridia Genotypes

The 11 families (24 participants) showed mutations that followed an autosomal dominant pattern. Table 3 summarizes the details of the identified *PAX6* mutations including nucleotide change, amino acid change, type of mutation and predicted functional outcome. Genetic data was not available from participants 5119 and 5124. Mutations that affect *PAX6* were found in 34 of 35 participants with aniridia who provided a saliva sample (20 unique variants), employing *PAX6* sequencing (n=25) and MPLA analysis (n=9). Three variants have not been reported previously. Figure 2 shows a schematic presentation of the deletions and mutations identified in *PAX6* and adjacent downstream regulatory regions.

PAX6 sequencing identified 15 different mutations, with five variants located in the paired domain, four in the linker region, one in the homeodomain and two in the proline-serine-threonine rich region. Untranslated regions of the *PAX6* gene (5'UTR: exons/introns 1–3) were involved in three different mutation variants.

Thirteen participants had mutations that introduce a premature termination codon (PTC), with or without a frameshift. All of these occurred > 50 base pairs upstream of the last exon/exon junction,

and thus the mRNA are expected to be targeted for degradation in the nonsense mediated decay pathway and result in haploinsufficiency.[33, 34] Two participants had mutations predicted to result in a PAX6 protein with a C-terminal extension (CTE) and nine had mutations predicted to cause splice errors. Partial deletions of *PAX6* were detected in two participants with sporadic aniridia. One was a 17 base pair deletion in exon 4 (GGCCCCCAGCCAGAGCC), followed by an A>T substitution that disrupts the Kozak sequence.[35] This mutation has not been reported previously. Without the Kozak sequence, the absence of protein is expected. This participant had severe corneal and lens opacities that hindered retinal imaging. The second person has a deletion that removes the last 25 base pairs of exon 5 through the first 61 base pairs of exon 6, including exon 5A (previously described by Grønskov *et al*.[36]). Seven from one family (no. 2), who have a splice site mutation (IV2-2delA) in the 5'UTR, have been described in detail previously.[10]

In nine participants, MPLA analysis identified five different multiple exon deletions, either within, upstream or downstream of the *PAX6* genomic region. One of these (*ELP4-DCDC1*) did not include any of the *PAX6* exons but was located downstream of the *PAX6* gene and contains 3' regulatory elements for *PAX6*.[37] Four of the large deletions included the *PAX6* coding exons, but only two of them included the retina-specific enhancer located in DNaseI hypersensitive sites (HS2–3) within the downstream regulatory region (DRR) between the *ELP4* and *PAX6* genes.[38] Without the enhancer, no messenger RNA is expected from the affected alleles.

No, *PAX6, FOXC1* or *PITX2* mutations could be detected for one sporadic case who had a classical aniridia phenotype with iris hypoplasia, moderate AAK and grade 3 foveal hypoplasia. No point mutations in the SIMO element were found for any of the participants.

Table 2. Overview of phenotypes in aniridia. Participants are sorted in the same way as in Table 3, that is according to whether the genotype is sporadic (above the broken line) or familial.

ID	Test Eye*	VA [logMAR]	AL [mm]	Iris hypoplasia	AAK grade	Nystagmus	FH grade	ON hypoplasia	Glaucoma	Lens status §
5110	OD	1.00 (HM)	21.29 (20.79)	Complete	3	Yes	N/A	Yes	Yes	P. phakic
5118	OD	0.74 (CF)	23.35 (24.80)	Complete	3	Yes	N/A	No	Yes	P. phakic
5121	OS	CF (CF)	26.08 (N/A)	Partial	3	Yes	N/A	No	No	N5/C1/P1
5126	OD	0.80 (0.88)	22.02 (21.68)	Complete	1	Yes	4	No	Yes	N1/C4/P4
5137	OD	0.70 (0.74)	23.47 (23.20)	Partial	1 (2)	Yes	3	No	No	N1/C3/P2
5138	OD	0.90	21.84 (21.64)	Complete	1	Yes	4	No	No	N1/C3/P1
5147	OD	0.50 (0.60)	22.64 (23.09)	Complete	2	Yes	3	No	No	N1/C3/P1
5149	OS	0.90 (1.10)	20.26 (20.21)	Partial	2 (3)	Yes	4	N/A	No	N2/C5/P3
5151	OS	CF (HM)	23.35 (23.39)	Complete	3	Yes	N/A	N/A	Yes	N1/C2/NA
5134	OD	0.18	21.66 (21.80)	Partial	1	No	1	No	No	P. phakic
5154	OD	0.72 (0.80)	22.27 (22.59)	Complete	1 (2)	Yes	2	No	No	N1/C4/P2
5119	OD	1.00 (1.30)	21.22 (N/A)	Complete	1 (3)	Yes	4	No	Yes	N1/C3/P1
5124	OD	0.40 (0.60)	24.01 (24.54)	Partial	0	No	0	No	No	N1/C1/P1
5113	OD	0.80 (1.00)	21.14 (21.40)	Complete	2	Yes	4	No	No	P. phakic
5129	OS	1.30 (CF)	21.50 (23.37)	Complete	3	Yes	N/A	No	Yes	P. phakic
5114	OD	0.86 (1.78)	23.97 (24.04)	Complete	1 (3)	Yes	3	Yes	Yes	Aphakic
5116	OD	0.40	25.66 (25.41)	Partial	2	No	2	No	No	P. phakic
5120	OS	0.22 (0.32)	23.80 (23.93)	Partial	1	No	2	No	No	N2/C1/P1
5123	OS	0.50 (1.30†)	22.72 (24.63)	Almost complete	2 (1)	No	2	No	No	N1/C3/P1
5135	OD	0.70 (0.80)	24.05 (23.25)	Complete	1	Yes	3	Yes	Yes	N2/C4/P3
5148	OS	0.60 (0.64)	21.04 (21.06)	Almost complete	2	No	4 (3)	No	Yes	P. phakic
5199	OD	0.20 (0.30)	25.55 (25.36)	Near normal	1	No	2	No	No	N0/C2/P0
5125	OD	0.74 (0.76)	24.13 (23.98)	Complete	1	Yes	3	No	Yes	N1/C2/P2
5127	OD	1.20 (1.10)	25.37 (26.51)	Almost complete	2	Yes	4	No (Yes)	Yes	P. phakic
5146	OS	CF (LP)	23.30 (N/A)	Complete	2 (3)	Yes	N/A	N/A	Yes	P. phakic
5131	OD	1.30 (CF)	24.42 (24.37)	Partial	1	Yes	4	Yes	Yes	Aphakic
5140	OD	0.70 (0.80)	20.97 (20.88)	Complete	2 (3)	Yes	4	No	No	N1/C4/P2
5141	OD	1.00 (0.90)	28.30 (28.08)	Partial	2	Yes	4	No	No	N1/C3/P1
5144	OD	0.74 (1.00)	23.55 (23.88)	Complete	2 (3)	Yes	3	No	No (Yes)	P. phakic
5145	OD	1.76 (1.80)	23.45 (22.65)	Complete	3	Yes	N/A	N/A	No	P. phakic
5117	OD	1.00 (1.10)	23.34 (23.35)	Complete	2 (1)	Yes	4	No	Yes	P. phakic
5128	OD	0.90 (1.10)	19.48 (19.44)	Complete	2 (3)	Yes	N/A	N/A	No	N1/C4/P4
5152	OD	1.30	23.21 (N/A)	Complete	3	Yes	N/A	N/A	Yes	N1/C3/P1
5130	OS	1.30 (LP)	26.59 (N/A)	Complete	3	Yes	N/A	Yes	Yes	Aphakic
5132	OS	0.56 (0.30)	25.74 (28.50)	Complete	0	No	1 (2)	No	Yes	P. phakic
5139	OD	0.00 (0.46‡)	22.95 (22.35)	Complete	0	No	0	No	No	N1/C1/P1
5155	OS	N/A	N/A (N/A)	Complete	0	No	N/A	N/A	No	N/A

Abbreviations: N/A, not available; VA, visual acuity; CF, counting fingers at 0.5m; LP, light perception; AL, axial length; FH, foveal hypoplasia grade; ON, optic nerve; P. phakic, pseudophakic

* The test eye is the eye included in retinal layer thickness analyses. Data from the other eye is noted in parenthesis if different from that of the test eye.

†Subluxated lens OD, not corrected for during VA measurement

‡Amblyopic OS

§ LOCS II grading[39]

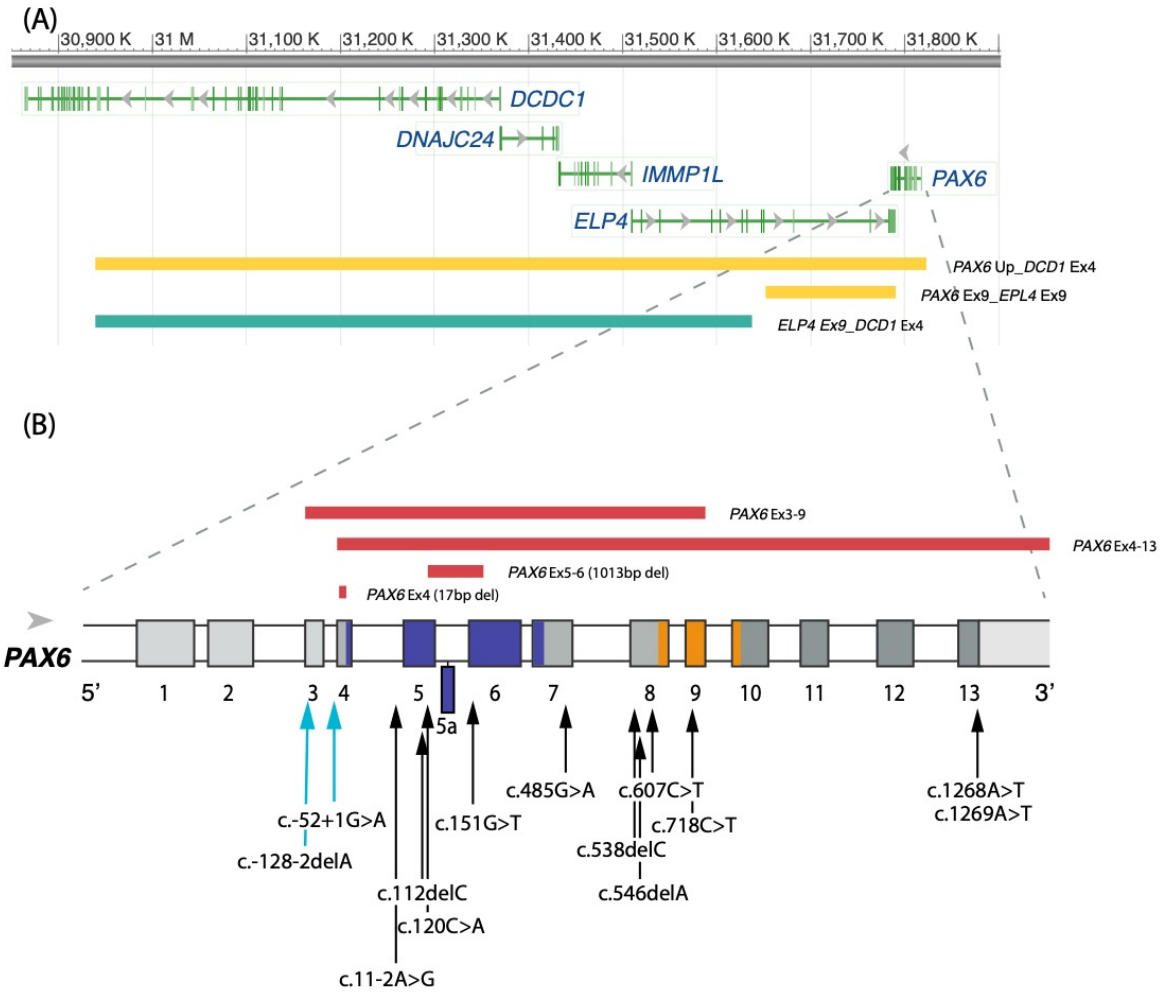

Figure 2. Schematic presentation of the deletions and mutations identified in PAX6 and adjacent downstream regulatory regions. (A) PAX6 is located at chromosome 11p13. The ruler at the top gives the nucleotide numbers for the region shown. By convention, the nucleotides that comprise each chromosome in the reference sequence are numbered consecutively starting at the tip of the petite (p) arm. The region shown is for the GRCh38/hg38 assembly of the human genome. The colored horizontal bars represent the size of the deletions identified in the participants with aniridia and are colored according retinal phenotype, green: FH grade 0–1; yellow: FH grade 1–2. (B). Zoomed in view of PAX6 gene structure. The gene has 14 exons and a 3' untranslated region (UTR) depicted as colored boxes (including exon 5a). The white boxes indicate introns. The protein coding region begins in exon 4 at position c.1. The protein domains encoded by the exons are color coded (blue: paired domain, grey: linker region, orange: homeodomain, dark grey: proline-serine-threonine domain). Mutations involving only the PAX6 gene found in this study are indicated as red bars above the gene showing deletions larger than 1 nucleotide. The arrows below the gene show the locations of point mutations, including single nucleotide deletions. The labeling convention for the arrows shows the coding region nucleotide number for the affected position which are positive if after the translation start site, or negative if in the 5' untranslated exons. The nucleotide number is followed by the identity of the nucleotide found in the reference sequence followed by ">" then by the nucleotide found in the mutant. Deletions are indicated by "del" followed by the identity of the deleted nucleotide. The arrows are color coded as follows: turquoise: FH grade 2–4; black FH grade 3–4.

Table 3. Summary of genotypes

ID	Inheritance	Family Nr.	Location	Nucleotide change	Amino acid change	Type of mutation #	NMD predicted
5110	Sporadic		Ex 5_6	Deletion *PAX6* Ex5_6 ‡		Deletion	Yes
5118	Sporadic		Ex 7	c.485G>A	p.(Trp162*)	Nonsense	Yes
5121	Sporadic		Ex 4	Deletion *PAX6* Ex4 §		Deletion	Yes
5126	Sporadic		Ex 8	c.607C>T	p.(Arg203*)	Nonsense	Yes
5137	Sporadic		Ex 5	c.120C>A	p.(Cys40*)	Nonsense	Yes
5138	Sporadic		Ex 8	c.546delA ||	p.(Gly184Glufs*23)	Frameshift	Yes
5147	Sporadic		-	Not found	-	-	-
5149	Sporadic		Ex 13	c.1268A>T	p.(*423Leuext15)	CTE	No
5151	Sporadic		Ex 9	c.718C>T	p.(Arg240*)	Nonsense	Yes
5134	Sporadic		Ex 9_13; *ELP4-Ex9*	Deletion *PAX6*, Ex 9_13 *ELP4,* Ex 9		Deletion	No mRNA expected
5154	Sporadic		Up_Ex1_13; E*LP4*, Ex9; *DCDC1*, Ex1+4	Deletion *PAX6* Upstream_ *DCDC1*, Ex4		Deletion	No mRNA expected
5113	Familial	1	Ex 8	c.538delC ||	p.(Gln180Argfs*27)	Frameshift	Yes
5129		1	Ex 8	c.538delC ||	p.(Gln180Argfs*27)	Frameshift	Yes
5114*	Familial	2	Int 2	c.-128-2delA (IVS2-2delA)		Splice	Most likely
5116*		2	Int 2	c.-128-2delA (IVS2-2delA)		Splice	Most likely
5120*		2	Int 2	c.-128-2delA (IVS2-2delA)		Splice	Most likely
5123*		2	Int 2	c.-128-2delA (IVS2-2delA)		Splice	Most likely
5135*		2	Int 2	c.-128-2delA (IVS2-2delA)		Splice	Most likely
5148*		2	Int 2	c.-128-2delA (IVS2-2delA)		Splice	Most likely
5199*		2	Int 2	c.-128-2delA (IVS2-2delA)		Splice	Most likely
5125†	Familial	3	Int 3	c.-52+1G>A (IVS3+1G>A)		Splice	Yes
5127	Familial	4	Ex 6	c.151G>T	p.(Gly51*)	Nonsense	Yes
5146		4	Ex 6	c.151G>T	p.(Gly51*)	Nonsense	Yes
5131	Familial	5	Ex 5	c.112delC	p.(Arg38Glyfs*30)	Frameshift	Yes
5140	Familial	6	Ex 13	c.1269A>T	p.(*423Tyrext15)	CTE	No
5141	Familial	7	Int 4	c.11-2A>G (IVS4-2A>G)		Splice	Yes
5144	Familial	8	Ex 9	c.718C>T	p.(Arg240*)	Nonsense	Yes
5145		8	Ex 9	c.718C>T	p.(Arg240*)	Nonsense	Yes
5117	Familial	9	Ex 3_9	Deletion *PAX6*, Ex3_9		Deletion	Yes
5128		9	Ex 3_9	Deletion *PAX6*, Ex3_9		Deletion	Yes
5152		9	Ex 3_9	Deletion *PAX6*, Ex3_9		Deletion	Yes
5130	Familial	10	Ex 4_13	Deletion *PAX6*, Ex4_13		Deletion	Yes
5132	Familial	11	E*LP4*, Ex9; *DCDC1*, Ex1+4	Deletion *ELP4*, Ex9_ *DCDC1*, Ex4		Deletion	Unknown
5139		11	E*LP4*, Ex9; *DCDC1*, Ex1+4	Deletion *ELP4*, Ex9_ *DCDC1*, Ex4		Deletion	Unknown
5155		11	E*LP4*, Ex9; *DCDC1*, Ex1+4	Deletion *ELP4*, Ex9_ *DCDC1*, Ex4		Deletion	Unknown

***** Participants previously reported[10]

† Participant harbours an additional variant in *PAX6* Ex10*:* c.831G>A, does not alter amino acid

‡ A 1013 bp deletion that removes the last 25 bp of exon 5 through the first 61 bp of exon 6

§ There is a 17 pb deletion (GGCCCCCAGCCAGAGCC), followed by an A>T substitution that disrupts the Kozak sequence. This deletion has not been reported previously

||These single nucleotide deletions have, to our knowledge, not been not reported previously. Slightly different nucleotide changes (c.551delG and c. 538C>T, respectively) are previously reported to give the same amino acid changes and are described as a cause of aniridia.

All genetic variants are predicted to be pathogenetic according to the ACMG classification scheme[40]

Retinal Layer Thicknesses

SD-OCT imaging was obtained of 26 persons with aniridia and 58 controls. Severe ocular media opacities (AAK > 2) limited the view of the posterior pole and/or severe nystagmus prohibited a reliable measurement or scan through the expected foveal center in ten participants with aniridia. One participant (5155) was not available for OCT imaging.

Figure 3 shows the variability in foveal morphology, including variability of inner and outer retinal structures, within and across foveal hypoplasia grades among those with aniridia. There was a statistically significant agreement in grading of foveal hypoplasia between the two graders ($\kappa = 0.883$, $P < 0.001$). Foveal hypoplasia was observed in 24 of 26 (92.3%) participants. The central fovea was thicker in aniridia (mean ± SD 311.6 ± 30.2 µm, range 232.5–357.8 µm) compared with the controls (229.4 ± 15.9 µm, 198.2–275.6 µm, $P < 0.001$). In contrast, the mean nasal and temporal perifoveal and parafoveal retinal thicknesses were significantly thinner in aniridia compared with the controls (all regions $P < 0.001$, Figure 4A). This was a consequence of thinner parafoveal and perifoveal inner (RNFL + GCL + IPL, Figure 4B) and outer retinal layers in aniridia (summarized in Table 4), whereas parafoveal and perifoveal INL and OPL were similar in both groups.

The outer retinal layers were significantly thinner in aniridia, across the whole horizontal meridian, compared with the controls, particularly in the foveal center (mean ± SD 156.3 ± 32.3 µm vs 210.8 ± 12.3 µm, $P < 0.001$; Figure 4C). The mean (SD) central foveal thicknesses of two of the component layers of the outer retina were thinner in participants with aniridia than the controls: ONL (73.0 ± 21.7 vs. 104.6 ± 12.9 µm; $P < 0.001$) and OS (29.0 ± 7.2 vs. 44.0 ± 3.2 µm; $P < 0.001$). Inner segment thickness was similar in the two groups (31.3 ± 3.7 vs. 33.7 ± 2.4 µm; $P = 0.5$*)* while the RPE tended to be slightly thicker in aniridia (32.4 ± 7.0 vs. 28.5 ± 3.7 µm; $P = 0.3$). Outer retinal layer thinning in the foveal center was associated with thinner nasal and temporal parafoveal and perifoveal retinal thickness (nasal parafovea: $r_p = 0.74$, $P < 0.001$; temporal parafovea: $r_p = 0.75$, $P < 0.001$; nasal perifovea: $r_p = 0.51$, $P = 0.009$; temporal perifovea: $r_p = 0.61$, $P = 0.001$) and ILM-IPL thickness (nasal parafovea: $r_p = 0.56$, $P =$

0.004; temporal parafovea: r_p = 0.45, P = 0.02; nasal perifovea: r_p = 0.52, P = 0.009; temporal perifovea: r_p = 0.59, P = 0.002).

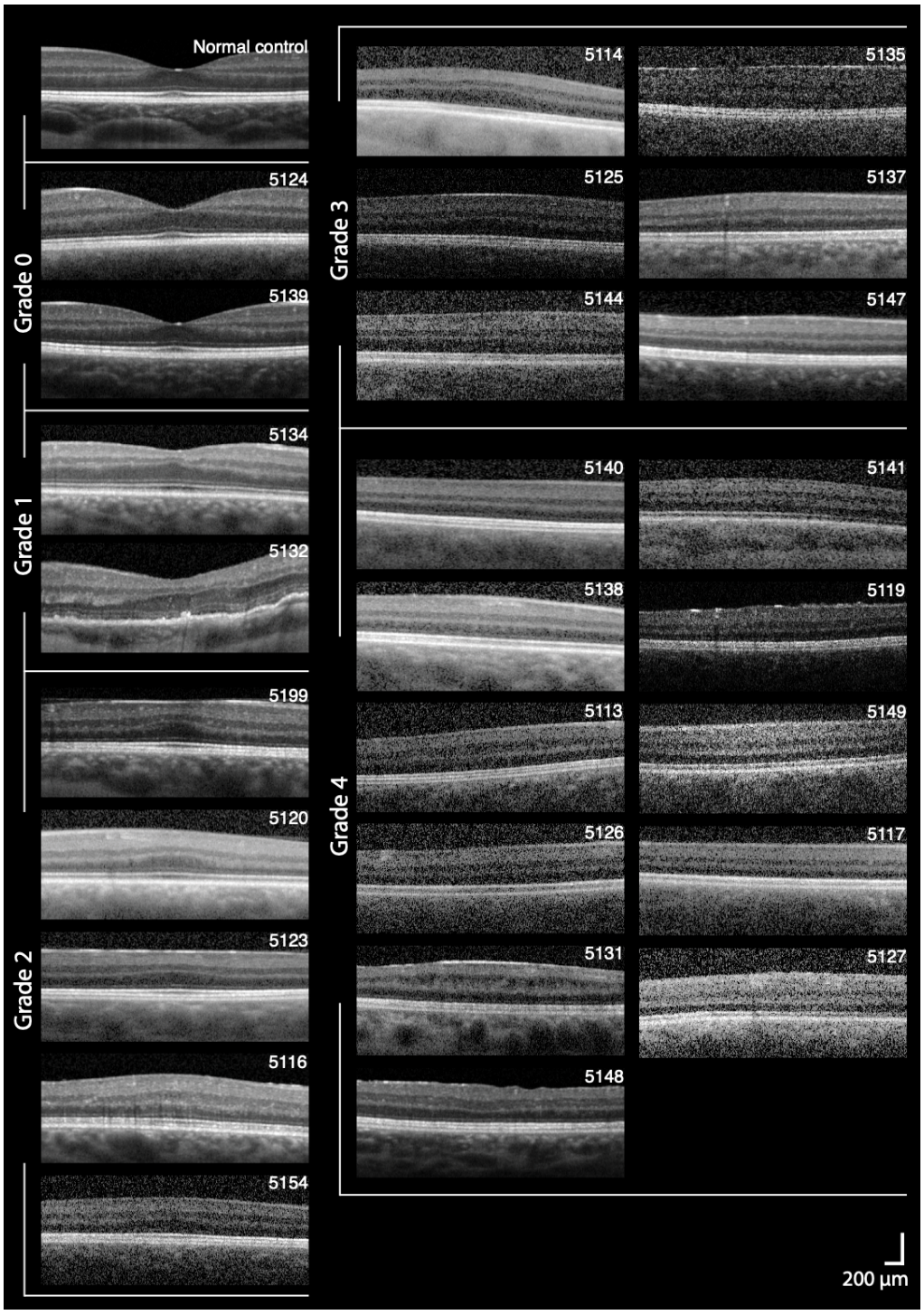

Figure 3. Variability in foveal morphology in aniridia. SD-OCT horizontal line scans through the expected foveal location are shown for the participants with aniridia and one normal control. The images are ordered from thickest (upper left) to thinnest (lower right) outer retinal layers within groups of foveal hypoplasia grade: grade 0 (no foveal hypoplasia), grade 1, grade 2, grade 3, and grade 4. Scale bar = 200 µm.

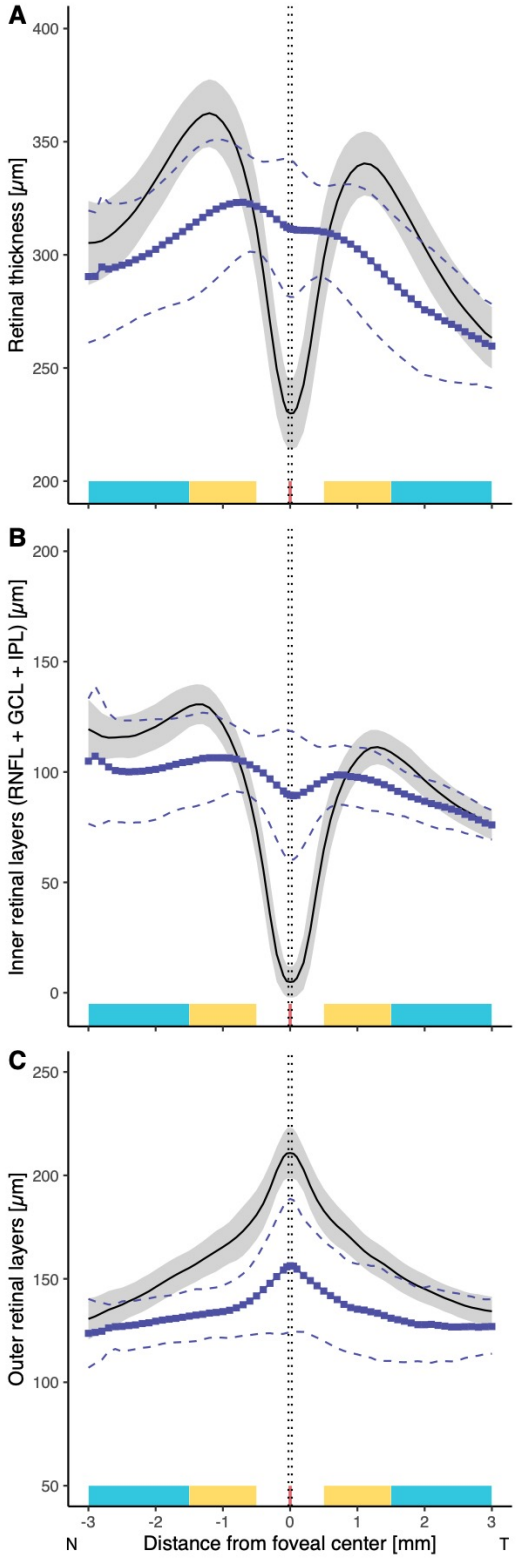

Figure 4. Graphs showing the variation in thickness of the (A) total retina, (B) inner retinal layers (ILM-IPL) and (C) outer retinal layers (ONL+IS+OS+RPE) along the horizontal meridian in aniridia compared with normal control participants. Black solid lines and the shaded area represent the normal mean ± SD and line with blue squares and dashed lines represent the mean ± SD for the participants with aniridia. The fovea, parafoveal and perifoveal regions along the nasal and temporal meridians are marked with red, yellow and turquoise, respectively.

Table 4. Differences in parafoveal (0.5–1.5 mm from the foveal center) and perifoveal (1.5–3.0 mm from the foveal center) retinal layer thicknesses between the participants with aniridia (n = 26) and normal controls. Outer nuclear thickness could only be calculated for a subset of the aniridia patients (n = 19).

Retinal layer	Mean difference [µm]	95% Confidence Interval		*P*-value	Mean difference [µm]	95% Confidence Interval		*P*-value
		Upper	Lower			Upper	Lower	
	Nasal parafovea				Temporal parafovea			
Inner retinal layers (RNFL + GCL + IPL)	-9.77	-4.69	-14.85	< 0.001	-3.29	2.33	-8.91	0.25
Inner nuclear layer	5.45	10.62	0.28	0.039	2.40	8.12	-3.33	0.41
Outer plexiform layer	4.63	9.80	-0.54	0.079	1.39	7.12	-4.33	0.63
Outer retinal layers (ONL + IS + OS + RPE)	-31.09	-26.09	-36.09	< 0.001	-30.96	-25.43	-36.48	< 0.001
Outer nuclear layer	-21.55	-18.52	-24.58	< 0.001	-26.33	-22.02	-30.65	< 0.001
	Nasal perifovea				Temporal perifovea			
Inner retinal layers (RNFL + GCL + IPL)	-16.91	-11.23	-22.59	< 0.001	-6.65	-2.46	-10.84	0.002
Inner nuclear layer	2.69	8.49	-3.10	0.36	-0.28	3.98	-4.55	0.90
Outer plexiform layer	4.82	10.62	-0.97	0.10	1.45	5.72	-2.81	0.50
Outer retinal layers (ONL + IS +OS + RPE)	-13.92	-8.33	-19.50	< 0.001	-14.50	-10.31	-18.69	< 0.001
Outer nuclear layer	-11.28	-8.42	-14.13	< 0.001	-15.45	-12.08	-18.82	< 0.001

We found a strong negative correlation between foveal outer retinal layer thickness and high-contrast logMAR visual acuity in aniridia (r_p = -0.80, P > 0.001). Multiple linear regression also showed that foveal outer retinal layer thickness was the strongest predictor of high-contrast logMAR visual acuity when AAK was ≤ grade 2 (r^2 = 0.66, P < 0.001; Figure 5). No correlations were observed between AL and foveal retinal thickness, except when AL < 21.5 mm which was only observed with grade 4 foveal hypoplasia and thin outer retinal layers. Analysis of variance followed by post-hoc Bonferroni-corrected pairwise t-tests revealed no significant differences in outer retinal thickness between a normal fovea and foveal hypoplasia grade 1 (p = 0.3), between grades 1 and 2 (p = 0.15), nor between grades 2 and 3 (p = 0.2). Foveal phenotypes did not correlate with iris phenotype.

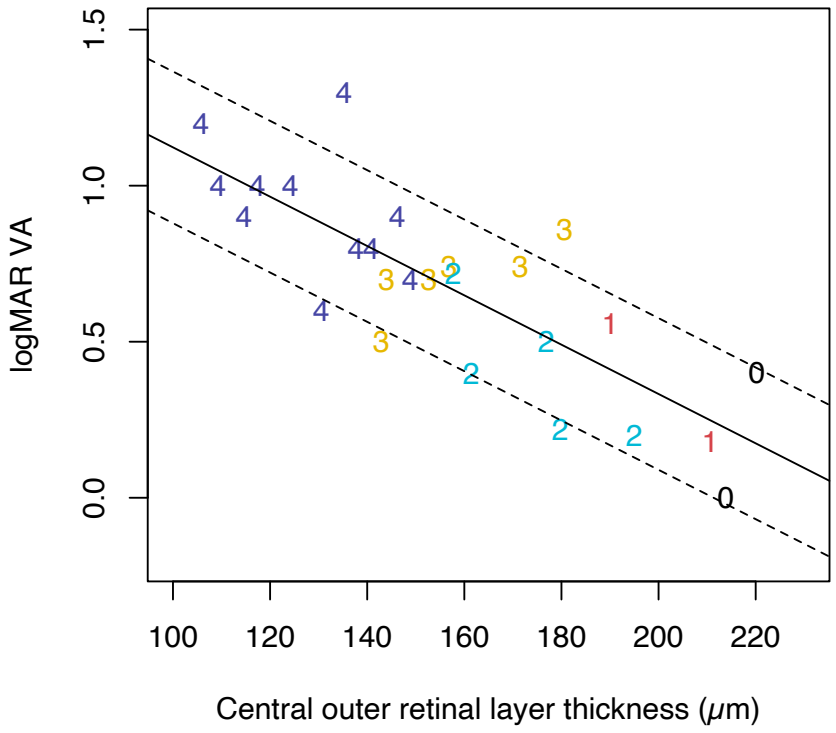

Figure 5. Relationship between foveal outer retinal layer thickness and high contrast logMAR visual acuity in aniridia. The number of the datapoint for each participant corresponds to their grade of foveal hypoplasia.

Genotype-Phenotype Correlations

All participants with a *PAX6* mutation had foveal hypoplasia. There was a large phenotypic variability among individuals with the same mutation, as well as between individuals with different mutations.

Participants with splice site mutations in the 5' untranslated region (5' UTR) of PAX6 (families 2 and 3) had, on average, thicker foveal outer retinal layers than those with mutations in the coding regions of the PAX6 gene (difference [range]: 27.7 [0.01–55.32] µm, P = 0.040; Figure 6). Those with mutations in PAX6 coding regions that introduced a PTC and predicted haploinsufficiency due to NMD had severe foveal hypoplasia (grade 3 or 4). In contrast, the participants who have large PAX6 deletions including the retina-specific enhancer had milder foveal hypoplasia (grades 1-2, Table 5). The family (no. 11) with a deletion in the 3' regulatory region (*ELP4-DCDC1*), but an intact PAX6 transcriptional region, had complete iris hypoplasia, but normal foveal shape or only mild foveal hypoplasia with outer retinal

layer thickness within the normal range (Figure 6). The two individuals with CTE mutations had complete foveal hypoplasia, thinning of outer retinal layers and short AL < 21 mm.

Table 5. Summary of the types of mutations and retinal phenotypes for the 26 participants who were imaged with OCT. The participants are ordered according to foveal hypoplasia grade corresponding to the OCT images in Figure 3.

ID	FH grade	Central retinal thickness [µm]	Central outer retinal thickness [µm]	Gender	Mutation	
					Type	Remarks
5124	0	239.27	220.22	M	Not available	
5139	0	232.48	213.88	F	Deletion *ELP4*, *DCD1*	Deletes retina enhancer
5134	1	296.73	210.63	F	Large deletion *PAX6*, *ELP4*	Deletes retina enhancer
5132	1	292.45	190.04	F	Deletion *ELP4*, *DCD1*	Deletes retina enhancer
5199	2	338.12	194.98	M	Splicing error *PAX6* 5'UTR	
5120	2	347.91	179.77	M	Splicing error *PAX6* 5'UTR	
5123	2	323.30	176.84	M	Splicing error *PAX6* 5'UTR	
5116	2	357.77	161.44	M	Splicing error *PAX6* 5'UTR	
5154	2	300.10	157.69	F	Large deletion *PAX6, ELP4*, *DCD1*	Deletes retina enhancer
5114	3	312.42	180.67	F	Splicing error *PAX6* 5'UTR	
5125	3	343.52	171.49	M	Splicing error *PAX6* 5'UTR	
5144	3	333.82	156.79	F	PTC – *PAX6* coding region	
5135	3	342.37	152.71	F	Splicing error *PAX6* 5'UTR	
5137	3	318.16	143.99	F	PTC – *PAX6* coding region	
5147	3	307.81	142.82	F	No mutation found	
5140	4	316.55	148.83	F	CTE – *PAX6* coding region	
5138	4	336.59	146.20	F	PTC – *PAX6* coding region	
5113	4	325.71	140.84	F	PTC – *PAX6* coding region	
5126	4	310.08	137.64	M	PTC – *PAX6* coding region	
5131	4	340.81	135.18	F	PTC – *PAX6* coding region	
5148	4	302.02	130.50	F	Splicing error *PAX6* 5'UTR	
5141	4	284.63	124.15	M	PTC – *PAX6* coding region	
5119	4	293.74	117.36	F	Not available	
5149	4	316.80	114.61	F	CTE – *PAX6* coding region	
5117	4	282.13	109.26	F	Large deletion *PAX6*	Intact retina enhancer
5127	4	305.73	105.72	F	PTC – *PAX6* coding region	

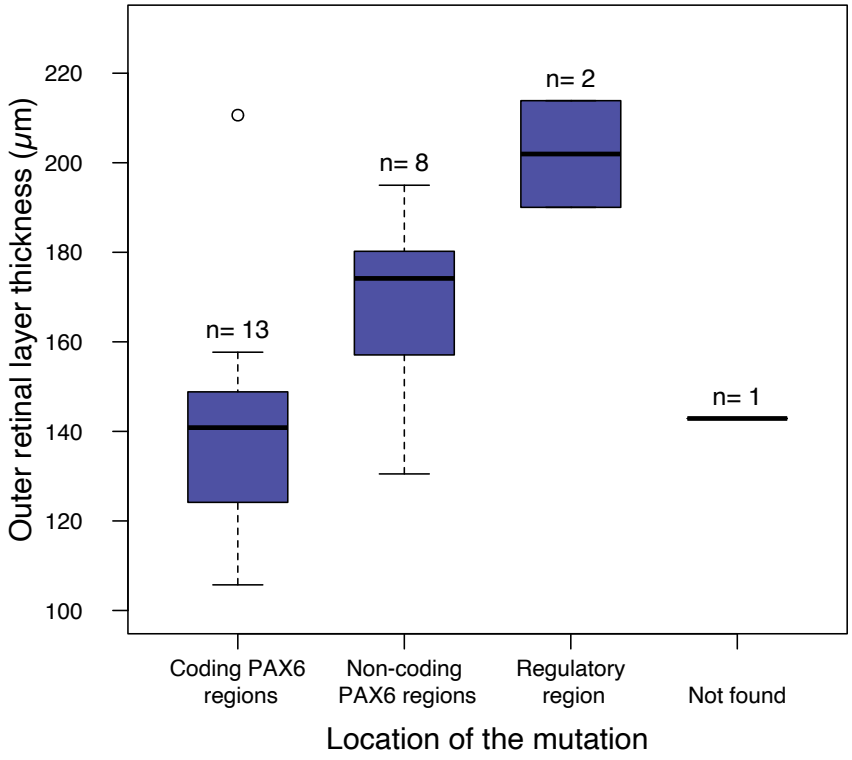

Figure 6. The boxplot shows the differences in foveal outer retinal layer thickness between participants who have mutations within *PAX6* coding regions, *PAX6* non-coding regions and 3' regulatory regions. One participant had no identified mutation.

Discussion

Mutations in the *PAX6* gene or in one or several of its regulatory regions were found in 97 % of the participants with aniridia, with three of 20 different pathogenic variants not reported previously. Comparison of the genotype with the detailed retinal phenotype in aniridia showed that all *PAX6* mutations were associated with varying degrees of arrested foveal development, reduced outer retinal thickness, and altered macular morphology. There was an association between the location of the gene mutation and macular phenotype. The better developed retinas were associated with mutations before the translational start codon (*PAX6* 5'UTR), deletions including the 3' regulatory region (*ELP4–DCDC1*) only, and in large *PAX6* deletions when the downstream regulatory region retina enhancer was deleted. This underscores the role of *PAX6* in foveal and macular development and indicates that residual PAX6 function may contribute to variation in phenotype depending on mutation location.

The mutations associated with the thickest foveal outer retinal layers and the mildest retinal phenotypes were mutations outside the *PAX6* gene (3' regulatory regions *ELP4-DCDC1*) followed by splice site mutations in the 5'UTR of *PAX6*. Mutations at these locations were generally associated with a better developed fovea than multiple *PAX6* exon deletions and mutations within the *PAX6* protein coding regions which are predicted to cause haploinsufficiency due to nonsense mediated decay of the mRNA. Deletions in 3' regulatory regions may affect *PAX6* expression through disruption of enhancer activity,[20] whereas variants in the untranslated regions may affect PAX6 function by altering normal splicing or disrupting open reading frames.[6] However, it is not known exactly how splice site mutations for the non-coding exons affect pre-mRNA splicing, mRNA expression level, or protein translation. The two variants in 5'UTR in the present study (c.-128-2delA and c. 52+1G>A) have been demonstrated to lead to skipping of exon 3 (in vitro) and exons 3-6 (reverse transcription-PCR), respectively, [6, 41] suggesting that the most likely outcome is haploinsufficiency.

It is clear that the contribution of each retinal layer to retinal thickness within the macula (central 6 mm) is considerably different in aniridia compared with the normal controls. During embryonic eye development, *PAX6* induces the differentiation of progenitor cells into retinal neurons.[42-44] The detailed analysis of the OCT images presented here shows that in eyes with aniridia, not only was the retina thicker and outer retinal layers thinner in the foveal center, but parafoveal and perifoveal inner and outer retinal layers were also significantly thinner than in the normal controls. This confirms previous findings in animal studies that loss off *PAX6* expression leads to a hypocellular macula.[42] It also corroborates the findings from other human studies,[11, 17] including a study using adaptive optics scanning light ophthalmoscopy, that revealed decreased macular cone photoreceptor density within one family with aniridia.[10] Thinner foveal outer retinal layers suggest that cone specialization and migration has not occurred to a full extent, resulting in immature foveal cones and decreased cone density. Absence of the IZ band (the photoreceptor – RPE apical processes interdigitation zone), observed in some of those with aniridia, may indicate immature foveal cone outer segments resulting in shorter cones with less indentation into the RPE. This could result in a hyperreflective signal from

the IZ that is more anterior than in a retina with longer and more mature cones (hence the tendency for the RPE to be thicker in aniridia).

The increased central foveal thickness in *PAX6*-associated aniridia appears to be caused by lack of centrifugal migration of the inner retinal layers away from the fovea. This is possibly related to the absence of a foveal avascular zone (FAZ) which is known to prevent the formation of a foveal pit.[25] PAX6 is important for the development of retinal ganglion cells[45] and for RPE specification and pigmentation.[46] The RPE and ganglion cells normally secrete pigment epithelium derive factor (PEDF), which prevents retinal blood vessels from invading the foveal region during early development.[25, 47] EphA6, which plays a role in regulating astrocyte migration across the retina, is also highly expressed by ganglion cells.[25] Thus, it is plausible that *PAX6* mutations affect the expression of anti-proliferative and anti-angiogenic factors in the developing foveal region which again lead to abnormal foveal vascularization.

Multiple exon deletions have previously been reported to result in a more severe corneal phenotype.[48] The same was observed here as four of seven participants with large *PAX6* deletions had corneal opacities that precluded retinal imaging. The three who were imaged (5134, 5154, 5117) had retinal phenotypes ranging from mild to severe (FH grade 1–4). Interestingly, the one participant (5117) who had a severe phenotype, had a deletion that included the region covered by the MLPA probes from *PAX6* exon 3 – 9, but left the DRR retina-specific enhancer intact. The mRNA from this deletion is likely to be unstable and be targeted to NMD. Thus, it appears that mutations that are predicted to target mRNA to destruction in NMD have a more severe phenotype than mutations that deleted the retina enhancer and thus do not produce any mRNA in the retina. The NMD pathway does not work with 100% efficiency, and there is variability in its efficiency even across family members with the same mutations.[49] Thus, one explanation for the difference in severity for participants lacking the retina enhancer versus those with a mutation that would be transcribed, but the mRNA targeted to destruction, is that a small amount of the mRNA escapes NMD. The escaped mRNA is expected to be

translated into a mutant protein that has a dominant negative effect. Variation in the efficiency of NMD across individuals may also contribute to the observed variability in phenotypes among family members with the same *PAX6* mutation.

CTE and PTC mutations were associated with moderate to severe retinal phenotypes. Myopia has been reported to be a common feature of CTE mutations,[8, 50] but the two in our cohort were both hyperopic with a short AL (< 21 mm). Aniridia has often been associated with small eyes, but our results show that there is large variability in ocular AL among those who have *PAX6*-associated aniridia. Only three participants were diagnosed with microphthalmia (AL < 21 mm)[51] accompanied by a severe retinal phenotype (FH grade 4, see 5140 and 5149 in figure 3; Ocular media opacities precluded OCT imaging in 5128). Normal eye growth is an important factor for emmetropization and is also thought to play a role in foveal maturation, including cone packing and elongation.[52] In normally developing eyes, a large part of foveal maturation and cone packing occurs after birth and up to the age of at least 16 years.[53] At birth, foveal photoreceptors are shorter than parafoveal and perifoveal photoreceptors, however they elongate as the eye grows and the fovea continues to mature.[53] The increased outer retinal layer thickness in the foveal center relative to the perifovea observed in some persons with *PAX6*-associated aniridia, therefore reflects photoreceptor development and foveal maturation after birth. This was evident in those who had a mutation in either 3' regulatory regions (*ELP4-DCDC1*) or splice site mutations in the 5'UTR of *PAX6*, but also in some participants with large *PAX6* deletions including the DRR (5134 and 5154). Longitudinal studies are required to understand the association between ocular axial growth and foveal maturation in aniridia, and the importance of refractive error correction and visual stimulation from an early age.

The effects of *PAX6* mutations are dose-dependent, thus mutations on both alleles will cause a very severe phenotype that usually are lethal before birth.[7] In the present study, participant 5125 exhibited classical aniridia and had two mutations, a splice site mutation (c.-52+1G>A) in intron 3 and a mutation in exon 10 (c.831 G>A). These two mutations are therefore likely to be present in one allele where the

former one (c.-52+1G>A) first terminates the PAX6 protein. Alternatively, the mutation in exon 10 (c.831G>A) is a silent mutation because it does not alter amino acid as reported previously,[41] although Mutation Taster[21] predicted that it would cause a splicing defect and be disease-causing.

No pathological sequence changes were observed in one sporadic case with classical aniridia indistinguishable from *PAX6*-associated aniridia. Next generation sequencing approaches such as whole genome sequence or whole exome analysis might be able to uncover the mutation in this individual. Somatic *PAX6* mosaicism has been described and might explain the presence of aniridia in persons without detectable *PAX6* mutations.[54] Mosaicism could also be a possible genetic factor to explain variable expressivity within families.[54]

A strength of this study was the detailed examination of foveal anatomy across a wide phenotypic and genotypic range of aniridia. Based on a reported prevalence of 1:72 000,[1] the 37 participants in this study represent > 50% of the persons who have aniridia in Norway and are therefore reasonably representative for persons with aniridia across the country. Despite limitations related to only being able to image with adequate quality in 26 participants with aniridia, the present analysis includes the full range of aniridia phenotypes.

Conclusions

The results presented here shows significant variation in outer retinal layer thickness measurements within each grade of foveal hypoplasia. Importantly, outer retinal layer thickness was the structural measure with the highest correlation with visual acuity in participants without severe central AAK. Notable examples are participants 5154 and 5199, both with FH grade 2, but participant 5154 have 35 µm thinner outer retinal layers than participant 5199 with correspondingly poorer visual acuity (0.72 vs. 0.20 logMAR, respectively). In clinical terms, this implies that qualitative grading (1–4) of foveal hypoplasia from OCT images is too coarse and may misclassify visual outcome for persons with aniridia.

PAX6 mutations were found to be associated with abnormal foveal formation and reduced number of neurons in the macula, with mutations in *PAX6* coding regions giving the worst outcome. The observed variation underscores the importance of careful retinal phenotypic characterization, even when the *PAX6* mutation is known, for predicting visual outcome after surgery, optical visual rehabilitation and future gene therapy. If photoreceptor development extends after birth in some eyes with *PAX6*-associated aniridia, as the increased foveal outer retinal layer thicknesses observed here indicates, it suggests that early visual stimulation and optimization of visual function is as important as it is in normally developing eyes. It may be a factor in improving foveal maturation outcome in adult life.

Acknowledgements

The authors are grateful to the Norwegian Association of Aniridia (Aniridi Norge) for the continued cooperation and support. The study was funded by the University of South-Eastern Norway and Aniridia Norway. Work done at the University of Washington was supported by NEI grants P30EY001730 and R01EY028118, and by unrestricted funds from Research to Prevent Blindness.

References

1. Edén U, Iggman D, Riise R, Tornqvist K. Epidemiology of aniridia in Sweden and Norway. *Acta Ophthalmologica*. 2008;86:727-729.
2. Shaw MW, Falls HF, Neel JV. Congenital Aniridia. *Am J Hum Genet*. 1960;12:389-415.
3. Ton CC, Hirvonen H, Miwa H, et al. Positional cloning and characterization of a paired box- and homeobox-containing gene from the aniridia region. *Cell*. 1991;67:1059-1074.
4. Lauderdale JD, Wilensky JS, Oliver ER, Walton DS, Glaser T. 3' deletions cause aniridia by preventing PAX6 gene expression. *Proc Natl Acad Sci U S A*. 2000;97:13755-13759.
5. Kleinjan DA, Seawright A, Schedl A, Quinlan RA, Danes S, van Heyningen V. Aniridia-associated translocations, DNase hypersensitivity, sequence comparison and transgenic analysis redefine the functional domain of PAX6. *Human Molecular Genetics*. 2001;10:2049-2059.
6. Plaisancie J, Tarilonte M, Ramos P, et al. Implication of non-coding PAX6 mutations in aniridia. *Hum Genet*. 2018;137:831-846.
7. Landsend ES, Utheim OA, Pedersen HR, Lagali N, Baraas RC, Utheim TP. The genetics of congenital aniridia-a guide for the ophthalmologist. *Surv Ophthalmol*. 2018;63:105-113.
8. Hingorani M, Williamson KA, Moore AT, van Heyningen V. Detailed ophthalmologic evaluation of 43 individuals with PAX6 mutations. *Invest Ophthalmol Vis Sci*. 2009;50:2581-2590.
9. Yokoi T, Nishina S, Fukami M, et al. Genotype-phenotype correlation of PAX6 gene mutations in aniridia. *Hum Genome Var*. 2016;3:15052.
10. Pedersen HR, Neitz M, Gilson SJ, et al. The Cone Photoreceptor Mosaic in Aniridia: Within-Family Phenotype-Genotype Discordance. *Ophthalmol Retina*. 2019;3:523-534.
11. Sannan NS, Gregory-Evans CY, Lyons CJ, et al. Correlation of novel PAX6 gene abnormalities in aniridia and clinical presentation. *Can J Ophthalmol*. 2017;52:570-577.
12. Gillespie FD. Aniridia, Cerebellar Ataxia, and Oligophrenia in Siblings. *Archives of Ophthalmology*. 1965;73:338-341.
13. Remez LA, Onishi A, Menuchin-Lasowski Y, et al. Pax6 is essential for the generation of late-born retinal neurons and for inhibition of photoreceptor-fate during late stages of retinogenesis. *Dev Biol*. 2017;432:140-150.
14. Shaham O, Menuchin Y, Farhy C, Ashery-Padan R. Pax6: a multi-level regulator of ocular development. *Prog Retin Eye Res*. 2012;31:351-376.
15. Casas-Llera P, Siverio A, Esquivel G, Bautista C, Alio JL. Spectral-domain optical coherence tomography foveal morphology as a prognostic factor for vision performance in congenital aniridia. *Eur J Ophthalmol*. 2018:1120672118818352.
16. Thomas MG, Kumar A, Mohammad S, et al. Structural grading of foveal hypoplasia using spectral-domain optical coherence tomography a predictor of visual acuity? *Ophthalmology*. 2011;118:1653-1660.
17. Pedersen HR, Hagen LA, Landsend ECS, et al. Color Vision in Aniridia. *Investigative Ophthalmology & Visual Science*. 2018;59:2142-2152.
18. Landsend ECS, Pedersen HR, Utheim OA, et al. Meibomian gland dysfunction and keratopathy are associated with dry eye disease in aniridia. *Br J Ophthalmol*. 2019;103:119-124.
19. den Dunnen JT, Dalgleish R, Maglott DR, et al. HGVS Recommendations for the Description of Sequence Variants: 2016 Update. *Hum Mutat*. 2016;37:564-569.
20. Bhatia S, Bengani H, Fish M, et al. Disruption of autoregulatory feedback by a mutation in a remote, ultraconserved PAX6 enhancer causes aniridia. *Am J Hum Genet*. 2013;93:1126-1134.
21. Schwarz JM, Cooper DN, Schuelke M, Seelow D. MutationTaster2: mutation prediction for the deep-sequencing age. *Nat Methods*. 2014;11:361-362.

22. Ansari M, Rainger J, Hanson IM, et al. Genetic Analysis of 'PAX6-Negative' Individuals with Aniridia or Gillespie Syndrome. *PLoS One*. 2016;11:e0153757.
23. Landsend ECS, Pedersen HR, Utheim OA, et al. Characteristics and Utility of Fundus Autofluorescence in Congenital Aniridia Using Scanning Laser Ophthalmoscopy. *Invest Ophthalmol Vis Sci*. 2019;60:4120-4128.
24. Lee H, Purohit R, Patel A, et al. In Vivo Foveal Development Using Optical Coherence Tomography. *Invest Ophthalmol Vis Sci*. 2015;56:4537-4545.
25. Provis JM, Dubis AM, Maddess T, Carroll J. Adaptation of the central retina for high acuity vision: cones, the fovea and the avascular zone. *Prog Retin Eye Res*. 2013;35:63-81.
26. Rohrschneider K. Determination of the location of the fovea on the fundus. *Invest Ophthalmol Vis Sci*. 2004;45:3257-3258.
27. Kass M, Witkin A, Terzopoulos D. Snakes: Active contour models. *International Journal of Computer Vision*. 1988;1:321-331.
28. Mishra A, Wong A, Bizheva K, Clausi DA. Intra-retinal layer segmentation in optical coherence tomography images. *Opt Express*. 2009;17:23719-23728.
29. González-López A, de Moura J, Novo J, Ortega M, Penedo MG. Robust segmentation of retinal layers in optical coherence tomography images based on a multistage active contour model. *Heliyon*. 2019;5:e01271-e01271.
30. Lujan BJ, Roorda A, Croskrey JA, et al. Directional optical coherence tomography provides accurate nuclear layer and Henle fiber layer measurements. *Retina*. 2015;35:1511-1520.
31. R Core Team. R: A language and environment for statistical computing. Vienna, Austria.: R Foundation for Statistical Computing; 2016.
32. Pinheiro JC, Bates DJ, DebRoy S, Sakar D, R Core Team. *nmle: Linear and Nonlinear Mixed Effects Models.* . R package version 3.1-141 2019.
33. Frischmeyer PA, Dietz HC. Nonsense-mediated mRNA decay in health and disease. *Hum Mol Genet*. 1999;8:1893-1900.
34. Tzoulaki I, White IM, Hanson IM. PAX6 mutations: genotype-phenotype correlations. *BMC Genet*. 2005;6:27.
35. Kozak M. The scanning model for translation: an update. *J Cell Biol*. 1989;108:229-241.
36. Gronskov K, Olsen JH, Sand A, et al. Population-based risk estimates of Wilms tumor in sporadic aniridia. A comprehensive mutation screening procedure of PAX6 identifies 80% of mutations in aniridia. *Hum Genet*. 2001;109:11-18.
37. Kikuta H, Laplante M, Navratilova P, et al. Genomic regulatory blocks encompass multiple neighboring genes and maintain conserved synteny in vertebrates. *Genome Res*. 2007;17:545-555.
38. Kleinjan DA, van Heyningen V. Long-range control of gene expression: emerging mechanisms and disruption in disease. *Am J Hum Genet*. 2005;76:8-32.
39. Chylack LT, Jr., Wolfe JK, Singer DM, et al. The Lens Opacities Classification System III. The Longitudinal Study of Cataract Study Group. *Arch Ophthalmol*. 1993;111:831-836.
40. Richards S, Aziz N, Bale S, et al. Standards and guidelines for the interpretation of sequence variants: a joint consensus recommendation of the American College of Medical Genetics and Genomics and the Association for Molecular Pathology. *Genet Med*. 2015;17:405-424.
41. Gronskov K, Rosenberg T, Sand A, Brondum-Nielsen K. Mutational analysis of PAX6: 16 novel mutations including 5 missense mutations with a mild aniridia phenotype. *Eur J Hum Genet*. 1999;7:274-286.
42. Klimova L, Kozmik Z. Stage-dependent requirement of neuroretinal Pax6 for lens and retina development. *Development*. 2014;141:1292-1302.
43. Oron-Karni V, Farhy C, Elgart M, et al. Dual requirement for Pax6 in retinal progenitor cells. *Development*. 2008;135:4037-4047.
44. Marquardt T, Ashery-Padan R, Andrejewski N, Scardigli R, Guillemot F, Gruss P. Pax6 is required for the multipotent state of retinal progenitor cells. *Cell*. 2001;105:43-55.

45. Hsieh YW, Yang XJ. Dynamic Pax6 expression during the neurogenic cell cycle influences proliferation and cell fate choices of retinal progenitors. *Neural Dev*. 2009;4:32.
46. Raviv S, Bharti K, Rencus-Lazar S, et al. PAX6 regulates melanogenesis in the retinal pigmented epithelium through feed-forward regulatory interactions with MITF. *PLoS Genet*. 2014;10:e1004360.
47. Kozulin P, Natoli R, Bumsted O'Brien KM, Madigan MC, Provis JM. The cellular expression of antiangiogenic factors in fetal primate macula. *Invest Ophthalmol Vis Sci*. 2010;51:4298-4306.
48. Lagali N, Wowra B, Fries FN, et al. PAX6 mutational status determines aniridia-associated keratopathy phenotype. *Ophthalmology*. 2019.
49. Nguyen LS, Wilkinson MF, Gecz J. Nonsense-mediated mRNA decay: inter-individual variability and human disease. *Neurosci Biobehav Rev*. 2014;46 Pt 2:175-186.
50. Souzeau E, Rudkin AK, Dubowsky A, et al. PAX6 molecular analysis and genotype-phenotype correlations in families with aniridia from Australasia and Southeast Asia. *Mol Vis*. 2018;24:261-273.
51. Harding P, Moosajee M. The Molecular Basis of Human Anophthalmia and Microphthalmia. *J Dev Biol*. 2019;7.
52. Springer AD, Hendrickson AE. Development of the primate area of high acuity, 3: temporal relationships between pit formation, retinal elongation and cone packing. *Vis Neurosci*. 2005;22:171-185.
53. Vajzovic L, Hendrickson AE, O'Connell RV, et al. Maturation of the human fovea: correlation of spectral-domain optical coherence tomography findings with histology. *Am J Ophthalmol*. 2012;154:779-789.e772.
54. Tarilonte M, Morin M, Ramos P, et al. Parental Mosaicism in PAX6 Causes Intra-Familial Variability: Implications for Genetic Counseling of Congenital Aniridia and Microphthalmia. *Front Genet*. 2018;9:479.

Doctoral dissertation no. 67
2020

—

The Retina in Congenital Aniridia
- Structural, Functional and Genetic Variability
Dissertation for the degree of Ph.D

—

Hilde Røgeberg Pedersen

—

ISBN: 978-82-7206-552-1 (print)
ISBN: 978-82-7206-553-8 (online)

usn.no